

**Discoveries of Anti-Müllerian hormone, its receptor,  
and a role to stimulates synthesis of collagen-specific chaperone HSP47  
in bovine oviducts and endometria**

ウシ子宮・卵管におけるアンチミュラーホルモンと受容体、  
ならびに、コラーゲン特異的シャペロン HSP47 の合成促進作用の発見

**Joint Graduate School of Veterinary Medicine  
Yamaguchi University**

**Raihana Nasrin FERDOUSY  
September 2022**

**Discoveries of Anti-Müllerian hormone, its receptor,  
and a role to stimulates synthesis of collagen-specific chaperone HSP47  
in bovine oviducts and endometria**

**A Dissertation**

*Submitted by*

**RAIHANA NASRIN FERDOUSY**

in Partial Fulfillment of the Requirement for the Degree of

**DOCTOR OF PHILOSOPHY  
(Reproductive Physiology and Management)**



**Joint Graduate School of Veterinary Medicine  
Yamaguchi University  
JAPAN**

**September, 2022**

## **Acknowledgements**

I am highly grateful to the Government of Japan, the Ministry of Education, Culture, Sports, Science and Technology, for sponsoring my study by providing me the Monbukagakusho (MEXT) Scholarship.

This dissertation work was carried out at the Laboratory of Reproduction, Department of Veterinary Clinical Sciences, Joint Graduate School of Veterinary Medicine, Yamaguchi University. This work has been realized through the intensive efforts and participation of many people. It is my pleasure to thank the many people who made my study and research possible.

First and foremost, I would like to thank my supervisor, Prof. Dr. Hiroya Kadokawa for his excellent knowledges, guidance, wisdom, unfaltering enthusiasm and patience. I am indebted to him for his continuous help and encouragement throughout the years not only in the academic aspects but also in my daily life. He and his wife's, Yukie Kadokawa positive approach to life and kindness are highly appreciated. They often went beyond the call of their duties to help patiently when I need help.

I am greatly thankful to my co-supervisors Prof. Dr. Mitsuhiro Takagi, Prof. Dr. Naoki Sasaki, Prof. Dr. Ken Kusakabe, and Prof. Dr. Takaaki Andou for their valuable comments, suggestions and guidance that made my preparation of this dissertation a reality. I am also thankful to all my teachers and office staffs for their kind support and help during my study.

I am highly grateful to the Yamaguchi Prefectural Government for allowing me to use their slaughter houses facilities and beef cattle farmers for allowing using their animals as sources of main data for the purpose of my study.

I am also thankful to my laboratory colleagues: Onalenna Kereilwe, Risa Saito, Obara Nishijima Laura Akari, Ritsuki Shiroma, Nguyen Thi Suong and Yuki Asato for their friendly assistance, encouragement and support in my studies. I also express my sincere thanks to my international, Japanese and Bangladeshi friends and their families, Hirakawa-no-Kaze-no Kai, Yamaguchi Red Cross, Yamaguchi city office and many other people and organizations that are not mentioned here, for their support to make my stay in Japan homely. I also acknowledge with thanks the great cooperation I received from the entire university community in terms of academic and social life during my study.

I would like to express my deepest appreciation and love to my parents, brothers, sisters, in-laws and all my family members for their everlasting encouragement, sacrifices, and kindness. Finally, I would like to thank my husband Tarif Abu Md Mamun and our daughters, for their unending love, sacrifices, patience, support and encouragement during my study. I would like to dedicate this dissertation to my parents who have been the source of my motivation for higher education.

## **Abstract**

Fertility decreases during aging in human and bovine females, but the exact pathophysiological mechanisms in the oviducts and uteri are not clarified yet. Anti-Müllerian hormone (AMH) is a glycoprotein that belongs to the transforming growth factor- $\beta$  superfamily. Plasma AMH concentrations can predict the fertility of adult female goats, ewes, cows, and women via unknown physiological mechanisms. This thesis study attempted to clarify whether AMH, and the main receptor for AMH, AMH receptor type 2 (AMHR2) have important roles for the age-related infertility.

In first, I investigated whether the primary receptor for AMH, AMHR2, is expressed in bovine oviducts and endometria. Reverse transcription–polymerase chain reaction (RT-PCR) detected expression of *AMHR2* mRNA in oviductal and endometrial specimens. Western blotting and immunohistochemistry were performed to analyse AMHR2 protein expression using anti-bovine AMHR2 antibody. Immunohistochemistry revealed robust AMHR2 expression in the tunica mucosa of the ampulla and isthmus, as well as in the glandular and luminal epithelium of the endometrium. The number of AMHR2-positive fibroblasts increased, suggesting the presence of fibrosis in the oviducts and uteri of old cows. *AMHR2* mRNA (measured RT-qPCR) and AMHR2 protein expression in these layers did not significantly differ among oestrous phases in adult Japanese Black (JB) cows ( $P > 0.1$ ). In addition, *AMHR2* mRNA and protein expression in these layers did not differ among old Holsteins (mean ( $\pm$ SEM) age  $91.9 \pm 6.4$  months) and young ( $26.6 \pm 0.8$  months) and old ( $98.8 \pm 10.2$  months) JB cows. Therefore, AMHR2 is expressed in bovine oviducts and endometria.

Other important hormones for endocrinological regulation have paracrine and autocrine roles. Therefore, in the next study, I investigated whether bovine oviducts and

endometria produce AMH. RT-PCR and western blotting detected AMH expression in oviductal and endometrial specimens. Immunohistochemistry revealed robust AMH expression in the ampulla and isthmus epithelia, and the glandular and luminal endometrial epithelia (caruncular endometria). The number of AMH-positive fibroblasts increased, suggesting the presence of fibrosis in the oviducts and uteri of old cows. *AMH* mRNA and protein expression in these layers did not significantly differ among estrous phases in adult JB heifers ( $p > .1$ ). Furthermore, the expression in these layers also did not differ among Holstein cows ( $93.8 \pm 5.8$  months old), JB heifers ( $25.5 \pm 0.4$  months old), and JB cows ( $97.9 \pm 7.9$  months old). We also compared AMH concentrations in the oviduct and uterine horn fluids among the three groups (measured by immunoassays). Interestingly, the AMH concentration in the oviduct fluid, but not in the uterine horn fluid, of Holstein cows was lower than those in JB heifers and cows ( $p < .05$ ). Therefore, bovine oviducts and endometria express AMH and likely secrete it into the oviduct and uterine fluids.

Collagen, the most abundant extra-cellular matrix in oviducts and uteri, performs critical roles in pregnancies. I hypothesised that the locations and amounts of both denatured collagen and the collagen-specific molecular chaperone 47-kDa heat shock protein (HSP47) in the oviducts and uteri of old cows are different compared with those of young heifers because of repeated pregnancies. Since detecting damaged collagen in tissues is challenging, we developed a new method that uses a denatured collagen detection reagent. Then, we compared damaged collagen in the oviducts and uteri between post-pubertal growing nulliparous heifers ( $22.1 \pm 1.0$  months old) and old multiparous cows ( $143.1 \pm 15.6$  months old). Further, I evaluated the relationship between denatured collagen and HSP47 by combining this method with fluorescence immunohistochemistry. Picro-

sirius red staining showed collagen in almost all parts of the oviducts and uteri. Expectedly, damaged collagen was increased in the oviducts and uteri of old cows. However, damaged collagen and HSP47 were not located in the same area in old cows. The number of HSP47-positive fibroblasts increased, suggesting the presence of fibrosis in the oviducts and uteri of old cows. These organs of old cows showed higher HSP47 protein amounts than those of heifers. However, the uteri, but not oviducts, of old cows had lower HSP47 mRNA amounts than those of heifers. These findings revealed the specific location and amounts of denatured collagen and HSP47 in the oviducts and uteri of old cows compared with those of heifers.

Therefore, I discovered the AMH, AMHR2 expression in several important layers of oviducts and uteri, and I discovered the increased AMH, AMHR2, and HSP47 in the fibroblasts after aging. However, still role of AMH, AMHR2 in oviducts and uteri were not clarified yet. Therefore, in the next study, I hypothesized that AMH stimulate HSP47 expression in fibroblast and epithelium. I cultured uterine fibroblasts and epithelial cells obtained from heifers. Then, I treated the cells with recombinant with increasing concentrations (0, 1, 10, or 100 ng mL<sup>-1</sup>) of AMH. Then, HSP47 expression was measured by western blotting. AMH stimulated ( $P < 0.05$ ) HSP47 expression in epithelial cells but not in fibroblasts. Therefore, these findings suggested the role of AMH to cause the abnormal high HSP47 expression in the oviducts and uteri of old cows.

In conclusion, this thesis discovered the AMH and AMHR2 in bovine oviducts and uteri, which have important roles for collagen synthesis via HSP47.

## **Table of Contents**

**Acknowledgements**

**i**

<b>Thesis Abstract</b>	<b>iii</b>
<b>Table of Contents</b>	<b>vi</b>
<b>List of Tables</b>	<b>xi</b>
<b>List of Figures</b>	<b>xii</b>
<b>List of Abbreviations</b>	<b>xxi</b>
<b>List of Companies</b>	<b>xxiv</b>

## **CHAPTER I**

<b>General Introduction</b>	<b>1-6</b>
-----------------------------	------------

## **CHAPTER II**

<b>Review of Literature</b>	<b>7-12</b>
2.1. Age-related infertility in cows	8
2.2. Importance of oviduct for early embryogenesis	8
2.3. Importance of uterus for early embryogenesis and pregnancy	9
2.4. AMH and AMHR2 for fertility and embryogenesis	10
2.5. Importance of collagen for fertility	11
2.6. Denatured collagen in aged animal	11
2.7. Importance of HSP47	12

## **CHAPTER III (Study I)**

### **AMHR2 expression in bovine oviducts and endometria: Comparison of AMHR2 mRNA and protein abundance between old Holstein and young and old JB**

#### **females**

Abstract	14
3.1. Introduction	15
3.2. Materials and methods	17
3.2.1. Animals and treatments	17
3.2.2. Samples collection	17
3.2.3. AMHR2 expression in oviduct and endometrium	17

3.2.4. RT-PCR, sequencing of amplified products, and homology search in gene databases	18
3.2.5. Western Blotting detection of AMHR2	22
3.2.6. Immunofluorescence staining and confocal microscopy	23
3.2.7. Oviductal and endometrial AMHR2 expression at different stages of the oestrous cycle	24
3.2.8. Comparison of AMHR2 expression among breeds and ages	24
3.2.9. RT-qPCR analysis of factors affecting <i>AMHR2</i> expression	25
3.2.10. Western blotting for factors affecting AMHR2 expression	28
3.2.11. Statistical analysis	28
3.3. Results	30
3.3.1. AMHR2 expression in oviduct and endometrium	30
3.3.2. Oviductal and endometrial AMHR2 expression at different stages of the oestrous cycle	31
3.3.3. Comparison of AMHR2 expression among breeds and ages	31
3.4. Discussion	39

## **CHAPTER IV (Study II)**

### **AMH is expressed and secreted by bovine oviductal and endometrial epithelial cells 42-73**

Abstract	43
4.1. Introduction	44
4.2. Materials and methods	46
4.2.1. Sample collection	46
4.2.2. AMH expression in oviduct and endometrium	46
4.2.3. Oviductal and endometrial AMH expression at different stages of the oestrous cycle	47
4.2.4. Comparison of AMH expression among breeds and ages	47
4.2.5. Analyze AMH concentration in the oviduct and uterine horn fluid	48

4.2.6. RT-PCR, sequencing of amplified products, and homology search in gene databases	49
4.2.7. Anti-AMH antibody used in this study	51
4.2.8. Western blotting for AMH detection	52
4.2.9. Fluorescent immunohistochemistry and confocal microscopy	53
4.2.10. RT-qPCR	54
4.2.11. AMH immunoassay	57
4.2.12. Statistical analysis	57
4.3. Results	58
4.3.1. AMH expression in oviduct and endometrium	58
4.3.2. Oviductal and endometrial AMH expression at different stages of the oestrous cycle	59
4.3.3. Comparison of AMH expression among breeds and ages	59
4.3.4. AMH concentration in the oviduct and uterine horn fluid	60
4.4. Discussion	70

## **CHAPTER V (Study III)**

### **Specific locations and amounts of denatured collagen and collagen-specific chaperone, HSP47, in the oviducts and uteri of old cows as compared with those of heifers**

Abstract	75
5.1. Introduction	76
5.2. Materials and methods	78
5.2.1. Sample collection	78
5.2.2. Development of the method for in situ detection of denatured collagen	79
5.2.3. Picro-sirius red staining for total collagen	80
5.2.4. RT-PCR, sequencing of amplified products, and homology search in gene databases	81
5.2.5. Western blotting for HSP47 detection	84

5.2.6. RT-qPCR analysis of <i>HSP47</i>	85
5.2.7. Immunofluorescence staining and confocal microscopy	88
5.2.8. Analysis of the 5'-flanking region of <i>SERPINH1</i>	89
5.2.9. Statistical analysis	89
5.3. Results	90
5.4. Discussion	103

## **CHAPTER VI (Study IV)**

### **AMH stimulates the HSP47 expression, in bovine uterine epithelial cells but not myofibroblasts 109-137**

Abstract	110
6.1. Introduction	111
6.2. Materials and methods	113
6.2.1. Sample collection	113
6.2.2. Antibodies and blocking peptides for immunohistochemistry and immunocytochemistry	113
6.2.3. Immunofluorescence staining and confocal microscopy	115
6.2.4. Culture of bovine epithelial cells and treatment with AMH	117
6.2.5. Culture of bovine uterine fibroblasts and treatment with AMH	119
6.2.6. Fluorescent immunocytochemistry	121
6.2.7. Effect of inhibition of the ERK pathway on AMH-induced HSP47 expression	121
6.2.8. Western Blotting for HSP47 detection	122
6.2.9. Statistical analysis	123
6.3. Results	125
6.4. Discussion	134

## **CHAPTER VII**

### **General Discussion and Conclusion 138-141**

7.1. General Discussion	139
-------------------------	-----

7.2. Conclusion	141
<b>References</b>	<b>142-159</b>

## **List of Tables**

### **CHAPTER III (Study I)**

Table 3.1	Details of the primers for RT PCR for <i>AMHR2</i>	21
Table 3.2	Details of the primers for RT-qPCRs for <i>AMHR2</i> , <i>C2orf29</i> and <i>SUZ12</i>	27
<b>CHAPTER IV (Study II)</b>		
Table 4.1.	Details of the primers for RT-qPCRs for <i>AMH</i>	56
<b>CHAPTER V (Study III)</b>		
Table 5.1	Details of the primers for RT PCR for <i>HSP47</i>	83
Table 5.2	Details of the primers for RT-qPCRs for <i>HSP47</i>	87

## List of Figures

### CHAPTER III (Study I)

- Fig. 3.1 Expression of *AMHR2* mRNA, as detected by reverse RT–PCR analysis 32  
(A) with cDNAs and (B) with NTC or NRCs. The electropherogram shows the expected size (320 bp) of PCR products of bovine *AMHR2* in the ovary, ampulla, isthmus and CAR and ICAR areas of the endometrium in healthy post pubertal heifers (A), but not in the NTC or NRCs in the ovary, ampulla, isthmus, CAR and ICAR areas (B)
- Fig. 3.2 Western blotting analysis of extracts from the ovary, ampulla, isthmus, 33  
CAR and ICAR areas in healthy post pubertal heifers using (A) anti-*AMHR2* antibody or (B) anti- $\beta$ -actin antibody.
- Fig. 3.3 *AMHR2* expression in (A) ampulla and (B) isthmus samples collected on 34  
Day 3 of the oestrous cycle, (C, D) CAR samples collected on Day 15 (low and high magnifications respectively) and (E, F) ICAR samples collected on Day 3 (E) and 21 (F) from healthy post-pubertal heifers. Nuclei were counterstained with DAPI. Differential interference contrast microscopy was used.
- Fig. 3.4 Relative *AMHR2* mRNA abundance in the in the (A) ampulla, (B) isthmus, 35  
(C) CAR and (D) ICAR areas in healthy post-pubertal heifers during the pre-ovulatory phase (pre-Ov; Days 19 to 21) and on Days 1-3, 8-12, and 5 to 17 of the oestrous cycle, as determined by RT-qPCR. Data were normalized against the geometric means of *C2orf29* and *SUZ12* abundance. Data are the mean  $\pm$  SEM. There were no significant differences ( $P > 0.05$ ) in *AMHR2* abundance across phases of the oestrous cycle.
- Fig. 3.5 Relative *AMHR2* protein expression, normalized against  $\beta$ -actin, in the (A) 36  
ampulla, (B) isthmus, (C) CAR and (D) ICAR areas in healthy post-pubertal heifers during pre-ovulatory phase (pre-Ov; Days 19 to 21) and on Days 1-3, 8-12, and 5 to 17 of the oestrous cycle, as determined by western blotting. There were no significant differences ( $P > 0.05$ ) in *AMHR2* expression across phases of the oestrous cycle.
- Fig. 3.6 Relative *AMHR2* mRNA abundance in the (A) ampulla, (B) isthmus, (C) 37  
CAR and (D) ICAR areas in healthy young adult JB heifers, old JB cows

and old Holsteins cows, as determined via RT-qPCR. Data were normalized against the geometric means of *C2orf29* and *SUZ12* abundance. Data are the mean  $\pm$  SEM. There were no significant differences ( $P > 0.05$ ) in *AMHR2* abundance among groups.

Fig. 3.7 Relative AMHR2 protein expression, normalized against  $\beta$ -actin, in the (A) 38 ampulla, (B) isthmus, (C) CAR and (D) ICAR areas in healthy young JB heifers, old JB cows, and old Holsteins cows, as determined via western blotting. Data are the mean  $\pm$  SEM. There were no significant differences ( $P > 0.05$ ) in AMHR2 expression among groups.

#### CHAPTER IV (Study II)

Fig. 4.1 Expression of *AMH* mRNA, detected by RT-PCR analysis. The 61 electropherogram shows the expected size (328 bp) of PCR products of bovine *AMH* in the ovary, ampulla, isthmus, and CAR and ICAR areas of the endometrium in post-pubertal heifers; no amplicons were observed in NTC and NRC conditions

Fig. 4.2 Western blotting using an anti-AMH rabbit antibody on protein extracts of 62 ovaries, ampulla, isthmus, and CAR and ICAR areas collected from post-pubertal heifers (A);  $\beta$ -actin was used as a loading control (B)

Fig. 4.3 Immunofluorescence staining of AMH in the ampulla samples of post- 63 pubertal heifers. Specimens were collected on day 3 (day 0 = day of estrus). Images were captured via laser-scanning confocal microscopy and show AMHR2 (light blue), AMH (green), cytokeratin (red), and counter-staining with DAPI nuclear stain (dark blue), and DIC microscopy (grayscale). The pink rectangle within the low magnification image indicates the position of the high magnification. In the merged photos, the pink arrows indicate the AMH signals in the luminal epithelium of mucosa. The brown arrows indicate signals in fibroblasts. Right panel (B) show negative controls staining using the normal animal IgGs. Scale bars represent 100  $\mu$ m in the low magnification. Scale bars represent 50  $\mu$ m in the enlarged merge of (A) and (C), and 100  $\mu$ m in other panels, which shown as pink rectangular.

- Fig. 4.4 Immunofluorescence staining of AMH in the isthmus samples of post- 64  
pubertal heifers. Specimens were collected on day 5 (day 0 = day of estrus).  
Images were captured via laser-scanning confocal microscopy and show  
AMHR2 (light blue), AMH (green), cytokeratin (red), and counter-staining  
with DAPI nuclear stain (dark blue), and DIC microscopy (grayscale). The  
pink rectangle within the low magnification image indicates the position of  
the high magnification. In the merged photos, the pink arrows indicate the  
AMH signals in the luminal epithelium of mucosa. The brown arrows  
indicate signals in fibroblasts. Right panel (B) show negative controls  
staining using the normal animal IgGs. Scale bars represent 100  $\mu\text{m}$  in the  
low magnification. Scale bars represent 50  $\mu\text{m}$  in the enlarged merge of (A)  
and (C), and 100  $\mu\text{m}$  in other panels.
- Fig. 4.5 Immunofluorescence staining of AMH in the CAR samples of post- 65  
pubertal heifers. Specimens were collected on day 13. Images were  
captured via laser-scanning confocal microscopy and show AMHR2 (light  
blue), AMH (green), cytokeratin (red), and counter-staining with DAPI  
nuclear stain (dark blue), and DIC microscopy (grayscale). In the merge  
photos of (A), cavity indicates the uterine cavity. The pink arrows indicate  
the AMH signals in the luminal epithelium of caruncle. The green arrows  
indicate AMH signals in the vasculature. Right panel (B) show negative  
controls staining using the normal animal IgGs1. Scale bars represent 100  
 $\mu\text{m}$  in (B), and 50  $\mu\text{m}$  in other panels.
- Fig. 4.6 Immunofluorescence staining of AMH in the ICAR samples of post- 66  
pubertal heifers. Specimens were collected on day 13. Images were  
captured via laser-scanning confocal microscopy and show AMHR2 (light  
blue), AMH (green), cytokeratin (red), and counter-staining with DAPI  
nuclear stain (dark blue), and DIC microscopy (grayscale). The pink arrows  
indicate the AMH signals in the epithelium of endometrial glands in  
intercaruncle. The green arrows indicate AMH signals in the vasculature.  
Right panel (B) show negative controls staining using the normal animal

IgGs. Scale bars represent 50  $\mu$ m in the enlarged merge of (A) and (C), and 100  $\mu$ m in other panels.

- Fig. 4.7 No significant differences in the relative expression levels of *AMH* mRNA (determined by the RT-qPCR) or protein (determined by western blotting) (all data are shown as the mean  $\pm$  SEM) in the ampulla (A, E), isthmus (B, F), CAR (C, G), or ICAR (D, H) samples of post-pubertal heifers during pre-ovulatory phase (Pre-Ov; day 19 to 21), day 1 to 3, day 8 to 12, or day 15 to 17. Relative *AMH* mRNA levels were determined by quantitative RT-PCR and normalized to the geometric means of *C2orf29* and *SUZ12* levels. Relative *AMH* protein expression levels were determined by western blotting and normalized to those of  $\beta$ -actin. The same letters indicate no significant differences ( $P > 0.05$ ) across phases. 67
- Fig. 4.8 No significant differences in the relative expression levels (shown as the mean  $\pm$  SEM) of *AMH* mRNA (determined by the RT-qPCR) or protein (determined by western blotting) in the ampulla (A, E), isthmus (B, F), CAR (C, G), or ICAR (D, H) samples among post-pubertal JB heifers, JB cows, and Holstein cows. The same letters indicate no significant differences ( $P > 0.05$ ) across phases. 68
- Fig. 4.9 *AMH* concentrations, as measured by enzyme immunoassays in the oviduct fluid on day 1 to 3 (A) or uterine fluid on day 8 to 14 (B), collected from post-pubertal JB heifers, JB cows, and Holstein cows. Different letters indicate significant differences ( $P < 0.05$ ) among groups. 69

## CHAPTER V (Study III)

- Fig. 5.1 Picro-sirius red staining for total collagen in ampulla, isthmus, and CAR and ICAR areas of the endometrium and myometrium in healthy post pubertal, growing and young nulliparous heifers (Young), and old multiparous JB beef cows (Old). The Picro-sirius red staining shows collagen in red, muscle fibres and cytoplasm in yellow, and complex in orange. 93

- Fig. 5.2 *In situ* detection of denatured collagen. The no-heated, non-digested young 94 tissues show very subtle signals of denatured collagen (red). In contrast, the old samples, in a manner similar to the heated or enzyme-digested young tissues, show strong signals corresponding to denatured collagen in the lamina propria and muscular layers of ampullae and isthmuses; the stroma of CAR and ICAR; the glandular epithelium of ICAR; and various myometrial cells.
- Fig. 5.3 Expression of *HSP47* detected via RT-PCR analysis. The 95 electropherogram shows the size (470 bp) expected from PCR products of bovine *HSP47* in the ampulla, isthmus, CAR, ICAR, and myometrium (Myo) in old cows. Bands were not present in the NTC and NRCs lanes.
- Fig. 5.4 Comparison of denatured collagen-rich areas (red) and HSP47-rich areas 96 (green) in the ampullae or isthmuses (collected on day 3 of the oestrous cycle) of Young and Old groups. Nuclei are counterstained with DAPI (dark blue). Unlike the Young, the Old specimens showed strong signal corresponding to denatured collagen in the lamina propria and muscular layers. The Old specimens showed strong signal corresponding to HSP47 in the epithelia of tunica mucosa and superficial stroma. Not many signals corresponding to colocalisation (yellow) were present in the Merge panels; scale bars are 50  $\mu$ m.
- Fig. 5.5 Comparison of denatured collagen-rich areas (red) and HSP47-rich areas 97 (green) in the CAR, ICAR, or Myo (collected on day 13 of the oestrous cycle) of Young and Old groups. Nuclei are counterstained with DAPI (dark blue). Both the Young and Old specimens showed signals corresponding to both denatured collagen and HSP47 in luminal epithelia, glandular epithelia, and stroma. Unlike the Young, the Old specimens also showed strong signals corresponding to both denatured collagen and HSP47 in the stroma and myometria. Particularly, the number of fibroblasts (green dots) increased. However, not many signals corresponding to colocalisation (yellow) were present in the Merge panels; scale bars are 50  $\mu$ m. The dark patches in old myometria are broken parts.

- Fig. 5.6 Comparison of HSP47-rich areas (green) and cytokeratin- or vimentin-rich areas (red) in the ampullae or isthmuses (collected on day 3 of the oestrous cycle), or the CAR, ICAR, or Myo (collected on day 13 of the oestrous cycle) of Old groups. Nuclei are counterstained with DAPI (dark blue); scale bars are 50  $\mu$ m. 99
- Fig. 5.7 Representative photos of western blotting analysis for HSP47 or anti- $\beta$ -actin mouse antibodies in extracts from ampulla, isthmus, CAR, ICAR, and myometrium (Myo) in the Young and Old groups (A). Relative HSP47 protein levels normalised to those of  $\beta$ -actin in the ampulla (B), isthmus (C), CAR (D), ICAR (E), or myometrium (F) in the Young and Old groups. The header in the upper corner of each graph represents the results of two-factor ANOVA followed by Fisher's PLSD test, including the effect of age (Young or Old) and effect of stage and interaction. Greek letters ( $\alpha$ ,  $\beta$ , or  $\chi$ ) above the grey left-side bars indicate significant between-stage differences in expression in Young samples; letters (a, b, or c) above the white right-side bars indicate significant between-stage differences in expression in Old samples (one-factor ANOVA followed by Fisher's PLSD test). N.S., non-significant. 100
- Fig. 5.8 Relative *HSP47* mRNA levels (mean  $\pm$  SEM) in the ampulla (A), isthmus (B), CAR (C), ICAR (D), or Myo (E) in healthy, post-pubertal growing nulliparous heifers (Young group) and old multiparous cows (Old group), as determined via RT-qPCR. Data were normalised to the geometric means of *C2orf29* and *SUZ12* levels. The header in the upper corner of each graph represents the results of two-factor ANOVA followed by Fisher's PLSD test, including the effect of age (Young or Old) and effect of stage and interaction. Greek letters ( $\alpha$ ,  $\beta$ , or  $\chi$ ) above the grey left-side bars indicate significant between-stage differences in expression in Young samples; letters (a, b or c) above the white right-side bars indicate significant between-stage differences in expression in Old samples (one-factor 102

ANOVA followed by Fisher's PLSD test). N.S. is abbreviation of non-significant.

Fig. 5.9 Supplementary Fig 1. Representative photos of western blotting using another anti-HSP47 mouse monoclonal antibody, clone M16.10A1 or anti- $\beta$ -actin mouse antibodies in extracts from ampulla, isthmus, CAR, ICAR, and myometrium (Myo) in the Young and Old groups. 108

## CHAPTER VI (Study IV)

Fig. 6.1 Comparison of AMHR2-rich areas (green), AMH-rich areas (light blue), and HSP47-rich areas (red) in the CAR, ICAR, and uterine myometrium (Myo) (collected on day 3 of the oestrous cycle) of young heifer (22 months old) and old cows (130 months old, collected on day 13 of the estrous cycle). Nuclei are counterstained with DAPI (dark blue). The specimens showed signals corresponding to both AMHR2 and HSP47 in luminal epithelia, glandular epithelia, and stroma. The Merge panels show signals indicating the colocalization (yellow arrows) of AMHR2 and HSP47. AMHR2-negative, AMH-negative, and HSP47-positive epithelial cells are indicated by white arrows and appear abundantly in the CAR (A) and Myo (C). AMHR2-positive, AMH-positive, and HSP47-positive myofibroblasts are indicated by brown arrows. The dark patches in old myometria are indicated by brown arrows. The dark patches in old myometria are broken parts. Scale bars: 50  $\mu$ m. 127

Fig. 6.2 Immunocytochemistry of cultured uterine epithelial cells for AMHR2 (green) with oxytocin receptor (A), HSP47 (B), or collagen type IV (C). Immunocytochemistry confirmed that all the cultured cells were cytokeratin-positive (A) and vimentin-negative (B), verifying pure epithelial cell culture. Scale bar: 20  $\mu$ m. 129

Fig. 6.3 Immunocytochemistry of cultured uterine myofibroblasts for AMHR2 (green) with oxytocin receptor (A), HSP47 (B), or collagen type IV (C). Immunocytochemistry confirmed that all the cultured cells were vimentin-positive (A) and cytokeratin-negative (B), verifying pure myofibroblast 130

culture. Scale bar: 20  $\mu$ m.

- Fig. 6.4 Representative photos of western blotting for HSP47 (A) or  $\beta$ -actin (B) 131  
using extracts of cultured uterine epithelial cells treated with AMH [final  
concentrations, 0, 1, 10 ng/mL, or 100 ng/mL (0.85 pM)], or with TGF- $\beta$ 1  
(final concentration, 0.85 pM). A dark 47 kDa band corresponding to  
HSP47 and a weak 75 kDa band were observed for control and all  
treatments. HSP47 levels were normalized to that of  $\beta$ -actin in both bands.  
The different letters (a or b) above the bars indicate significant difference  
in HSP47 expression due to different treatments (One-factor ANOVA  
followed by Fisher's PLSD test).
- Fig. 6.5 Representative photos of western blotting for HSP47 (A) or  $\beta$ -actin (B) 132  
using extracts of cultured uterine myofibroblasts treated with AMH [final  
concentrations, 0, 1, 10 ng/mL, or 100 ng/mL (0.85 pM)], or TGF- $\beta$ 1 (final  
concentrations, 0.85 pM). A main 47 kDa band corresponding to HSP47  
and a weak 75 kDa band were observed. HSP47 levels were normalized to  
that of  $\beta$ -actin in both bands. The same letters (a) above the bars indicate  
no significant differences in HSP47 expression due to different treatments  
(One-factor ANOVA followed by Fisher's PLSD test).
- Fig. 6.6 Representative photos of western blotting for HSP47 (A) or  $\beta$ -actin (B) 133  
using extracts of cultured uterine epithelial cells treated with AMH (final  
concentrations, 100 ng/mL) with or without pre-treatment with U0126. The  
different letters (a or b) above the bars indicate significant difference in  
HSP47 expression due to different treatments (One-factor ANOVA  
followed by Fisher's PLSD test).
- Fig. 6.7 Supplementary Fig. 1. Comparison of AMHR2-rich areas (green), AMH- 137  
rich areas (light blue), and HSP47-rich areas (red) in the ampullae or  
isthmuses (collected on day 3 of the estrous cycle) of old cow uteri (130  
months old). Nuclei are counterstained with DAPI (dark blue). The old  
specimens showed strong signals corresponding to both AMHR2 and  
HSP47 in the epithelia of tunica mucosa and superficial stroma. The merge

panels show signals corresponding to colocalization of AMHR2 with HSP47 (yellow arrows). AMHR2-positive, AMH-positive, and HSP47-positive myofibroblasts are indicated by brown arrows. Scale bars: 50  $\mu\text{m}$ .

## List of Abbreviations

AFC	: Antral follicle count
AI	: Artificial insemination
AMH	: Anti-Müllerian hormone
AMHR2	: Anti-Müllerian hormone receptor type 2
ANOVA	: Analysis of variance
BLAST	: Basic nucleotide local alignment search tool
BMP	: Bone morphogenetic protein
Bp	: Base pair
BSA	: Bovine serum albumin
cDNA	: Complementary deoxyribonucleic acid
C	: Celsius
C2orf29	: Chromosome 2 open reading frame 29
CAR	: Caruncle
CCD	: Charge-coupled device
CO <sub>2</sub>	: Carbon dioxide
Cq	: Quantification cycle
CVs	: Coefficients of variation
DAPI	: 4',6-diamidino-2-phenylindole
DDBJ	: DNA Data Bank of Japan
DIC	: Differential interference contrast
DMEM	: Dulbecco's modified eagle's medium
DNA	: Deoxyribonucleic acid
EBI	: European Bioinformatics Institute
ECL-Prime	: Enhanced chemiluminescence-prime
ECM	: Extra-cellular matrix
EIA	: Enzyme immunoassay
ELISA	: Enzyme-Linked Immuno Sorbent Assay
ERE	: Estrogen-responsive element
ERK	: extracellular signal-regulated kinase pathways

EDTA	: Ethylenediaminetetraacetic acid
FBS	: Fetal bovine serum
FSH	: Follicle stimulating hormone
h	: Hour(s)
HEPES	: 4-(2-hydroxyethyl)-1-piperazineethanesulfonic acid
HCl	: Hydrogen chloride
HRP	: Horseradish peroxidase
HSP47	: Heat shock 47 kDa protein
ICAR	: Intercaruncle
IgG	: Immunoglobulin G
IVF	: In vitro fertilization
JB	: Japanese Black
kbp	: Kilo Base pair
KCl	: Potassium chloride
kDa	: Kilo Dalton
IU	: International Units
kg	: Kilogram (s)
L	: Liter (s)
LH	: Luteinizing hormone
MAPK	: Mitogen-activated protein kinase enzymes
MIF	: Macrophage migration inhibitory factor
MIS	: Mullerian Inhibiting Substance
min	: Minute (s)
mL	: Mililiter (s)
mM	: Millimolar
mm	: Millimeter
mRNA	: Messenger ribonucleic acid
n	: Number
NCBI	: National Center for Biotechnology Information
NaCl	: Sodium chloride
Na <sub>2</sub> HPO <sub>4</sub>	: Disodium hydrogen phosphate

ND	: Nano Drop
ng	: Nanogram(s)
nM	: Nanomolar
NRCs	: No reverse transcription controls
NTC	: No template control
OCT	: Optimal cutting temperature
PBS	: Phosphate buffered saline
PCR	: Polymerase chain reaction
PFA	: Paraformaldehyde
pg	: Pico gram
PLSD	: Protected least significant difference
PRE	: Progesterone-responsive element
Post-OV	: Post-ovulation
PVDF	: Polyvinylidene fluoride
R2	: Reactions with a coefficient of determination
RE	: response element
RNA	: Ribonucleic acid
RT-PCR	: Reverse transcription-polymerase chain reaction
RT-qPCR	: Reverse transcription-quantitative polymerase chain reaction
SDS	: Sodium Dodecyl Sulfate
SEM	: Standard error of mean
Smad	: Small mothers against decapentaplegic
SUZ12	: Suppressor of zeste 12
TGF	: Transforming growth factor
T-PER	: Tissue protein extraction reagent
$\mu$ L	: Microliter
$\mu$ g	: Microgram
$\mu$ m	: Micrometer
$\mu$ M	: Micromolar

## List of Companies Supplying Chemicals or Instruments Used in This Study

<b>Name of company</b>	<b>Address</b>
Abcepta Inc.	San Diego, CA, USA
Adobe	San Jose, CA, USA
Aviva Systems Biology	CA, USA
Bethyl Laboratories Inc.	Montgomery, TX, USA
Bio-Rad	Hercules, CA, US
Bioss antibodies Inc.	Woburn, MA, USA
Carl Zeiss	Göttingen, Germany
Cytiva	Marlborough, MA, USA
Eclipse Ci	Nikon, Tokyo, Japan
Enzo Life Sciences, Inc.	Farmingdale, New York. USA
Enzo Biochem Inc.	New York. USA
Fujifilm	Tokyo, Japan
Funakoshi	Tokyo, Japan
GE Healthcare	Amersham, UK
Gelstar, Lonza	Allendale, NJ, US
Genetyx	Tokyo, Japan
Gibco	Grand Island, NY, USA
Ibidi	Grafelfing, Germany
Leica Microsystems	Wetzlar, Germany
Matsunami-Glass	Osaka, Japan
Molecular Research Centre Inc.	Cincinnati, OH, USA
Nacalai Tesque, Inc.	Kyoto, Japan
NanoDrop Technologies Inc.	Wilmington, DE, USA
Nippon Gene	Tokyo, Japan
Nitta Gelatin Inc.	Futamata, Yao-shi, Osaka

Peptide Institute Inc.	Osaka, Japan
PluriSelect Life Science	Leipzig, Germany
R & D systems	Minneapolis, MN, US
Red rock software	Salt Lake, UT, USA
Sakura Fintechical Co. Ltd.	Tokyo, Japan
SAS Institute, Inc.	Cary, NC, USA
Scrum Inc.	Tokyo, Japan
ScyTek laboratories Inc.	Logan, UT, USA
Shiraimatsu Corp. Ltd.	Osaka, Japan
Sigma-Aldrich	St. Louis, MO, USA
Takara Bio Inc.	Shiga, Japan
Thermo Fisher Scientific	Waltham, MA, US
Toyobo Co. Ltd	Osaka, Japan
Vector Laboratories Inc.	Burlingame, CA, USA
Wako Pure Chemicals	Osaka, Japan
Yamato Kohki	Saitama, Japan

## **CHAPTER I**

### **General Introduction**

Old age is associated with infertility in various animals, including women and cows (Osoro and Wright 1992; Scheffer et al. 2018). Little is known for details of mechanism for reproductive longevity (Chenoweth, 1994). However, in an early study by Erickson *et al.* (1976), aging was associated with infertility, specially 55% of the cows become infertile by 13 years of age. Wathes, (2012) reported that the infertility is the main reason for culling of dairy cows, because of the inhibited of conception, owing to intrinsic problems in the embryo and/or to a poor-quality reproductive tract environment. Therefore, clarifying mechanism of reproductive aging is very important.

Ovaries regulate the oviducts and endometria through estradiol and progesterone secreted from mid-sized or large-sized follicles or corpora lutea (Pohler et al. 2012; Binelli et al. 2018). However, it is unclear, whether preantral and small antral follicles, which account for the majority of follicles in ovaries, secrete any hormone to regulate the oviducts and endometria. We wondered whether preantral and small antral follicles are the ‘silent majority’ in the ovaries.

The oviduct is the first site of maternal body contact with the early embryo. Oviduct plays important roles to accomplish gamete transport, fertilization and embryo development in a timely manner and to provide a healthy embryo to the uterus (Kolle et al., 2009; Besenfelder et al., 2012). For the early-stage embryo, the oviduct seems to supply any growth factor as well as nutrients via oviductal fluid (Hugentobler et al., 2010; Besenfelder et al., 2012).

The uterus provides an environment for an embryo that develop into a fetus and complete pregnancy. Abnormal stromal fibroblasts in myometrium causes adenomyosis in uterus, and is associated with infertility in humans (Zhai *et al.* 2020). Uterine fluids ensure

uterine fluid homeostasis and facilitate embryo-maternal interactions in mammalian species, including humans (Zhang *et al.* 2017).

Anti-Müllerian hormone (AMH) is a member of the transforming growth factor (TGF)- $\beta$  family, and its well-known secretion is from the preantral and small antral follicles in female animals (Bhide and Homburg 2016). AMH has been well-characterized at the ovarian level; that is, with regarding to its roles in regulating follicular development (Hernandez-Medrano *et al.* 2012) and inhibiting follicular atresia (Seifer and Merhi 2014). Blood AMH concentration is a useful blood marker for antral follicle counts (AFCs) in the Wagyu breed (Hirayama *et al.* 2019), as well as in dairy cows and women (Arouche *et al.* 2015; Sefrioui *et al.* 2019). Mossa and Ireland (2019) have shown that dairy cows with a low AFC have lower concentrations of AMH and a thinner endometrium than cows with high AFC. In various animals, including women and cows, circulating AMH concentrations can help predict the number of high-quality embryos produced (Arouche *et al.* 2015; Sefrioui *et al.* 2019). The number of high-quality embryos results from synchronous regulation by the spermatozoa, ovum, oviduct, and endometrium. Further, plasma AMH concentrations are positively correlated with pregnancy rates in various animals, including women and cows (Ribeiro *et al.* 2014; Josso 2019). Indeed, recent studies have shown an increased risk of miscarriage among women with low blood AMH concentrations (Tarasconi *et al.* 2017; Lytle Schumacher *et al.* 2018). Recent studies have revealed extragonadal roles of AMH mediated by activation of its primary receptor, AMHR2, in gonadotrophs in the anterior pituitaries of rats and bovines (Garrel *et al.* 2016; Kereilwe *et al.* 2018). However, limited information is available regarding the exact mechanisms underlying this association.

Blood AMH concentrations are highest in pubertal girls and gradually decrease starting at age 25 until it is undetectable after menopause (Dewailly *et al.* 2014), suggesting

that low AMH is a marker for ovarian aging (Bhide and Homburg 2016). Studies on the relationship between age and plasma AMH concentration in adult female ruminants are not common, but one study showed that old Wagyu (syn. Japanese Black) cows have higher blood AMH concentrations than post pubertal heifers and young cows (Koizumi and Kadokawa 2017). Therefore, age may be a determinant of blood AMH concentration.

Collagen, one of the most extra-cellular matrix (ECM) proteins, exerts a critical role in successful pregnancies, and abnormal collagen expression is associated with recurring miscarriages in women (Li *et al.* 2019, Shi *et al.* 2020). The bovine endometrium, similar to that of other mammals, changes morphologically throughout the oestrous cycle (Arai *et al.* 2013). Furthermore, dysregulation of ECM remodelling in bovine endometrium may impair fertility (Scolari *et al.* 2016).

Denaturation of collagen is increased due to various diseases, including cancer, osteoporosis, and arthritis (Fields 2013, Ito and Nagata 2019). Denatured collagen was studied by electron microscopy for corneal immune injury (Mohos and Wagner 1969). It was technically challenging to detect damaged collagen in tissues until the recent development of a collagen hybridising peptide (Zitnay *et al.* 2017) and a denatured collagen detection reagent (Takita *et al.* 2019). The latter is a biotin-labelled collagen-mimetic peptide that hybridises with the denatured portion of collagen. It enables the detection of denatured collagen via western blotting as well as through visualisation of heat damaged collagen fibrils in mouse fibroblasts (Takita *et al.* 2019).

Forty-seven kilodalton heat shock protein, HSP47, encoded by *SERPINH1*, is the sole procollagen-specific molecular chaperone that is essential for correct folding of the unique, triple-helical structure of collagen (Ito and Nagata 2019). HSP47 also plays important roles in the synthesis of collagen as well as in the prevention of procollagen aggregation (Duarte

and Bonatto 2018). Therefore, HSP47 can be used to detect the location of active collagen synthesis in the oviducts and uteri.

In the first study, I hypothesized that AMHR2 is expressed in oviducts and endometria and if it has any role to regulate oviducts and endometria. Other important hormones for endocrinological regulation have paracrine and autocrine roles. Therefore, in the second study, I investigated whether bovine oviducts and endometria produce AMH for paracrine and autocrine signaling. I evaluated the relationship between AMH expression in the bovine oviducts and endometria and oestrous stage, age and breed.

Collagen have critical roles in pregnancies. In the third study, I hypothesized that the locations and amounts of both denatured collagen and HSP47 in the oviducts and uteri of old cows are different compared to those of young heifers. In the first part of this study, we developed a new method using the denatured collagen detection reagent to compare young and old oviducts and uteri. Then, we evaluated the relationship between denatured collagen and HSP47. Still role of AMH, AMHR2 in oviducts and uteri were not clarified yet. Therefore, in the fourth study, I evaluated the colocalization of AMHR2 and HSP47; then I hypothesized that AMH stimulates HSP47 expression in epithelial cells and fibroblasts of bovine uteri.

This thesis consists of nine chapters. In Chapter I (General Introduction), I explained the background information and main objectives of the study. In Chapter II, I reviewed the literatures directly or indirectly related to my thesis. Chapters III and IV deal with expression of AMHR2 and AMH in oviducts and endometria and that their expressions are age related. In Chapter V, I determined the locations and amounts of both denatured collagen and HSP47 expression. In Chapter VI, I evaluated the effect of AMH to stimulates HSP47 expression in

bovine uterine epithelial cells and fibroblasts. Finally, I discussed the main findings of the present study to conclude in chapter VII.

## **CHAPTER II**

### **Review of Literature**

## **2.1. Age-related infertility in cows**

Infertility increases after aging in various animals, including women and cows (Osoro and Wright 1992; Scheffer *et al.* 2018); however, limited information is available regarding the exact mechanisms underlying this association among animals. Little is known for details of mechanism for reproductive longevity in bovines. In study by Erickson *et al.* (1976), 55% of the cows became infertile by 13 years of age. Also, Wathes, (2012) reported that infertility is the main reason for culling dairy cows. Wathes, (2012) reported that old cows have suppressed conception rate owing to intrinsic problems in the embryo and/or to a poor-quality reproductive tract environment. Therefore, clarifying mechanism of reproductive aging is very important.

## **2.2. Importance of oviduct for early embryogenesis**

Oviduct is the site where the maternal body first contacts with the early embryo. Oviducts are stage for a series of important events, e.g., gamete maturation, capacitation, sperm selection and early embryo development, and all of these must precisely initiate and complete (Kolle *et al.* 2009; Besenfelder *et al.* 2012). Ovum and sperm enter the oviduct from opposite ends and fuse to form an embryo. To meet all these demands, the oviduct consists of the infundibulum, ampulla and isthmus, which consist of longitudinal and circular aligned muscle layers, endothelial ciliated and non-ciliated cells. The isthmus is the functional sperm reservoir, and ampulla is the site for acrosome reaction in ruminants (Hunter, 2005).

Oviductal fluid secreted mainly by the non-ciliated epithelial cells, and oviductal fluid

may provide growth factors as well as nutrients for the early embryo (Cox and Leese, 1997; Yaniz *et al.* 2000; Gray *et al.* 2001). Oviducts modulate its local mechanisms at the molecular level during the presence of gametes and embryos, which represent the first exchange of signals between the maternal environment and embryo (Holt and Fazeli, 2010; Kolle *et al.* 2010). The oviduct exhibits an extraordinary flexibility that is hormonally driven and exactly timed according to the embryonic stage (Abe and Hoshi, 2008; Nakahari *et al.* 2011), and the epithelium is the layer directly contact with ovum, sperm and embryo. During early embryo development, the embryo needs support by the oviduct to establish pregnancy.

### **2.3. Importance of uterus for early embryogenesis and pregnancy**

The uterus provides an environment for an embryo to develop into a fetus and reside until the completion of pregnancy. Bovine endometrium consists of caruncular (CAR) and intercaruncular (ICAR) regions. In the intercaruncular regions, there are stroma fibroblast cells and luminal epithelial and glandular epithelial cells those have essential functions during pregnancy establishment (Chaney *et al.* 2021). Uterine epithelial cells also play important roles in the uterine defence against microbial infection (Hillmer *et al.* 2020). Abnormal stromal fibroblasts in myometrium causes adenomyosis in uterus, and is associated with infertility (Zhai *et al.* 2020).

Hormonal imbalance is a cause of infertility. Also, thin endometrium, fibroids, adenomyosis, and endometriosis, can affect uterine receptivity and limit the ability to conceive and implantation of an embryo (Taylor, 2018).

Uterine fluid is the medium for sperm and embryo transport, extracellular vesicles and mobile RNAs, ions and proteins, ensure uterine fluid homeostasis and facilitate embryo-maternal interactions (Zhang *et al.* 2017).

#### **2.4. AMH and AMHR2 for fertility and embryogenesis**

AMH is a member of the TGF- $\beta$  family, secreted from the preantral and small antral follicles in female animals (Bhide and Homburg 2016). AMH has been well-characterized at the ovarian level, i.e., with respect to its roles in regulating follicular development (Hernandez-Medrano *et al.* 2012) and inhibiting follicular atresia (Seifer and Merhi 2014). Blood AMH concentration is a useful blood marker for antral follicle counts in the Wagyu breed (Hirayama *et al.* 2019), as well as in dairy cows and women (Arouche *et al.* 2015; Sefrioui *et al.* 2019). Mossa and Ireland (2019) have shown that dairy cows with a low AFC have lower concentrations of AMH and thinner endometrium than those in cows with high AFC. Circulating AMH concentrations can help predict the number of high-quality embryos produced by various animals, including women and cows (Arouche *et al.* 2015; Sefrioui *et al.* 2019). The number of high-quality embryos results from synchronous regulation by the sperm, ovum, oviduct, and endometrium. Further, plasma AMH concentrations are positively correlated with pregnancy rates in various animals, including women and cows (Ribeiro *et al.* 2014; Josso 2019). Indeed, recent studies have shown an increased risk of miscarriage among women with low blood AMH concentrations (Tarasconi *et al.* 2017; Lyttle *et al.* 2018). These data suggest the importance of AMH for proper reproductive function in ruminants.

Recent studies have revealed extragonadal roles of AMH. by the activation of its primary receptor, AMHR2, in gonadotrophs in the anterior pituitaries of rats and bovines (Garrel *et al.* 2016; Kereilwe *et al.* 2018). Therefore, AMHR2 may be expressed in the oviducts and the endometria to mediate any yet unknown roles of AMH.

Several studies found that AMH may be involved in the fertility, pregnancy. It plays role in fertility management in cattle (Mossa *et al.* 2017). Circulating AMH is a reliable marker of the antral follicle population of an animal as well as directly correlated to an animal's response to a superovulation protocol. AMH may be valuable as a reproductive management tool (Alward and Bohlen, 2020). AMH was used as treatment of endometriosis stromal and epithelial cell growth and induces cell cycle arrest and apoptosis in endometriosis cells (Signorile *et al.* 2014). AMH causes growth inhibition of epithelial ovarian cancer cells and cell lines in vitro and in vitro via AMHR2 receptor-mediated mechanism (Kim *et al.* 2014).

## **2.5. Importance of collagen for fertility**

Collagen, one of the most abundant ECM proteins, exerts a critical role in successful pregnancies, and abnormal collagen expression is associated with recurring miscarriages in women (Li *et al.* 2019, Shi *et al.* 2020). The bovine endometrium, similar to that of other mammals, changes morphologically throughout the oestrous cycle (Arai *et al.* 2013). Furthermore, dysregulation of ECM remodeling in bovine endometrium may impair fertility (Scolari *et al.* 2016).

## **2.6. Denatured collagen in aged animal**

Denaturation of collagen is increased due to various diseases, including cancer, osteoporosis, and arthritis (Fields 2013, Ito and Nagata 2019). Denatured collagen was studied by electron microscopy for corneal immune injury (Mohos and Wagner 1969). It was technically challenging to detect damaged collagen in tissues until the recent development of a collagen hybridising peptide (Zitnay *et al.* 2017) and a denatured collagen

detection reagent (Takita *et al.* 2019). The latter is a biotin-labelled collagen-mimetic peptide that hybridises with the denatured portion of collagen. It enables the detection of denatured collagen via western blotting as well as through visualisation of heat damaged collagen fibrils in mouse fibroblasts (Takita *et al.* 2019).

Repeated pregnancy and parturition increases the denatured collagen. Another possible reason for such an increase in the levels of denatured collagen may be infection and inflammation because lipopolysaccharides decrease collagen synthesis in myometrial explants from women (Wendremaire *et al.* 2013). The tunica mucosa of oviducts and epithelia of the endometrium are located adjacent to the lumen, and thus, the structure of these layers may be susceptible to damage or frequent changes. denatured collagen-rich areas, damaged structure may remain uncured. This may explain the increased infertility observed in older beef cows (Osoro and Wright 1992). Those data suggest the importance to denatured collagen study.

## **2.7. Importance of HSP47**

HSP47, encoded by *SERPINH1*, is a sole procollagen-specific molecular chaperone that is essential for correct folding of the unique, triple-helical structure of collagen (Ito and Nagata 2019). HSP47 also plays important roles in the synthesis of collagen as well as in the prevention of procollagen aggregation (Duarte and Bonatto 2018). Therefore, HSP47 is central in detecting the location of active collagen synthesis in the oviducts and uteri. However, there are no previous studies for any importance of HSP47 in oviduct and uterus.

## **CHAPTER III**

**(Study I)**

**AMHR2 expression in bovine oviducts and endometria: Comparison of  
AMHR2 mRNA and protein abundance between old Holstein and young  
and old JB females**

## Abstract

AMH is a glycoprotein produced by granulosa cells of the preantral and small antral follicles that has multiple important roles in the ovaries. Recent studies have revealed extragonadal AMH regulation of gonadotropin secretion from bovine gonadotrophs. In this Chapter, I investigated whether the primary receptor for AMH, AMHR2, is expressed in bovine oviducts and endometria. RT-PCR detected expression of *AMHR2* mRNA in oviductal and endometrial specimens. Western blotting and immunohistochemistry were performed to analyze AMHR2 protein expression using anti-bovine AMHR2 antibody. Immunohistochemistry revealed robust AMHR2 expression in the tunica mucosa of the ampulla and isthmus, as well as in the glandular and luminal epithelium of endometrium. *AMHR2* mRNA and AMHR2 protein expression in these layers did not significantly differ among oestrous phases in adult JB cows ( $P > 0.1$ ). In addition, *AMHR2* mRNA and protein expression in these layers did not differ among old Holsteins (mean ( $\pm$ SEM) age  $91.9 \pm 6.4$  months) and young ( $26.6 \pm 0.8$  months) and old ( $98.8 \pm 10.2$  months) JB cows. Therefore, AMHR2 is expressed in bovine oviducts and endometria.

### 3.1. Introduction

Ovaries regulate the oviducts and endometria through estradiol and progesterone secreted from mid-sized or large-sized follicles or corpora lutea (Pohler *et al.* 2012; Binelli *et al.* 2018). However, it is unclear, whether preantral and small antral follicles, which account for the majority of follicles in ovaries, secrete any hormone to regulate the oviducts and endometria. We wondered whether preantral and small antral follicles are the ‘silent majority’ in the ovaries.

AMH is a member of the TGF- $\beta$  family, and is primarily secreted by the preantral and small antral follicles in female animals (Bhide and Homburg 2016). AMH has been well-characterized at the ovarian level; that is, with regard to its roles in regulating follicular development (Hernandez-Medrano *et al.* 2012) and inhibiting follicular atresia (Seifer and Merhi 2014). Blood AMH concentration is a useful blood marker for AFCs in the JB breed (Hirayama *et al.* 2019), as well as in dairy cows and women (Arouche *et al.* 2015; Sefrioui *et al.* 2019). Mossa and Ireland (2019) have shown that dairy cows with a low AFC have lower concentrations of AMH and a thinner endometrium than cows with high AFC. In various animals, including women and cows, circulating AMH concentrations can help predict the number of high-quality embryos produced (Arouche *et al.* 2015; Sefrioui *et al.* 2019). The number of high-quality embryos results from synchronous regulation by the spermatozoa, ovum, oviduct, and endometrium. Further, plasma AMH concentrations are positively correlated with pregnancy rates in various animals, including women and cows (Ribeiro *et al.* 2014; Josso 2019). Recent studies have revealed extragonadal roles of AMH mediated by activation of its primary receptor, AMHR2, in gonadotrophs in the anterior pituitaries of rats and bovines (Garrel *et al.* 2016; Kereilwe *et al.* 2018). Therefore, AMHR2 may be expressed in the oviducts and the endometria to mediate any yet unknown roles of

AMH. Indeed, recent studies have shown an increased risk of miscarriage among women with low blood AMH concentrations (Tarasconi *et al.* 2017; Lyttle Schumacher *et al.* 2018).

Old age is associated with infertility in various animals, including women and cows (Osoro and Wright 1992; Scheffer *et al.* 2018); however, limited information is available regarding the exact mechanisms underlying this association. Several studies in humans have linked aging to plasma AMH concentrations. Blood AMH concentrations are highest in pubertal girls and gradually decrease starting at age 25 until it is undetectable after menopause (Dewailly *et al.* 2014), suggesting that low AMH is a marker for ovarian aging (Bhide and Homburg 2016). Studies on the relationship between age and plasma AMH concentration in adult female ruminants are not common, but one study showed that old JB (syn. Japanese Black) cows have higher blood AMH concentrations than post pubertal heifers and young cows (Koizumi and Kadokawa 2017). Therefore, age may be a determinant of the AMHR2 expression levels in the oviducts and endometria, although there may be species differences.

Oviductal and endometrial AMHR2 expression is unknown in any species; however, AMHR2 is expressed in women with endometriosis and uterine adenomyosis (Signorile *et al.* 2014; Kim *et al.* 2018). Therefore, in the present study we investigated the hypothesis that AMHR2 is expressed in bovine oviducts and endometria. A previous study showed breed-dependent differences in circulating AMH concentrations among dairy cow breeds (Ribeiro *et al.* 2014). Infertility in Holsteins is a critical issue in the dairy industry worldwide (Kadokawa and Martin 2006). Therefore, the aim of this study was to evaluate the association between oviductal and endometrial AMHR2 expression and various physiological factors, such as stage of the oestrous cycle, age, and breed.

## **3.2. Materials and Methods**

### **3.2.1. Animals and treatments**

All experiments were performed according to the Guiding Principles for the Care and Use of Experimental Animals in the Field of Physiological Sciences (Physiological Society of Japan; available at <http://physiology.jp/wp-content/uploads/2015/07/Guiding-principles.pdf>, accessed 1 May 2018) and were approved by the Committee on Animal Experiments of Yamaguchi University.

### **3.2.2. Samples collection**

Oviductal and endometrial samples from cattle managed by contracted farmers in western Japan. Since the bovine spongiform encephalopathy disaster in 2002, all cattle born in Japan since 2003 are registered in a database at birth with an individual identification number. This number must be shown on an ear tag, carcass, and meat packages sold by butchers. Japanese farmers and consumers can obtain information, including breed, birth date, farm, movement from farm to farm, date and place of livestock auction and slaughter by querying the server of the National Livestock Breeding Center of Japan. We used both individual identification numbers and information given by the contracted farmers for the cattle in this study.

### **3.2.3. AMHR2 expression in oviduct endometrium**

Experiment investigated whether AMHR2 is expressed in the oviduct and endometrium in heifers using RT-PCR, western blotting, and immunofluorescence staining. The ampulla, isthmus, CAR, and ICAR area of endometria were obtained from four post-pubertal (26 months of age) JB heifers at a local abattoir. The four heifers were at Days 3, 8,

15, and 21 of the oestrous cycle (where Day 0 = day of oestrus), as determined via macroscopic examination of the ovaries and uterus (Miyamoto *et al.* 2000). The ampulla, isthmus, CAR, and ICAR samples collected were from the side ipsilateral to ovulation in the three heifers at Days 3, 8, or 15 of the cycle, but from the side ipsilateral to the dominant follicle in the remaining heifer at day 21 of the cycle. Ampullar samples were collected from areas at least 3 cm away from the fimbriated infundibulum as well as from the ampullary-isthmic junction, and the isthmus samples were collected from areas also at least 3 cm away from the ampullary-isthmic junction as well as from the utero-tubal junction. Half of the ampulla and half of the isthmus were frozen in liquid nitrogen and stored at -80°C until RNA or protein extraction. The remaining halves of the ampulla and isthmus were stored in 4% PFA at 4°C for 16 h for immunohistochemistry studies. The middle area of uterine horn was opened longitudinally using scissors, and CAR areas were carefully dissected so as not to include ICAR areas; subsequently, ICAR areas were cut off. The CAR and ICAR samples were frozen in liquid nitrogen and preserved at -80°C until RNA or protein extraction or stored in 4% PFA at 4°C for 16 h for immunohistochemistry studies.

Since granulosa cells in small antral follicles express AMHR2 (Poole *et al.* 2016), ovarian tissue specimens were harvested from the same heifers as positive AMHR2 controls for RT-PCR and western blotting analysis.

#### **3.2.4. RT-PCR, sequencing of amplified products, and homology search in gene databases**

Total RNA was extracted from the ovary, ampulla, isthmus, CAR, or ICAR areas from the four heifers using RNazol RT Reagent (Molecular Research Center) according to the

manufacturer's protocol. The extracted RNA samples were treated with ribonuclease-free deoxyribonuclease (Thermo Fisher Scientific) to eliminate possible genomic DNA contamination. Using a NanoDrop ND-1000 spectrophotometer (NanoDrop Technologies), the concentration and purity of each RNA sample were evaluated to ensure the ratio of absorbance at 260nm: 280nm was in the acceptable range of 1.8–2.1. The mRNA quality of all samples was verified by electrophoresis of total RNA followed by staining with ethidium bromide, and the 28S:18S ratios were 2:1. The cDNA was synthesized from 1 µg total RNA per sample using SuperScript IV VILO Master Mix (Thermo Fisher Scientific) according to the manufacturer's protocol. NRCs were prepared for RT-PCR; they were generated by treating the extracted RNA with the same deoxyribonuclease but not with cDNA synthetase.

In order to determine the expression of *AMHR2* mRNA in the samples, PCR was conducted using the primer pair reported previously by our group (Kereilwe *et al.* 2018), which was designed by Primer3 (<http://www.ncbi.nlm.nih.gov/tools/primer-blast/>, accessed 8 April 2020) based on reference sequence of bovine *AMHR2* NCBI reference sequence of bovine *AMHR2* is NM\_001205328.1, because one of PCR primers must span the exon-exon junction. Table 3.1 details the primers used for RT-PCR. Using a Veriti 96-Well Thermal Cycler (Thermo Scientific), PCR was performed using 20 ng of cDNA, 20 ng RNA as the NRC or water as the NTC, and polymerase (Tks Gflex DNA Polymerase, Takara Bio) under the following thermocycles reported by our group (Kereilwe *et al.* 2018): 94 °C for 1 min for pre-denaturing followed by 35 cycles of 98°C for 10 s, 60°C for 15 s, and 68°C for 30 s. PCR products were separated on 1.5% agarose gel by electrophoresis with a molecular marker [Gene Ladder 100 (0.1-2kbp), Nippon Gene], stained with fluorescent stain (Gelstar; Lonza), and observed using a CCD imaging system (GelDoc; Bio-Rad). The PCR products were purified with the NucleoSpin Extract II kit (Takara Bio) and then sequenced with a

sequencer (ABI3130, Thermo Fisher Scientific) using one of the PCR primers and the Dye Terminator v3.1 Cycle Sequencing Kit (Thermo Fisher Scientific). The sequences obtained were used as query terms with which to search the homology sequence in the DDBJ, GenBank and EBI Data Bank using the BLAST optimized for highly similar sequences (available on the NCBI website).

**Table 3.1.** Details of the primers for RT-PCR for *AMHR2*

Gene	Primer	Sequence 5'-3'	Position		Size (bp)
			Nucleotide	Exon	
<i>AMHR2</i>	Forward	AGATTTGCGACCTGACAGCAG	1272– 1292	9-10	320
	Reverse	CTTCCAGGCAGCAAAGTGAG	1572– 1591	11	

### 3.2.5. Western Blotting detection of AMHR2

Proteins were extracted from the ovary (used as positive controls), ampulla, isthmus, CAR, or ICAR samples from the four heifers, and western blotting was performed as described previously (Kereilwe *et al.* 2018). The extracted protein sample (33.4µg total protein in 37.5µl) was mixed in 12.5µl of 4x Laemmli sample buffer (Bio-Rad) containing 10% (v/v) β-mercaptoethanol, then boiled for 3 min at 100 °C. The boiled protein samples were quickly cooled down on ice, and then a 12 µl aliquot of the boiled protein samples (8 µg of total protein) was loaded onto a polyacrylamide gel along with a molecular weight marker and resolved by electrophoresis on sodium dodecyl sulfate-polyacrylamide gels at 100 V for 90 min. Proteins were then transferred to PVDF membranes. Membranes were blocked with 0.1% Tween 20 and 5% non-fat dry milk for 1h at 25 °C. Next, immunoblotting was performed with our original anti-AMHR2 chicken antibody (Kereilwe *et al.* 2018; 1:25,000 dilution) overnight at 4 °C. The anti-AMHR2 chicken antibody binds to the extracellular region located near the N terminus of the AMHR2, and full details for this antibody have been published previously (Kereilwe *et al.* 2018). After washing, the PVDF membranes were incubated with HRP-conjugated anti- chicken IgG goat antibody (Bethyl laboratories; 1:50,000 dilution) at 25 °C for 1 h. Protein bands were visualized using an ECL-Prime chemiluminescence kit (GE Healthcare) and CCD imaging system (Fujifilm). Previous studies utilizing western blotting for AMHR2 reported that human, mouse, and bovine AMHR2 are present as dimers, full-length monomers, or cleaved monomers (Faure *et al.* 1996; Hirschhorn *et al.* 2015; Kereilwe *et al.* 2018). Thus, we defined bovine AMHR2 bands based on band size as one of these structure types. After antibodies were removed from the PVDF membrane with stripping solution, the membrane was used for

immunoblotting with the anti- $\beta$ -actin mouse monoclonal antibody (1:50,000 dilution; A2228; Sigma-Aldrich).

### **3.2.6. Immunofluorescence staining and confocal microscopy**

After storage in 4% paraformaldehyde in PBS at 4°C for 16 h, tissue blocks were placed in 30% sucrose-PBS until the blocks were infiltrated with sucrose. Tissue blocks were then subjected to immunofluorescence staining using previously described protocols (Nahar *et al.* 2013; Kereilwe *et al.* 2018). Briefly, 15- $\mu$ m sections were prepared and mounted on slides. The sections were treated with 0.3% Triton X-100-PBS for 15 min and were then blocked by incubating with 0.5 mL of PBS containing 10% normal goat serum (Wako Pure Chemicals) for 1 h at room temperature. The slides were incubated with the same anti-AMHR2 chicken antibody (Kereilwe *et al.* 2018; 1:1,000 dilution) for 12 h at 4°C, followed by incubation with Alexa Fluor Alexa Fluor 488 goat anti-chicken IgG (Thermo Fisher Scientific; diluted to 1  $\mu$ g/mL) and DAPI (Wako Pure Chemicals) for 2 h at room temperature.

The stained sections on slides were observed using a confocal microscope (LSM710; Carl Zeiss) equipped with diode (405 nm), argon (488 nm) lasers. Images obtained by fluorescence microscopy were scanned with a 20 $\times$  or 40 $\times$  objective and recorded by a CCD camera system controlled by ZEN2012 black edition software (Carl Zeiss). In the confocal images obtained after immunohistochemistry analysis, the DAPI is shown in blue and AMHR2 is shown in green. To verify the specificity of the signals, several negative controls were included in which the primary antiserum had been omitted or pre-absorbed with 5 nM of the antigen peptide (Kereilwe *et al.* 2018) or in which normal chicken IgG (Wako Pure Chemicals) was used instead of the primary antibody.

### **3.2.7. Oviductal and endometrial AMHR2 expression at different stages of the oestrous cycle**

Experiment was conducted to compare AMHR2 expression in oviductal and endometrial samples among stages of the oestrous cycle using RT-qPCR and western blotting (described below).

Samples of the ampulla, isthmus, CAR and ICAR tissues were harvested from adult (26-month-old) non-pregnant healthy JB heifers in the pre-ovulatory phase (Days 19-21; n = 5), Days 1 to 3 (n = 5), Days 8 to 12 (n = 5), or Days 15 to 17 (n = 5), as determined by macroscopic examination of the ovaries and uterus (Miyamoto *et al.* 2000). Samples were obtained at the local abattoir and immediately frozen in liquid nitrogen and stored at  $-80^{\circ}\text{C}$  until RNA or protein extraction.

### **3.2.8. Comparison of AMHR2 expression among breeds and ages**

Experiment was conducted to compare AMHR2 expression in oviductal and endometrial samples based on age or breed utilizing the RT-qPCR and western blotting (described below)

Samples of the ampulla, isthmus, CAR, and ICAR tissues were harvested during the luteal phase (day 8 to 12) from healthy post-pubertal JB heifers (mean ( $\pm$  SEM)  $26.6 \pm 0.8$  months of age; n = 6; young JB group), old JB cows ( $98.8 \pm 10.2$  months of age; n = 6; old JB group) and old Holstein cows ( $91.9 \pm 6.4$  months of age; n = 6; old Holstein group) from the local abattoir. These three groups were compared for four reasons. (1) it was not possible to obtain samples from post pubertal Holstein heifers because they are kept in dairy farms for milking purposes. (2) in a previous study (Kereilwe and Kadokawa 2019), we compared

AMH expression levels in gonadotrophs between old Holsteins (about 80 months old) and young and old JB females (26 and 90 months old respectively) and found significant differences in AMH mRNA and protein between them. (3) we previously discovered significant difference in blood AMH concentrations between old JB cows and young JB heifers (81 and 22 months old respectively) (Koizumi and Kadokawa 2017); and (4) farmers kill old JB cows after completing parturition a sufficient number of times to obtain beef, usually after 84 months of age. All heifers and cows in the three groups were non-lactating and non-pregnant, with no follicular cysts, luteal cysts, or other ovarian or uterine disorders upon macroscopic ovarian examination of ovaries (Kamomae 2012). The old Holstein cows were killed because they had not become pregnant after at least five AI attempts. Unlike JB and Holstein, other breeds of cattle (such as Angus, Hereford, and Guernsey) are very rare in Japan; thus, we were unable to collect samples from these other breeds.

### **3.2.9. RT-qPCR analysis of factors affecting AMHR2 expression**

After preparation of high-quality total RNA and cDNA synthesis using the protocol described above, *AMHR2* mRNA expression was compared among oestrous phases or among the young JB, old JB, and old Holstein groups using RT-qPCR and data analyses as described previously (Nahar and Kadokawa 2017; Kereilwe *et al.* 2018).

The primers for *AMHR2* were designed using Primer Express Software v3.0 (Thermo Fisher Scientific), based on reference sequences. The primer sequences are detailed in Table 3.2. *AMHR2* expression levels were normalized against the geometric mean of the expression levels of two house-keeping genes, namely chromosome 2 open reading frame 29 (*C2orf29*) and suppressor of zeste 12 (*SUZ12*), selected using Normfinder program (Vandesompele *et al.* 2002; available at <http://moma.dk/normfinder-software>, accessed 2

June 2019) and amplified using previously reported primers (Rekawiecki *et al.* 2012; Nahar and Kadokawa 2017), because these two are the most stable and reliable housekeeping genes in the bovine oviducts and endometria (Walker *et al.* 2009; Nahar and Kadokawa 2017).

Gene expression was measured in duplicate by RT-qPCR with 20 ng cDNA, using CFX96 Real Time PCR System (Bio-Rad) and Power SYBR Green PCR Master Mix (Thermo Fisher Scientific), together with a 6-point relative standard curve and an NRC. Standard 10-fold dilutions of purified and amplified DNA fragments were prepared. Temperature conditions for all genes were as follows: 95°C for 10 min for pre-denaturation; five cycles each of 95°C for 15s and 66°C for 30s; and 40 cycles each of 95°C for 15s and 60°C for 60s. Melting curve analyses were performed at 95°C for each amplicon and each annealing temperature to ensure the absence of smaller non-specific products such as dimers. To optimize the RT-qPCR assay, serial dilutions of a cDNA template were used to generate a standard curve by plotting the log of the starting quantity of the dilution factor against the C<sub>q</sub> value obtained during amplification of each dilution. All the C<sub>q</sub> values of the unknown samples ( $\pm$ SEM)  $22.85 \pm 0.15$  were between the highest (8.00) and lowest (30.33) standards for *AMHR2* in RT-qPCR. Further, all the C<sub>q</sub> values of the unknown samples were between the highest and lowest standards for *C2orf29* or *SUZ12* in real-time PCR. Reactions with a coefficient of determination (R<sup>2</sup>) > 0.98 and efficiency between 95% and 105% were considered optimized. The intra-assay CVs of real-time PCRs were <6%. The concentration of PCR products was calculated by comparing C<sub>q</sub> values of unknown samples against the standard curve using appropriate software (CFXmanagerV3.1, Bio-Rad). Then the *AMHR2* amount was divided by the geometric mean of *C2orf29* and *SUZ12* in each sample.

**Table 3.2.** Details of the primers for RT-qPCRs for *AMHR2*, *C2orf29* and *SUZ12*

Gene	Primer	Sequence 5'-3'	Position		Size (bp)
			Nucleotide	Exon	
<i>AMHR2</i>	Forward	TGGGAGATTATGAGTCGCTGC	1249–	9	52
			1269		
	Reverse	GTGGTGGTCTGCTGTCAGGT	1281–	9-10	
			1300		
<i>C2orf29</i>	Forward	TCAGTGGACCAAAGCCACCTA	928–948	3	170
	Reverse	CTCCACACCGGTGCTGTTCT	1077–	4	
			1097		
<i>SUZ12</i>	Forward	CATCCAAAAGGTGCTAGGATA	1441–	13	160
		GATG	1465		
	Reverse	TTGGCCTGCACACAAGAATG	1581–	14	
			1600		

### **3.2.10. Western blotting for factors affecting AMHR2 expression**

Expression of AMHR2 protein were compared in the ampulla, isthmus, CAR and ICAR areas was compared among estrous phases or among young JB, old JB and old Holsteins groups using previously reported protocols for western blotting and data analyses (Kereilwe *et al.* 2018; Kereilwe and Kadokawa 2018). Briefly, boiled samples (8  $\mu\text{g}$  total protein of each sample) were loaded on a polyacrylamide gel along with the molecular weight marker and four standard samples (2, 4, 8, and 16  $\mu\text{g}$  total protein for each of five randomly selected samples diluted with protein extraction reagent). MultiGauge v.3.0 software (Fujifilm) was used to quantify the signal intensity of the protein bands. The intensities of band of AMHR2 (full-length form) in the 16, 8, 4, and 2  $\mu\text{g}$  protein samples were set as 100%, 50%, 25%, and 12.5%, respectively, and the intensity of other samples was calculated as a percentage of these standards using MultiGauge software. After antibodies were removed from the PVDF membrane with stripping solution, the membrane was used for immunoblotting with the anti- $\beta$ -actin mouse monoclonal antibody. The intensities of the  $\beta$ -actin band for 16-, 8-, 4-, and 2- $\mu\text{g}$  protein samples were set as 100%, 50%, 25%, and 12.5%, respectively, and the intensity of other samples was calculated as a percentage of these standards using MultiGauge software. AMHR2 expression levels were normalized against  $\beta$ -actin expression in each sample.

### **3.2.11. Statistical analysis**

Statistical analyses were performed using Stat View version 5.0 for Windows (SAS Institute, Inc.). Grubb's test verified the absence of outliers. The Shapiro-Wilk's test and Kolmogorov-Smirnov Lilliefors test verified the normality of distribution of each variable.

The F-test verified homogeneity of variance of all of variables between stages of oestrous cycle and ages. One-factor ANOVA followed by post-hoc comparisons using Fisher's PLSD test was performed for the four stages comparisons. One-factor ANOVA followed by Fisher's PLSD test was used to test the significance of differences between old Holstein cows, young JB's and old JB's. The level of significance was set at two-tailed  $P < 0.05$ . Data are expressed as mean  $\pm$  SEM.

### 3.3. Results

#### 3.3.1. AMHR2 expression in oviduct and endometrium

PCR products of the expected size (320 bp), indicating *AMHR2*, were obtained from the ovary, ampulla, isthmus, CAR, and ICAR areas, as revealed through agarose gel electrophoresis (**Fig. 3.1A**). Bands of PCR products from ovary, CAR, and ICAR areas were stronger than bands from the ampulla. Neither the NTC nor any of the NRCs yielded any PCR amplified products (**Fig. 3.1B**). A homology search against gene databases for the sequenced amplified products revealed bovine *AMHR2* (NM\_001205328.1) as the best match, with a query coverage of 100%; e-value, 0.0; maximum alignment identity, 99%. No other bovine gene exhibited homology with the PCR product herein, thus indicating that the amplified product was indeed *AMHR2*.

*AMHR2* expression in the ampulla, isthmus, CAR, ICAR areas and in positive control ovarian specimens were analysed via western blot analysis using the anti-*AMHR2* antibody (**Fig. 3.2**). The western blot showed similar protein bands for *AMHR2* among all tissue samples (**Fig. 3.2A**). However, full length bands and cleaved bands were stronger in ovary, CAR and ICAR samples than ampulla and isthmus. No protein bands were observed for the negative control membranes, wherein the primary antiserum was pre-absorbed with the antigen peptide.

**Fig. 3** shows the results of immunofluorescence staining for *AMHR2* in the ampulla, isthmus, CAR, and ICAR areas. Robust, high-intensity fluorescent signals of *AMHR2* localized in the tunica mucosa of ampulla (**Fig. 3.3A**) and isthmus (**Fig. 3.3B**). Strong *AMHR2* signals were also localized in the luminal epithelium of endometrial glands (**Fig.**

3.3C, 3.3D), and the epithelium of endometrium glands (Fig. 3.3E, 3.3F). In addition, the uterine stroma contained showed the AMHR2 signals (Fig. 3.3 C, 3.3D).

### **3.3.2. Oviductal and endometrial AMHR2 expression at different stages of the oestrous cycle**

RT-qPCR and western blotting revealed no significant differences in *AMHR2* mRNA (Fig. 3.4) or AMHR2 protein (Fig. 3.5) expression levels among various estrous phases in the ampulla, isthmus, CAR, and ICAR areas.

### **3.3.2. Comparison of AMHR2 expression among breeds and ages**

RT-qPCR and western blotting revealed no significant differences in *AMHR2* mRNA (Fig. 3.6) of AMHR2 protein (Fig. 3.7) expression levels in the ampulla, isthmus, CAR, and ICAR areas among old Holsteins and young and old JB's cows.

**(A) RT-PCR with cDNAs**

**(B) RT-PCR with NTC, or NRCs**

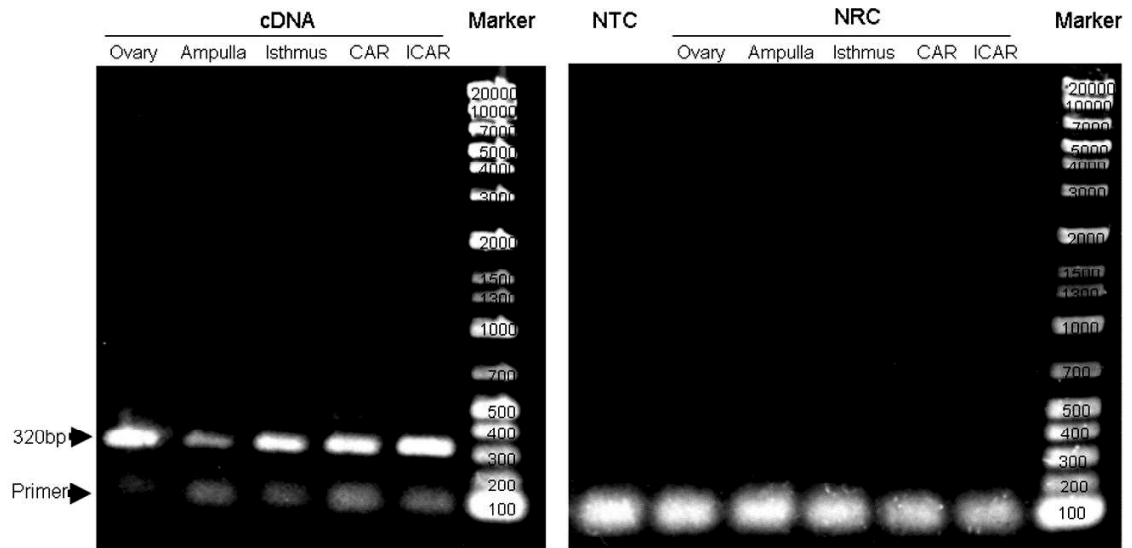
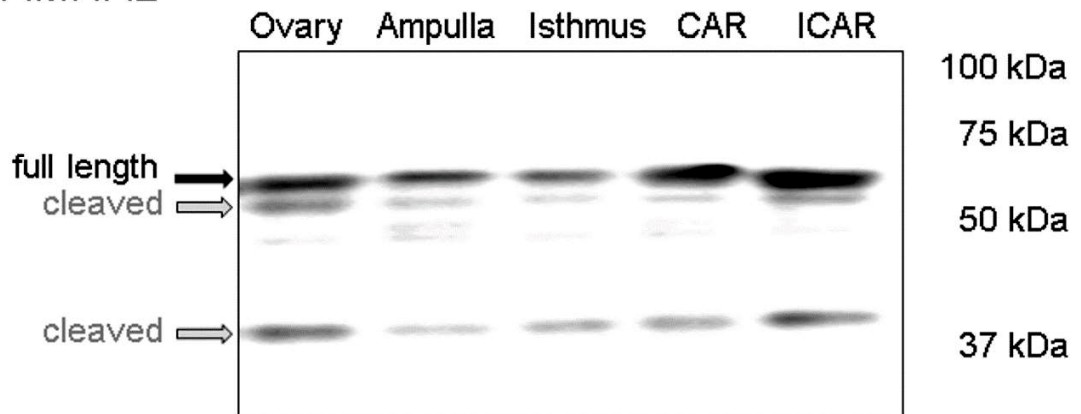


**Fig. 3.1.** Expression of *AMHR2* mRNA, as detected by RT-PCR analysis (A) with cDNAs and (B) with NTC or NRCs. The electropherogram shows the expected size (320 bp) of PCR products of bovine *AMHR2* in the ovary, ampulla, isthmus, and CAR and ICAR areas of the endometrium in healthy post-pubertal heifers (A) but not in the NTC or NRCs in the ovary, ampulla, isthmus, CAR, and ICAR areas (B).

(A) AMHR2



(B)  $\beta$ -actin



**Fig. 3.2.** Western blotting analysis of extracts from the ovary, ampulla, isthmus, CAR and ICAR areas in healthy post-pubertal heifers using (A) an anti-AMHR2 antibody or (B) an anti- $\beta$ -actin mouse antibody.

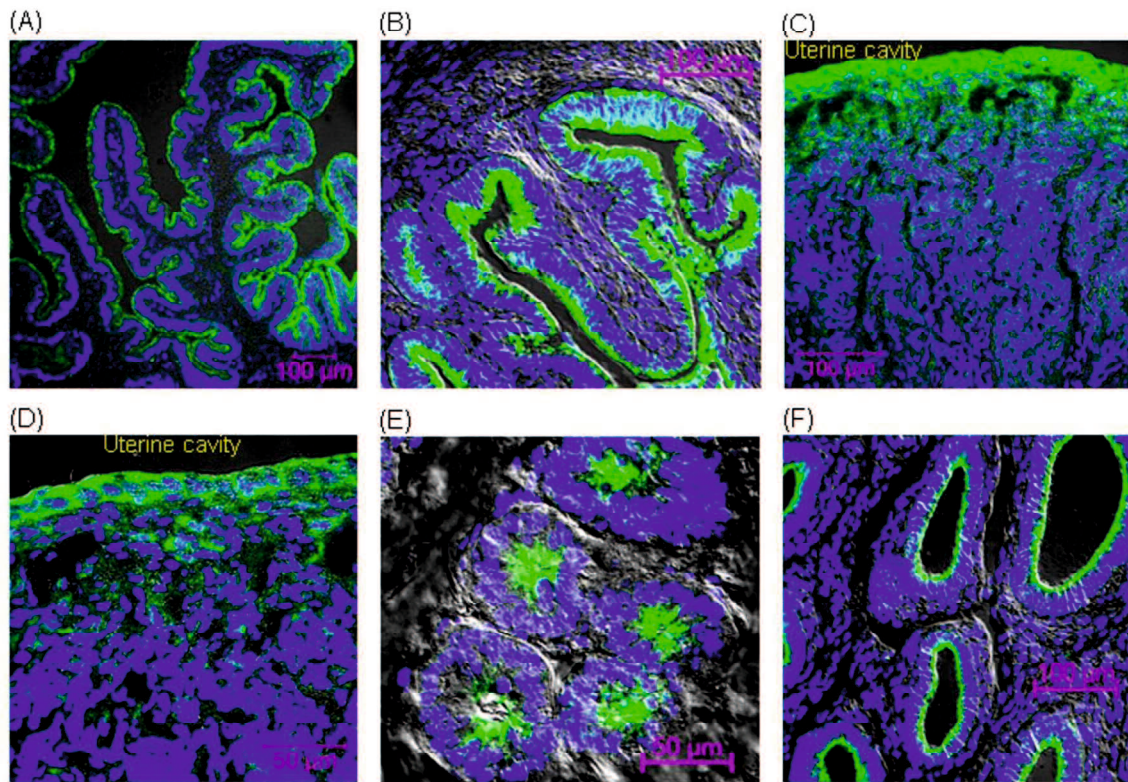


**Fig. 3.3.** AMHR2 expression in (A) ampulla and (B) isthmus samples collected on Day 3 of the oestrous cycle, (C, D) CAR samples collected on Day 15 (low and high magnification respectively) and (E and F) ICAR samples collected at Days 3 (E) and 21 (F) from healthy post-pubertal heifers. Nuclei were counterstained with counterstained with DAPI. Differential interference contrast microscopy was used.

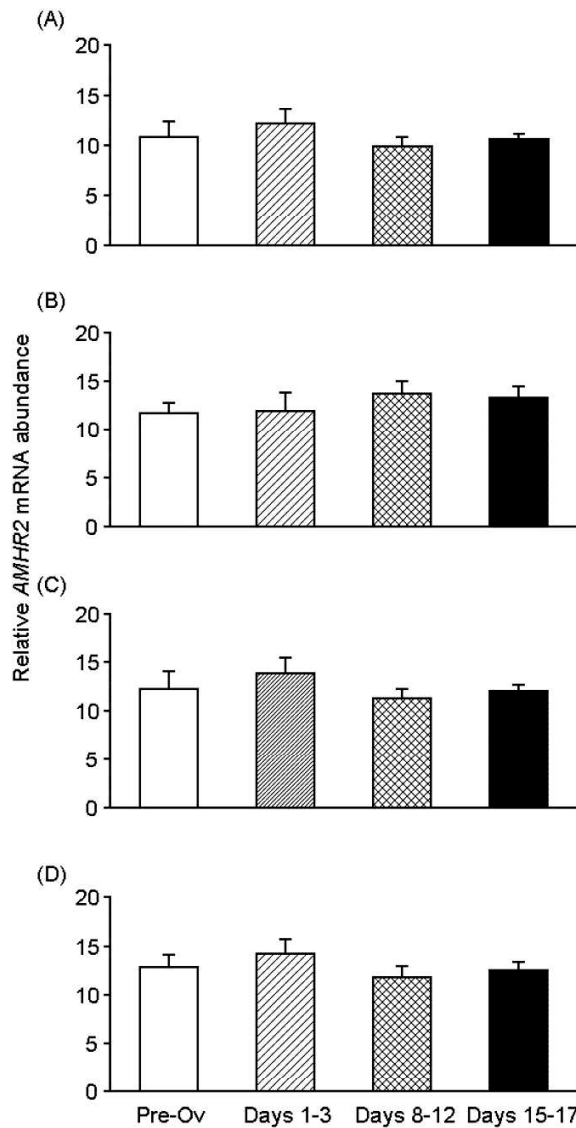


**Fig. 3.4.** Relative *AMHR2* mRNA abundance in the in the (A) ampulla, (B) isthmus, (C) CAR and (D) ICAR areas in healthy post-pubertal heifers during the pre-ovulatory phase (pre-Ov; Days 19 to 21) and on Days 1-3, 8-12, and 5 to 17 of the oestrous cycle, as determined by RT-qPCR. Data were normalized against the geometric means of *C2orf29* and *SUZ12* abundance. Data are the mean  $\pm$  SEM. There were no significant differences ( $P > 0.05$ ) in *AMHR2* abundance across phases of the oestrous cycle.

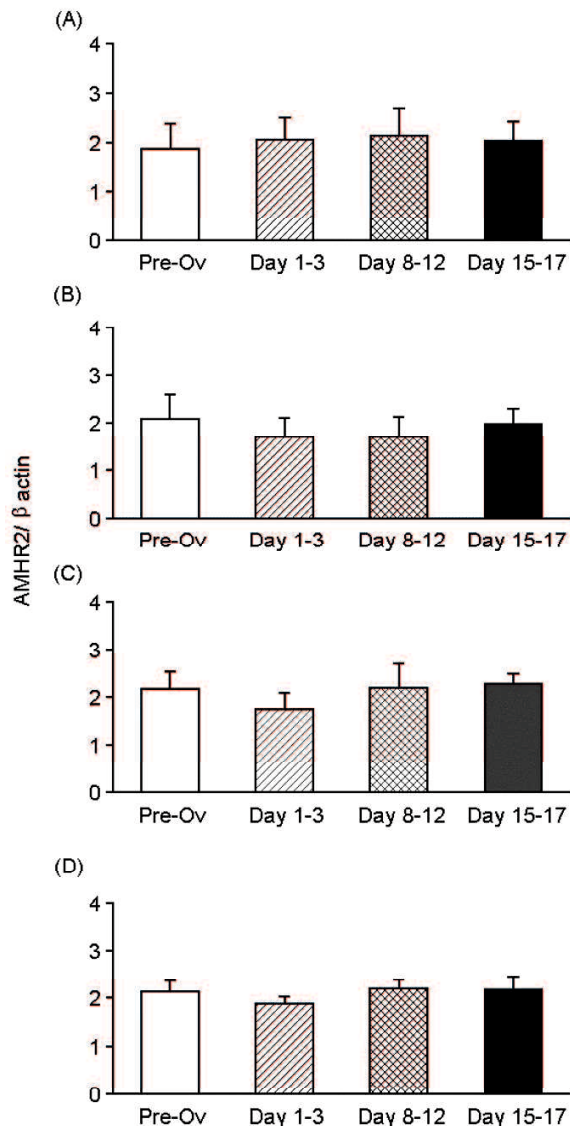


**Fig. 3.5.** Relative AMHR2 protein expression, normalized against  $\beta$ -actin, in the (A) ampulla, (B) isthmus, (C) CAR and (D) ICAR areas in healthy post-pubertal heifers during pre-ovulatory phase (pre-Ov; Days 19 to 21) and on Days 1-3, 8-12, and 5 to 17 of the oestrous cycle, as determined by western blotting. There were no significant differences ( $P > 0.05$ ) in AMHR2 expression across phases of the oestrous cycle.

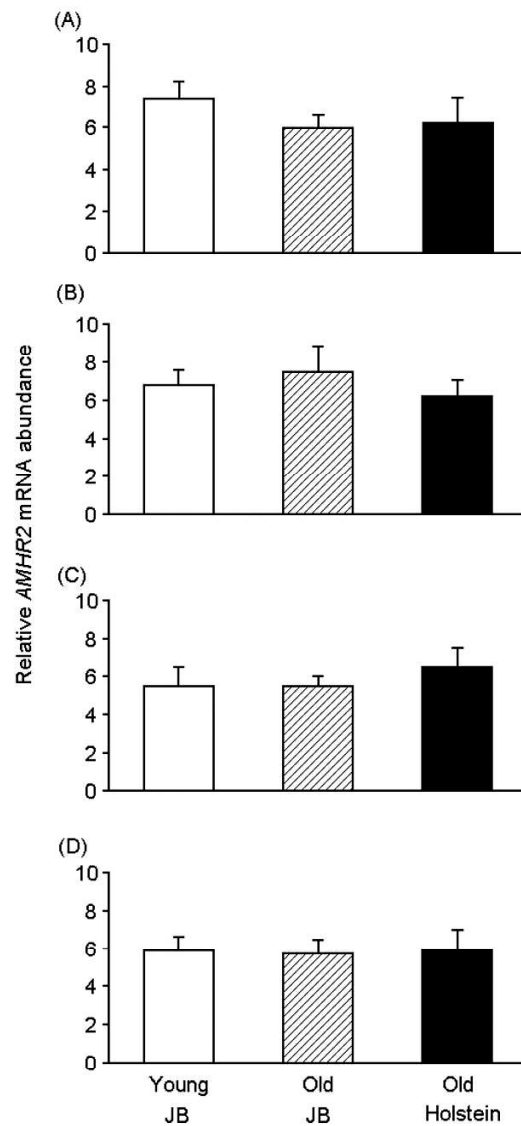


**Fig. 3.6.** Relative *AMHR2* mRNA abundance in the (A) ampulla, (B) isthmus, (C) CAR and (D) ICAR areas in healthy young adult JB heifers, old JB cows and old Holsteins cows, as determined via RT-qPCR. Data were normalized against the geometric means of *C2orf29* and *SUZ12* abundance. Data are the mean  $\pm$  SEM. There were no significant differences ( $P > 0.05$ ) in *AMHR2* abundance among groups.

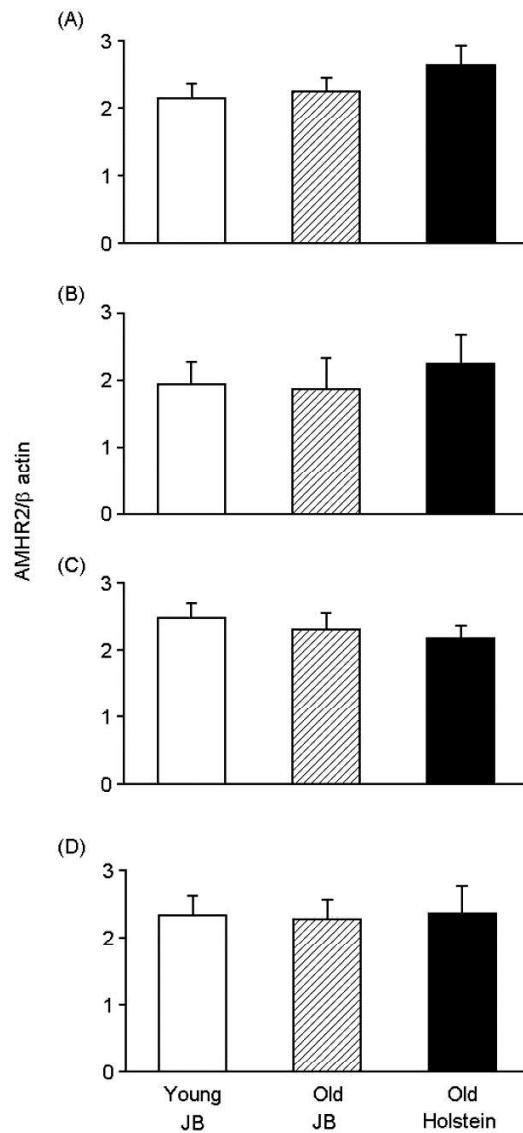


**Fig. 3.7.** Relative AMHR2 protein expression, normalized against  $\beta$ -actin, in the (A) ampulla, (B) isthmus, (C) CAR and (D) ICAR areas in healthy young JB heifers, old JB cows, and old Holsteins cows, as determined via western blotting. Data are the mean  $\pm$  SEM. There were no significant differences ( $P > 0.05$ ) in AMHR2 expression among groups.

### 3.4. Discussion

To the best of our knowledge, the present study is the first to report AMHR2 expression in the oviducts among all species. Immunofluorescence analysis using anti-bovine AMHR2 antibody revealed robust high-intensity signals in the tunica mucosa of ampulla and isthmus and in the glandular and luminal epithelium of endometria, leading to the speculation regarding the potential roles of AMHR2 in these layers.

AMH contributes to regression of the Müllerian duct to prevent the development of the oviducts and uterus in male fetuses (Rey *et al.* 2003), thereby potentially clarifying why the role of AMH in the oviduct has not been studied. Recently, after completion of the present series of experiments, Kim *et al.* (2019) reported AMHR2 expression in healthy human endometrial tissues. Although Kim *et al.* (2019) did not study fluctuations in endometrial AMHR2 expression during the menstrual cycle, no significant differences were reported between proliferative and secretory endometria. Furthermore, in the present study, no significant difference in AMHR2 expression was reported in the ampulla, isthmus, CAR, and ICAR areas among different stages of the oestrous cycle in heifers. In addition, previous studies have not reported considerable changes in circulating AMH concentrations during the oestrous cycle in ruminants *in vivo*, including JB (El-Sheikh Ali *et al.* 2013; Pfeiffer *et al.* 2014; Koizumi and Kadokawa 2017). Therefore, constitutively expressed AMHR2 in the tunica mucosa of the ampulla and isthmus and in the glandular and luminal epithelium of the endometrium may not play a temporal role, e.g., during sperm capacitation and fertilization (Croxatto 2002; Hunter 2005). These layers in the oviducts and endometria provide growth factors and nutrients for embryogenesis in various animals, including cattle (Hugentobler *et al.* 2010; Besenfelder *et al.* 2012). Women with low blood AMH concentrations are at an increased risk of miscarriage (Tarasconi *et al.* 2017; Lyttle *et al.*

2018). Therefore, further studies are required to clarify whether AMHR2 in these tissue layers play critical roles in embryo development and conception.

Endometria and oviducts are subject to pathogens present in the spermatozoa and seminal plasma (Kelly *et al.* 1997; Quayle 2002), and pathogens and endotoxins penetrate the uterus via the cervix (Herath *et al.* 2007; Tang *et al.* 2013). Circulating AMH concentrations are significantly lower in women with lymphoma than in healthy women and have been highly correlated with some cytokines, suggesting potential associations with the cytokine network (Paradisi *et al.* 2016). Therefore, further studies are required to clarify whether AMHR2 in the tunica mucosa of ampulla and isthmus and the glandular and luminal epithelium of the endometrium plays important roles in the immune system.

Fertility is decreased with old age in beef cows (Osoro and Wright 1992). In the present study, no significant difference was observed in AMHR2 expression in the oviducts and endometria among old Holsteins and young and old JB cows. However, blood AMH concentrations are influenced by age in cows (Koizumi and Kadokawa 2017); old JB cows have significantly higher blood AMH concentrations (100 pg/ml) than young cows (1–10 pg/ml) throughout the postpartum period (Koizumi and Kadokawa 2017). Therefore, the AMHR2 in oviducts and endometria in old JB cows may contribute to infertility among old cows. The association of age with oviductal and endometrial AMHR2 expression has not been reported previously in any species; hence, the present results cannot be compared with previous results. The present results regarding the effects of breed and age on AMHR2 expression should be interpreted with caution because we could not obtain specimens from young Holsteins. Therefore, further studies are required to clarify whether AMHR2 in oviducts and endometria has an important role in infertility in old cows.

Herein, multiple protein bands were observed for AMHR2 upon western blotting, in agreement with previous reports on various animals, including bovine (Faure *et al.* 1996; Hirschhorn *et al.* 2015; Kereilwe *et al.* 2018) showing that AMHR2 is present as a full-length and cleaved monomer (Faure *et al.* 1996; Hirschhorn *et al.* 2015) and because AMHR2 is glycosylated (Faure *et al.* 1996). In conclusion, AMHR2 is expressed in the oviducts and endometria of heifers and cows.

## **CHAPTER IV**

**(Study II)**

**AMH is expressed and secreted by bovine oviductal  
and endometrial epithelial cells**

## Abstract

In this Chapter, I investigated whether bovine oviducts and endometria produce AMH (for paracrine and autocrine signaling). RT-PCR and western blotting detected AMH expression in oviductal and endometrial specimens. Immunohistochemistry revealed robust AMH expression in the ampulla and isthmus epithelia, and the glandular and luminal endometrial epithelia (caruncular endometria). *AMH* mRNA and protein expression in these layers did not significantly differ among estrous phases in adult JB heifers ( $P > 0.1$ ). Furthermore, the expression in these layers also did not differ among old Holsteins cows ( $93.8 \pm 5.8$  months old), JB young heifers ( $25.5 \pm 0.4$  months old), and JB cows ( $97.9 \pm 7.9$  months old). We also compared AMH concentrations in the oviduct and uterine horn fluids among the three groups (measured by immunoassays). Interestingly, the AMH concentration in the oviduct fluid, but not in the uterine horn fluid of Holsteins cows, was lower than that those in JB heifers and cows' females ( $P < 0.05$ ). Therefore, bovine oviducts and endometria express AMH and likely secrete it into the oviduct and uterine fluids.

#### 4.1. Introduction

AMH is a member of the TGF- $\beta$  family. Preantral and small antral follicles secrete AMH in female animals (Bhide & Homburg, 2016). AMH expression is well-characterized in ovaries and plays important roles in regulating follicular development (Hernandez-Medrano *et al.* 2012) and inhibiting follicular atresia (Sefrioui *et al.* 2019). Concentrations of circulating AMH can help to predict the number of high-quality embryos produced by various mammals, including cows and humans (Arouche *et al.* 2015; Sefrioui *et al.* 2019). High-quality embryos result from synchronous regulation by the sperm, ovum, oviduct, and endometrium. Further, plasma AMH concentrations are positively correlated with pregnancy rates in various animals, including humans and cows (Josso, 2019; Ribeiro *et al.* 2014).

Accordingly, women with low blood AMH concentrations have an increased risk of miscarriage (Lyttle *et al.* 2018; Tarasconi *et al.* 2017). Moreover, mares with delayed uterine clearance have significantly lower blood AMH concentrations than those without delayed uterine clearance (Gharagozlou *et al.* 2013). Therefore, AMH might play vital roles in the oviduct and endometrium. AMH can act at the extragonadal level by activating its primary receptor, AMHR2, in the gonadotrophs of anterior pituitaries of rats and bovines (Garrel *et al.* 2016; Kereilwe & Kadokawa, 2019). We have previously shown that bovine gonadotrophs express AMH, which likely acts in paracrine and autocrine manner (Kereilwe *et al.* 2018). Endometrial tissues of healthy women also express AMHR2 (Kim *et al.*, 2019). We recently discovered that AMHR2 is expressed in parts of the bovine oviducts and uterus that are important for fertility and embryogenesis, namely, the epithelium of the tunica mucosa of the ampulla and isthmus, the epithelium of uterine glands, and the luminal epithelium of the endometrium (Ferdousy *et al.* 2020). Therefore, these tissues might express AMH for different paracrine and autocrine roles.

Old age is associated with decreased fertility in cows and humans (Osoro & Wright, 1992; Scheffer *et al.* 2018); however, the exact mechanisms underlying this association remains unclear. Several studies in humans have linked aging to plasma AMH concentrations. Blood AMH concentrations are highest in pubertal girls and gradually decrease starting at age 25 until they are undetectable after menopause (Dewailly *et al.* 2014), suggesting that low AMH is a marker of ovarian aging (Bhide & Homburg, 2016). Studies on the relationship between age and plasma AMH concentrations in adult female ruminants are not common, but one study showed that old JB cows have higher blood AMH concentrations than post-pubertal heifers and young cows (Koizumi & Kadokawa, 2017). Therefore, age might be a determinant of AMH expression levels in the oviducts and endometria, although there could be species-specific differences as well.

Therefore, in this study, we evaluated the association between oviductal and endometrial AMH expression and various physiological factors, such as the stage of the estrous cycle, age, and breed. We also compared AMH concentrations in the oviduct and uterine horn fluids collected from old Holsteins cows and JB heifers and cows.

## **4.2. Materials and methods**

### **4.2.1. Sample collection**

All experiments were performed according to the Guiding Principles for the Care and Use of Experimental Animals in the Field of Physiological Sciences (Physiological Society of Japan) and approved by the Committee on Animal Experiments of Yamaguchi University.

### **4.2.2. AMH expression in oviduct and endometrium**

Experiment was conducted to evaluate whether AMH was expressed in the oviduct and endometrium in heifers utilizing RT-PCR, western blotting, and immunofluorescence staining. We obtained the ipsilateral side of the ampulla, isthmus, caruncular, and intercaruncular area of endometria from four post-pubertal (26 months of age) JB heifers at a local abattoir. The four heifers were at days 2 to 3, 8 to 12, 15 to 17, and 19 to 21 (day 0 = day of estrous), as determined via macroscopic examination of the ovaries and uterus (Miyamoto *et al.* 2000). The ampulla, isthmus, caruncle, and intercaruncle samples collected were from the side ipsilateral to ovulation in the three heifers from days 2 to 3, 8 to 12, or 15 to 17 but were from the side ipsilateral to the dominant follicle in the remaining heifer at day 19 to 21. We collected ampullar samples from areas at least 3 cm from the fimbriated infundibulum, from the ampullary–isthmic junction, and the isthmus samples from areas also at least 3 cm from the ampullary–isthmic junction, and the utero-tubal junction. Half of the ampulla and half of the isthmus were frozen in liquid nitrogen and preserved at  $-80^{\circ}\text{C}$  until RNA or protein extraction. The remaining halves of the ampulla and isthmus were stored in 4% paraformaldehyde at  $4^{\circ}\text{C}$  for 16 hr for immunohistochemistry. The middle area of the uterine horn was opened longitudinally using scissors, and caruncle tissues were carefully dissected so as not to include the intercaruncle; then, intercaruncle areas were excised. The

collected caruncle and intercaruncle samples were frozen in liquid nitrogen and preserved at  $-80\text{ }^{\circ}\text{C}$  until RNA or protein extraction or stored in 4% PFA at  $4\text{ }^{\circ}\text{C}$  for 16 hr for immunohistochemistry. Granulosa cells in preantral and small antral follicles express AMH (Campbell *et al.* 2012; Kereilwe *et al.* 2018). Therefore, we also collected ovarian tissue samples from the same heifers to use as a positive control of AMH expression for RT-PCR and western blotting assays.

#### **4.2.3 Oviductal and endometrial AMH expression at different stages of the oestrous cycle**

Experiment was conducted to compare AMH expression in oviductal and endometrial samples among different stages of the estrous cycle utilizing quantitative RT-PCR and western blotting described subsequently. The ampulla, isthmus, caruncle, and intercaruncle tissues were harvested from adult (26-month-old) non-pregnant JB heifers in the pre-ovulatory phase (day 19 to 21;  $n = 5$ ), day 1 to 3 ( $n = 5$ ), day 8 to 12 ( $n = 5$ ), or day 15 to 17 ( $n = 5$ ), as determined via macroscopic examination of the ovaries and uterus (Miyamoto *et al.* 2000). Samples were obtained at the local abattoir and immediately frozen in liquid nitrogen and preserved at  $-80\text{ }^{\circ}\text{C}$  until RNA or protein extraction.

#### **4.2.4. Comparison of AMH expression among breeds and ages**

Experiment was conducted to compare AMH expression in oviductal and endometrial samples based on age or breed utilizing the quantitative RT-PCR and western blotting described subsequently. The ampulla, isthmus, caruncle, and intercaruncle tissues were harvested during the luteal phase (day 8 to 12) from post-pubertal JB heifers ( $25.5 \pm 0.4$  months of age;  $n = 6$ ), JB cows ( $97.9 \pm 7.9$  months of age;  $n = 6$ ), and Holstein cows ( $93.8$

$\pm 5.8$  months of age;  $n = 6$ ) from the local abattoir. We compared these three groups due to the following reasons. First, it was impossible to obtain samples from post-pubertal Holstein heifers since they were kept in dairy farms for milking purposes. Second, in our previous study (Kereilwe *et al.* 2018), we compared expression levels of AMH in gonadotrophs between Holsteins cows (approximately 80 months of age), and young JB heifers (approximately 26 months of age) and cows (approximately 90 months of age), finding significant differences in *AMH* mRNA and AMH protein among them. Third, we previously observed a significant difference in blood AMH concentrations between JB cows (approximately 81 months of age) and JB heifers (approximately 22 months of age) (Koizumi & Kadokawa, 2017). The collected samples were frozen in liquid nitrogen and preserved at  $-80$  °C until RNA or protein extraction. All heifers and cows in the three groups were non-lactating and non-pregnant, with no follicular cysts, luteal cysts, or other ovarian or uterine disorders upon macroscopic ovarian examination (Kamomae, 2012). The Holstein cows were slaughtered because they had not become pregnant after at least five artificial insemination attempts.

#### **4.2.5. Analyze AMH concentration in the oviduct and uterine horn fluid**

Experiment was conducted to analyze AMH concentrations in the oviduct and uterine horn fluids using an AMH enzyme immunoassay. We collected oviduct fluids on day 1 to 3, that is when oocytes are in oviduct (El-Banna & Hafez, 1970), and uterine horn fluids on day 8 to 14 in order to compare AMH concentrations among groups of JB heifers ( $26.2 \pm 0.7$  months of age;  $n = 6$ ), JB cows ( $111.0 \pm 12.2$  months of age;  $n = 6$ ), and Holstein cows ( $91.9 \pm 6.4$  months of age;  $n = 6$ ). The females were killed at the slaughterhouse; the ipsilateral sides of oviducts to ovulation were closed at the uterine end and then cut to

separate the uterine end from the utero-tubal junction. The oviducts were then separated from the surrounding connective tissue. A blunt 20-gauge needle was inserted from the infundibulum side of the oviducts and used to gently flush the oviducts with 0.01 M phosphate-buffered 0.14 M saline (pH 7.3) (PBS; 2mL/oviduct). The resultant oviductal fluids were collected from the opposite sides of the oviducts and pooled into 2-mL microtubes. For the collection of uterine fluids, a blunt 20-gauge needle was inserted into the tip of a cut uterine horn in which the uterine-body side had been closed by artery forceps. After gently flushing with PBS (10mL/horn), the resultant fluids were collected from the tip of the cut uterine horn and pooled into 50-mL tubes. Tubes were centrifuged at  $800 \times g$  for 20 min at 4° C, and the supernatants were stored at -35° C until analyzed for AMH.

#### **4.2.6. RT-PCR, sequencing of amplified products, and homology search in gene databases**

We utilized the same RT-PCR and sequencing methods as reported previously (Kereilwe *et al.* 2018) to determine the expression of *AMH* mRNA in the ovary, ampulla, isthmus, caruncle, or intercaruncle from the four heifers for experiment 1. Briefly, total RNA was extracted from the samples using RNeasy RT Reagent (Molecular Research Center Inc.) according to the manufacturer's protocol. The extracted RNA samples were treated with ribonuclease-free deoxyribonuclease (Thermo Fisher Scientific) to eliminate possible genomic DNA contamination. The concentration and purity of each RNA sample were evaluated to ensure that the A260/A280 nm ratios were in the acceptable range of 1.8–2.1. The mRNA quality of all samples was verified by electrophoresis of total RNA followed by staining with ethidium bromide, and confirming that the 28S:18S ratios were 2:1. The cDNA was synthesized from 1 µg of the total RNA per sample using Superscript IV VILO Master

Mix (Thermo Fisher Scientific) according to the manufacturer's protocol. NRCs were prepared for RT-PCR; they were generated by treating the extracted RNA with the same deoxyribonuclease but not with cDNA synthetase. PCR was conducted using the previously reported primers (Kereilwe *et al.* 2018): nucleotides 1486–1813, forward primer: 5'-GCTCATCCCCGAGACATAACC- 3'; reverse primer: 5'-TTCCCGTGTTTAATGGGGCA-3'). Primers were designed by the Primer3 algorithm (<https://www.ncbi.nlm.nih.gov/tools/primer-blast/>) based on a reference sequence of bovine *AMH* NCBI reference sequence of bovine *AMH* is NM\_173890. The expected PCR-product size of *AMH* using the primer pair is 328 bp. Using a Veriti 96-Well Thermal Cycler (Thermo Fisher Scientific), PCR was performed using 20 ng of cDNA, 20 ng RNA as the NRC or water as the NTC, and polymerase (Tks Gflex DNA Polymerase) under the following thermocycling conditions: 94 °C for 1 min for pre-denaturation followed by 35 cycles of 94 °C for 60 sec, 60 °C for 15 sec, and 68 °C for 30 sec. PCR products were separated on 1.5% agarose gels by electrophoresis along with a molecular marker [Gene Ladder 100 (0.1–2 kbp), Nippon Gene], stained with fluorescent stain (Gelstar, Lonza), and observed using a CCD imaging system (GelDoc; Bio-Rad). The PCR products were purified with the NucleoSpin Extract II kit (Takara Bio Inc.) and subsequently, sequenced with a sequencer (ABI3130, Thermo Fisher Scientific) using one of the PCR primers and the Dye Terminator v3.1 Cycle Sequencing Kit (Thermo Fisher Scientific). The sequences obtained were used as query terms to search the homology sequence in the DNA Data Bank of NCBI using the BLAST optimized for highly similar sequences (available on the NCBI website).

#### 4.2.7. Anti-AMH antibody used in this study

We utilized the same anti-human AMH rabbit polyclonal antibody (ARP54312; Aviva Systems Biology) that we previously verified with bovine ovaries (Kereilwe *et al.* 2018) to determine the expression of AMH in the bovine samples by western blotting and immunohistochemistry. Human AMH is secreted as a homodimeric precursor consisting of two identical monomers (560 amino acids; NCBI accession number AAA98805.1) (Mamsen *et al.* 2015). Each monomer consists of two domains, specifically (i) a mature C-terminal region, which becomes bioactive after proteolytic cleavage and binds AMHR2, and (ii) a pro-region, which is important for AMH synthesis and extracellular transport. The human AMH precursor is cleaved at amino acid 451 (arginine) between the two domains. The pro-region has another cleavage site at amino acid 229 (arginine), causing three potential cleavage products, namely pro-mid-mature, mid-mature, and mature (Mamsen *et al.* 2015). The bovine AMH precursor monomer (575 amino acids; NCBI accession number NP\_776315.1) has a 91% sequence homology to the human protein. The bovine AMH precursor contains an arginine cleavage site between the two domains at amino acid 466 but not at the residue corresponding to amino acid 229. The rabbit polyclonal anti-AMH antibody recognizes the mature C-terminal form of human AMH (corresponding to amino acids 468–517; SVDLRAERSVLIPETYQANNCQGVCGWPQSDRNPRYGNHVLLKMQARG). This sequence has 98% homology to amino acids 483–532 of the mature C-terminal form of bovine AMH but no homology to other bovine proteins, as determined based on protein BLAST.

#### 4.2.8. Western blotting for AMH detection

Western blotting was performed as described previously (Kereilwe *et al.* 2018). Briefly, proteins were extracted from the ampulla, isthmus, and caruncle, or intercaruncle, or ovary samples (used as positive controls) from the four heifers used in experiment 1. The extracted protein sample (33.4  $\mu$ g of total protein in 37.5  $\mu$ l) was mixed in 12.5  $\mu$ l of 4x Laemmli sample buffer (Bio-Rad) containing 10% (v/v)  $\beta$ -mercaptoethanol, and then boiled for 3 min at 100 °C. The boiled protein samples were quickly cooled on ice. Then, 12  $\mu$ l of boiled protein samples (8  $\mu$ g of total protein) was loaded onto a sodium dodecyl sulfate-polyacrylamide polyacrylamide gel (Any KD Criterion TGX precast gel; 567-1125; Bio-Rad) along with a molecular weight marker (Precision Plus Protein All Blue Standards; Bio-Rad) and resolved by electrophoresis at 100 V for 90 min. Proteins were then transferred to PVDF membranes. Blocking was performed with 5% non-fat dry milk containing 0.1% tween 20 for 1 hr at 25 °C; subsequently, immunoblotting was performed with the anti-AMH rabbit antibody (1:25,000 dilution) overnight at 4 °C. After washing the membrane with 10 mM tris-HCl (pH 7.6) containing 150 mM NaCl and 0.1% tween 20, the PVDF membrane was incubated with HRP-conjugated anti-rabbit IgG goat antibody (Bethyl Laboratories, Inc., 1:50,000 dilution) for 1 hr at 25 °C. Protein bands were visualized using an ECL-Prime chemiluminescence kit (GE Healthcare) and CCD imaging system (Fujifilm). We defined bovine AMH bands based on band size as the AMH precursor or the mature form (four sizes) according to previous studies (Mamsen *et al.* 2015; Kereilwe *et al.* 2018). Antibodies were removed from the PVDF membrane with a stripping solution (Nacalai Tesque Inc.); then, the membrane was used for immunoblotting with the anti- $\beta$ -actin mouse monoclonal antibody (A2228, 1:50,000 dilution; Sigma-Aldrich).

Western blotting was also conducted to compare AMH protein expression levels in the ampulla, isthmus, caruncle, and intercaruncle among different estrous phases or the groups of JB heifers, JB cows, and Holstein cows groups from experiment 2 or 3. Briefly, boiled samples (8  $\mu$ g total protein of each sample) were loaded on a polyacrylamide gel along with the molecular weight marker and four standard samples (2, 4, 8, and 16  $\mu$ g total protein for each of five randomly selected samples diluted with protein extraction reagent). MultiGauge v.3.0 software (Fujifilm) was used to quantify the signal intensity of the protein bands. The intensities of bands representing AMH (as the mature C-terminal form) for 16, 8, 4, and 2  $\mu$ g protein samples were set as 100%, 50%, 25%, and 12.5%, respectively, and the intensity of other samples was calculated as a percentage of these standards using MultiGauge software. After antibodies were removed from the PVDF membrane with a stripping solution, the membrane was used for immunoblotting with the anti- $\beta$ -actin mouse monoclonal antibody. The intensities of the  $\beta$ -actin band for 16, 8, 4, and 2  $\mu$ g protein samples were set as 100%, 50%, 25%, and 12.5%, respectively, and the intensity of other samples was calculated as a percentage of these standards using MultiGauge software. The AMH expression level was normalized to that of  $\beta$ -actin in each sample.

#### **4.2.9. Fluorescent immunohistochemistry and confocal microscopy**

We utilized the same method of immunohistochemistry to detect ovarian AMH and AMHR2 as reported previously (Kereilwe *et al.* 2018; Kereilwe & Kadokawa, 2019) for experiment 1. Briefly, the fixed tissue blocks were placed in 30% sucrose PBS until the blocks were infiltrated with sucrose. The blocks were then frozen in an embedding medium (Tissue-Tek OCT compound; Sakura Finetechnical Co. Ltd) and maintained at  $-80^{\circ}\text{C}$ . Next, the blocks were sectioned into 15- $\mu$ m-thick cross-sections using a cryostat (Leica

Microsystems Pty Ltd) and mounted on microscope slides (MAS coat Super frost; Matsunami-Glass). The sections were treated with 0.3 % triton X-100-PBS for 15 min and blocked by incubating them with 0.5 mL of PBS containing 10% normal goat serum (Wako Pure Chemicals) for 1 hr at room temperature. The slides were incubated with a cocktail of primary antibodies containing the anti-AMH (Kereilwe *et al.* 2018), anti-AMHR2 (Kereilwe & Kadokawa, 2019), anti-cytokeratin antibodies (Sigma-Aldrich) (all diluted as 1:1,000) for 12 hr at 4 °C. After the primary antibody incubation, the sections were washed twice with PBS and then incubated with a cocktail of fluorochrome-conjugated secondary antibodies (Alexa Fluor 488 goat anti-chicken IgG, Alexa Fluor 546 goat anti-mouse IgG, and Alexa Fluor 647 goat anti-rabbit IgG [all from Thermo Fisher Scientific and diluted to 1 µg/mL]) and DAPI (Wako Pure Chemicals) for 4 hr at room temperature.

The stained sections on slides were observed by confocal microscopy (LSM710; Carl Zeiss) equipped with a diode laser 405 nm, argon laser 488 nm, and HeNe laser 533 nm. Images obtained by fluorescence microscopy were scanned with a 20×, 40×, 63× or 100× objective and recorded with a CCD camera system controlled by ZEN2012 black edition software (Carl Zeiss). The DAPI is shown in blue, and AMH is shown in green in the confocal images. To verify the specificity of the signals, we included several negative controls in which the primary antiserum had been omitted, or in which normal rabbit IgG, normal mouse IgG, and normal chicken IgG (all from Wako Pure Chemicals) were used instead of the primary antibody.

#### **4.2.10. RT-qPCR**

RT-qPCR was performed to compare *AMH* expression among estrous phases or the groups of JB heifers, JB cows, and Holstein cows' groups in experiment 2 or 3. The

preparation of high-quality total RNA and cDNA synthesis was performed as described herein. We utilized the same method of RT-qPCR and the same primers to measure *AMH* mRNA or two housekeeping genes, *C2orf29* and *SUZ12*. Table 4.1 lists the primer sequences for *AMH* and the two housekeeping genes.

Levels of gene expression were measured in duplicate by quantitative RT-qPCR analyses with 20 ng cDNA, using the CFX96 Real Time PCR System (Bio-Rad) and Power SYBR Green PCR Master Mix (Thermo Fisher Scientific), with a six-point relative standard curve, the NTC, and the NRC. Standard 10-fold dilutions of purified and amplified cDNA fragments were prepared. The cycle conditions for all genes were: 95 °C for 10 min for pre-denaturation; five cycles each of 95 °C for 15 sec and 66 °C for 30 sec; 40 cycles each of 95 °C for 15 sec, and 60 °C for 60 sec. Melting curve analyses were performed at 95 °C for each amplicon and each annealing temperature to ensure the absence of smaller non-specific products, such as dimers. To optimize the RT-qPCR assay, serial dilutions of a cDNA template were used to generate a standard curve by plotting the log of the starting quantity of the dilution factor against the C<sub>q</sub> value obtained during amplification of each dilution. Reactions with a coefficient of determination (R<sup>2</sup>) > 0.98 and efficiency between 95 and 105% were optimized. The coefficients of variation of RT-qPCR were less than 6%. The concentration of PCR products was calculated by comparing the C<sub>q</sub> values of unknown samples with the standard curve using software CFX managerV3.1 (Bio-Rad). The gene expression levels of *AMH* genes were normalized to the geometric mean of the expression levels of two housekeeping genes; thus, the *AMH* amount was divided by the geometric mean of *C2orf29* and *SUZ12* in each sample.

**Table 4.1.** Details of the primers used for RT-qPCRs

Gene name		Primer sequence 5'-3'	Position		Size (bp)
			Nucleotide	Exon	
<i>AMH</i>	forward	GGGTTAGCCCTTACCCTGC	683–701	3	121
	reverse	GTAACAGGGCTGGGGTCTTT	784–803	4	

#### **4.2.11. AMH immunoassay**

AMH concentrations in samples of the oviduct and uterine fluids were assessed by using a bovine AMH ELISA kit (Ansh Labs) using a protocol described previously (Akbarinejad *et al.* 2019). The pair of mouse monoclonal antibodies used has epitopes in the N-terminal or C-terminal of the mature C-terminal form of bovine AMH. The ELISA has no cross-reactivity with bovine LH, FSH, inhibins, and activins (personal communication with Dr. Ajay Kumar of Ansh Labs). The detection limit was 0.011 ng/mL, and the intra- and inter-assay coefficient of variation were 4.3% and 8.6%, respectively.

#### **4.2.12. Statistical analysis**

The statistical analyses were performed using Stat View version 5.0 for Windows (SAS Institute, Inc.). The Grubb's test was used to verify the absence of outliers. The Shapiro-Wilk test or the Lilliefors test were used to evaluate the normality or log-normality of each variable, respectively all variables were normally distributed. The F-test was used to verify the homogeneity of variance of all variables between estrous stages and ages. Using Grubb's test, we verified that there were no outliers for the variables. ANOVA and Fisher's PLSD test were used to evaluate differences in AMH mRNA or protein expression in either the ampulla, isthmus, caruncle, or intercaruncle collected from bovines at different estrous stages or different groups. ANOVA and Fisher's PLSD tests were also used to evaluate differences in the logarithm of AMH concentrations in the oviduct or uterine fluids collected from females at different estrous stages or different groups. The level of significance was set at  $P < 0.05$ . Data are expressed as mean  $\pm$  standard error of the mean (SEM).

### 4.3. Results

#### 4.3.1. AMH expression in oviduct and endometrium

An amplicon of 328 bp, indicating *AMH*, was obtained from samples of the ovary, ampulla, isthmus, caruncle, and intercaruncle and confirmed using agarose gel electrophoresis (**Fig. 4.1**). Neither the NTC nor NRC yielded any PCR-amplified products. A homology search against the gene databases for the sequenced amplified products revealed bovine *AMH* (NM\_173890.1) as the best match, with a query coverage of 100%, e-value of 0.0, and maximum alignment identity of 99%. No other bovine gene displayed homology with the PCR-product described, indicating that the amplified product was bovine *AMH*.

AMH expression in the ampulla, isthmus, caruncle, and intercaruncle, and in ovarian specimens used as positive controls was analyzed via western blotting (**Fig. 4.2**). Similar protein bands for AMH were observed among all the tissue samples (**Fig. 4.2A**). The ovary, isthmus, caruncle, and intercaruncle, however, showed multiple bands for full-length AMH, whereas the ampulla showed a single band for full-length AMH. The mature C-terminal form was found only in the ovary and intercaruncle but not in the ampulla, isthmus, and caruncle. No protein bands were observed on the blotting membranes used as negative controls, on which the primary antiserum had been pre-absorbed with an antigen peptide.  $\beta$ -actin was the loading control, as shown in Figure **4.2B**.

**Fig. 4.3** and **Fig. 4.4** show the results of immunofluorescence staining for cytokeratin, AMHR2, and AMH in the ampulla or isthmus samples. Immunohistochemistry revealed robust AMH expression in the epithelium of the tunica mucosa, shown as a cytokeratin-positive layer, of the ampulla (**Fig. 4.3A, 4.3C**) and isthmus (**Fig. 4.4A, 4.4C**), where AMH receptor type 2 was also expressed. Further, fibroblasts, which were cytokeratin-negative, too expressed AMH. **Fig. 4.5** and **Fig. 4.6** show the results of immunofluorescence staining

for cytokeratin, AMHR2, and AMH in the caruncle or intercaruncle samples. The strong AMH signals were localized to the luminal epithelium (**Fig. 4.5A, 4.5C**), the vasculature in the stroma (**Fig. 4.5A**), and the epithelium of endometrial glands (**Fig. 4.6A, 4.6C**). Negative control staining using the normal IgGs showed no immunostaining signal in these layers or cells (**Fig. 4.3B, 4.4B, 4.5B, 4.6B**).

**Fig. 4.3 and Fig. 4.4** show the results of immunofluorescence staining for cytokeratin, AMHR2, and AMH. Immunohistochemistry revealed robust AMH expression in the epithelium of the tunica mucosa, shown as a cytokeratin-positive layer, of the ampulla (**Fig. 4.3A**) and isthmus (**Fig. 4.3C**), where AMHR2 was also expressed. Further, fibroblasts, which were cytokeratin-negative, too expressed AMH. The strong AMH signals were localized to the luminal epithelium (**Fig. 4.5A**), the vasculature in the stroma (**Fig. 4.5A**), and the epithelium of endometrial glands (**Fig. 4.6C**). Negative control staining using the normal IgGs showed no immunostaining signal in these layers or cells (**Fig. 4.3B, 4.4B**).

#### **4.3.2. Oviductal and endometrial AMH expression at different stages of the oestrous cycle**

RT-qPCR and western blotting revealed no significant differences in *AMH* mRNA and protein expression among various estrous phases in the ampulla (**Fig. 4.7A, 4.7E**), isthmus (**Fig. 4.7B, 4.7F**), caruncle (**Fig. 4.7C, 4.7G**), and intercaruncle (**Fig. 4.7D, 4.7H**).

#### **4.3.3 Comparison of AMH expression among breeds and ages**

There were no significant differences in AMH mRNA and protein expression levels in the ampulla (**Fig. 4.8A, 4.8E**), isthmus (**Fig. 4.8B, 4.8F**), caruncle (**Fig. 4.8C, 4.8G**), and

intercaruncle (**Fig. 4.8D, 4.8H**) among the Holsteins cows and the JB heifers and cows' females.

#### **4.3.4 AMH concentration in the oviduct and uterine horn fluid**

AMH concentrations in the oviduct fluids on day 1 to 3 of old Holsteins cows were lower than those in the oviduct fluids of young and old JB heifers and cows' females ( $P < 0.05$ ; **Fig. 4.9A**). AMH concentrations in uterine horn fluid on day 8 to 14, did not differ among these three groups (**Fig. 4.9B**).

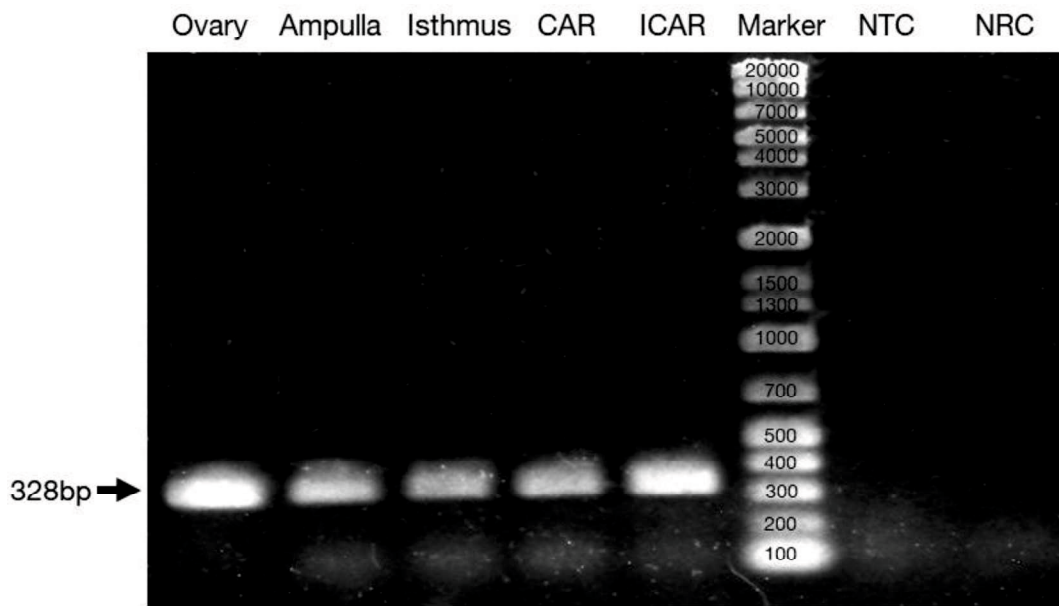
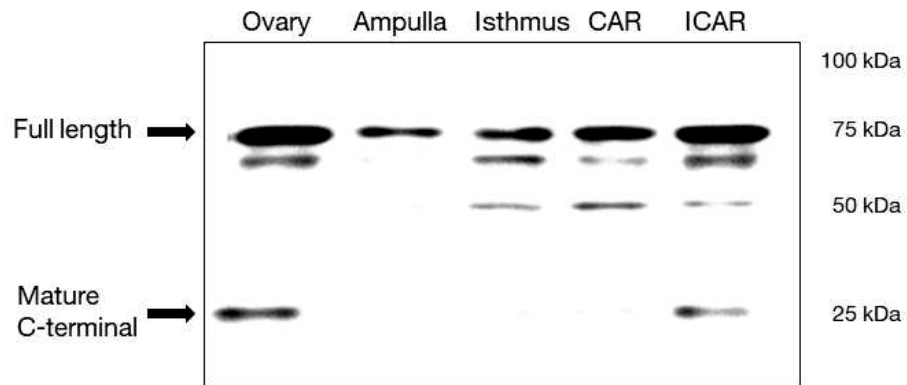


**Fig. 4.1.** Expression of *AMH* mRNA, detected by RT-PCR analysis. The electropherogram shows the expected size (328 bp) of PCR products of bovine *AMH* in the ovary, ampulla, isthmus, and CAR and ICAR areas of the endometrium in post-pubertal heifers; no amplicons were observed in the NTC and NRC conditions.

(A) AMH



(B)  $\beta$ -actin

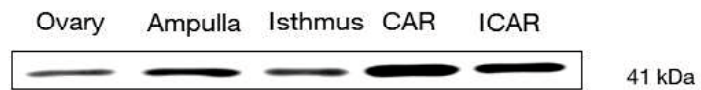


**Fig. 4.2.** Western blotting using an anti-AMH rabbit antibody on protein extracts of ovaries, ampulla, isthmus, and CAR and ICAR areas collected from post-pubertal heifers (A);  $\beta$ -actin was used as a loading control (B).

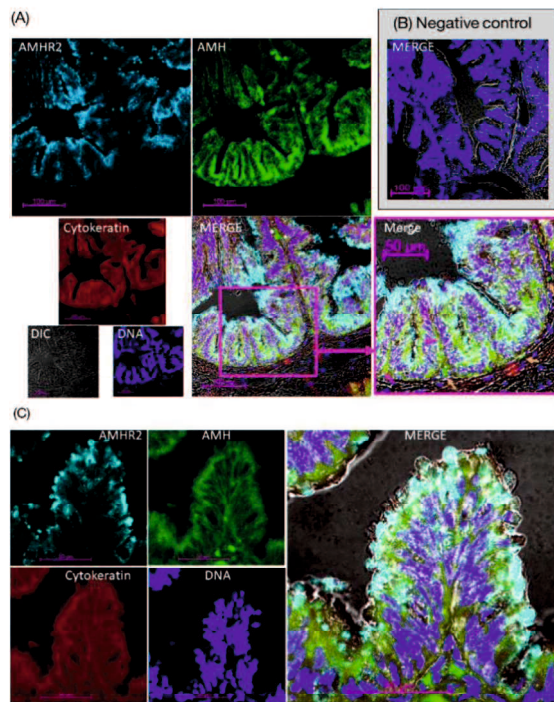


**Fig. 4.3.** Immunofluorescence staining of AMH in the ampulla samples of post-pubertal heifers. Specimens were collected on day 3 (day 0 = day of estrous). Images were captured via laser-scanning confocal microscopy and show AMHR2 (light blue), AMH (green), cytokeratin (red), and counter-staining with DAPI nuclear stain (dark blue), and differential interference contrast (DIC) microscopy (grayscale). The pink rectangle within the low magnification image indicates the position of the high magnification. In the merged photos, the pink arrows indicate the AMH signals in the luminal epithelium of mucosa. The brown arrows indicate signals in fibroblasts. Right panel (B) show negative controls staining using the normal animal IgGs. Scale bars represent 100  $\mu\text{m}$  in the low magnification. Scale bars represent 50  $\mu\text{m}$  in the enlarged merge of (A) and (C), and 100  $\mu\text{m}$  in other panels, which shown as pink rectangular.

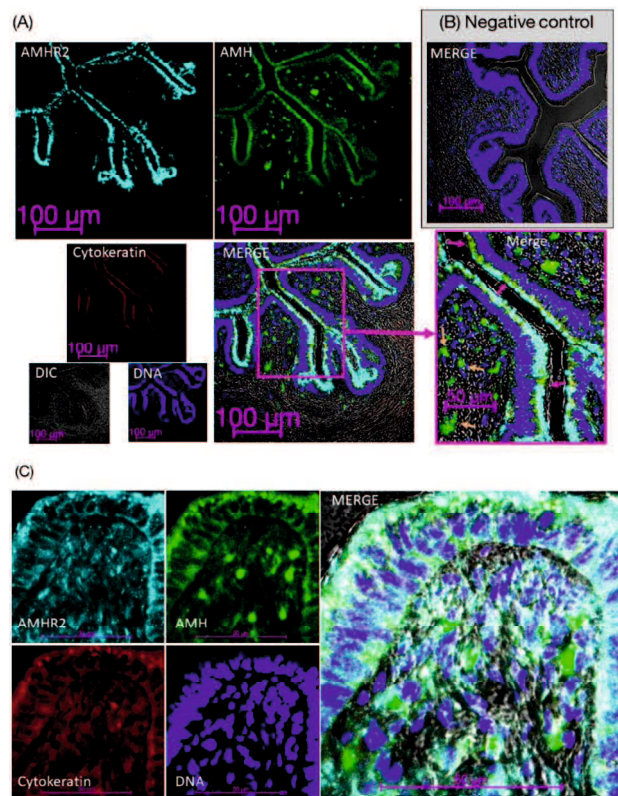


**Fig. 4.4.** Immunofluorescence staining of AMH in the isthmus samples of post-pubertal heifers. Specimens were collected on day 5 (day 0 = day of estrous). Images were captured via laser-scanning confocal microscopy and show AMHR2 (light blue), AMH (green), cytokeratin (red), and counter-staining with DAPI nuclear stain (dark blue), and DIC microscopy (grayscale). The pink rectangle within the low magnification image indicates the position of the high magnification. In the merged photos, the pink arrows indicate the position of the high magnification. In the merged photos, the pink arrows indicate the AMH signals in the luminal epithelium of mucosa. The brown arrows indicate signals in fibroblasts. Right panel (B) show negative controls staining using the normal animal IgGs. Scale bars represent 100 μm in the low magnification. Scale bars represent 50 μm in the enlarged merge of (A) and (C), and 100 μm in other panels.

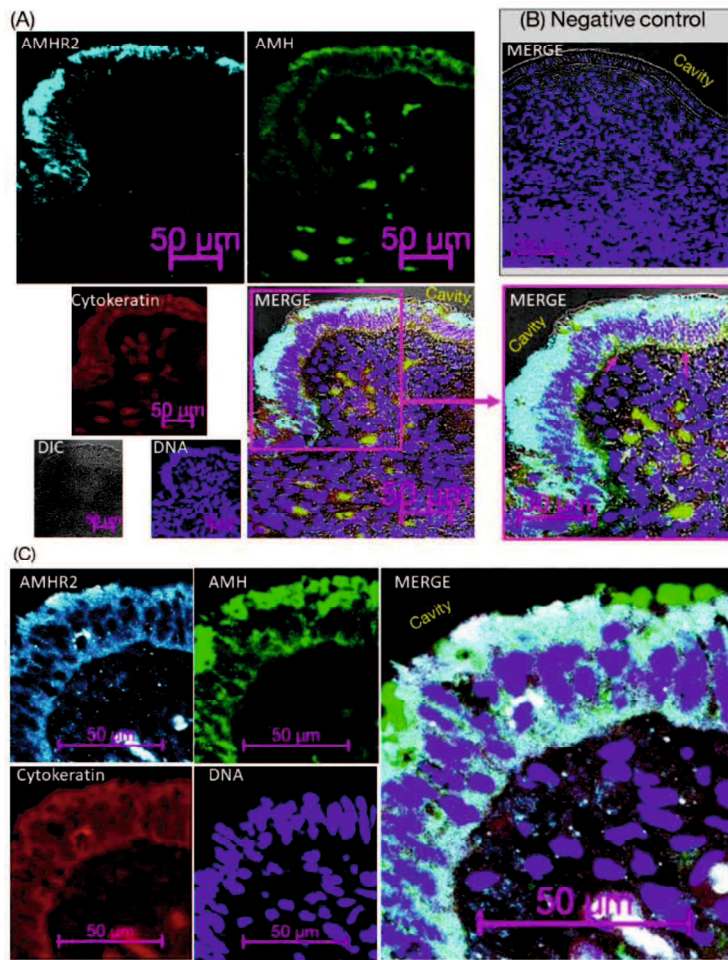


**Fig. 4.5.** Immunofluorescence staining of AMH in the caruncle samples of post-pubertal heifers. Specimens were collected on day 13. Images were captured via laser-scanning confocal microscopy and show AMHR2 (light blue), AMH (green), cytokeratin (red), and counter-staining with DAPI nuclear stain (dark blue), and DIC microscopy (grayscale). In the merge photos of (A), cavity indicates the uterine cavity. The pink arrows indicate the AMH signals in the luminal epithelium of caruncle. The green arrows indicate AMH signals in the vasculature. Right panel (B) show negative controls staining using the normal animal IgGs1. Scale bars represent 100  $\mu\text{m}$  in (B), and 50  $\mu\text{m}$  in other panels.

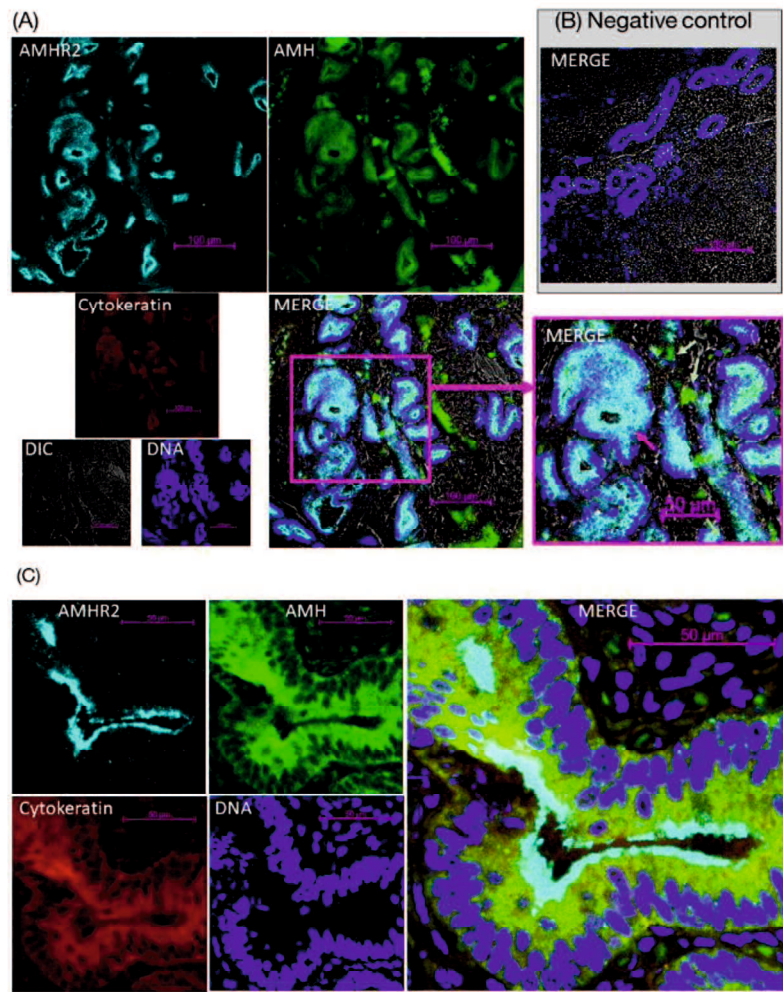


**Fig. 4.6.** Immunofluorescence staining of AMH in the intercaruncle samples of post-pubertal heifers. Specimens were collected on day 13. Images were captured via laser-scanning confocal microscopy and show AMHR2 (light blue), AMH (green), cytokeratin (red), and counter-staining with DAPI nuclear stain (dark blue), and DIC microscopy (grayscale). The pink arrows indicate the AMH signals in the epithelium of endometrial glands in intercaruncle. The green arrows indicate AMH signals in the vasculature. Right panel (B) show negative controls staining using the normal animal IgGs. Scale bars represent 50  $\mu\text{m}$  in the enlarged merge of (A) and (C), and 100  $\mu\text{m}$  in other panels.

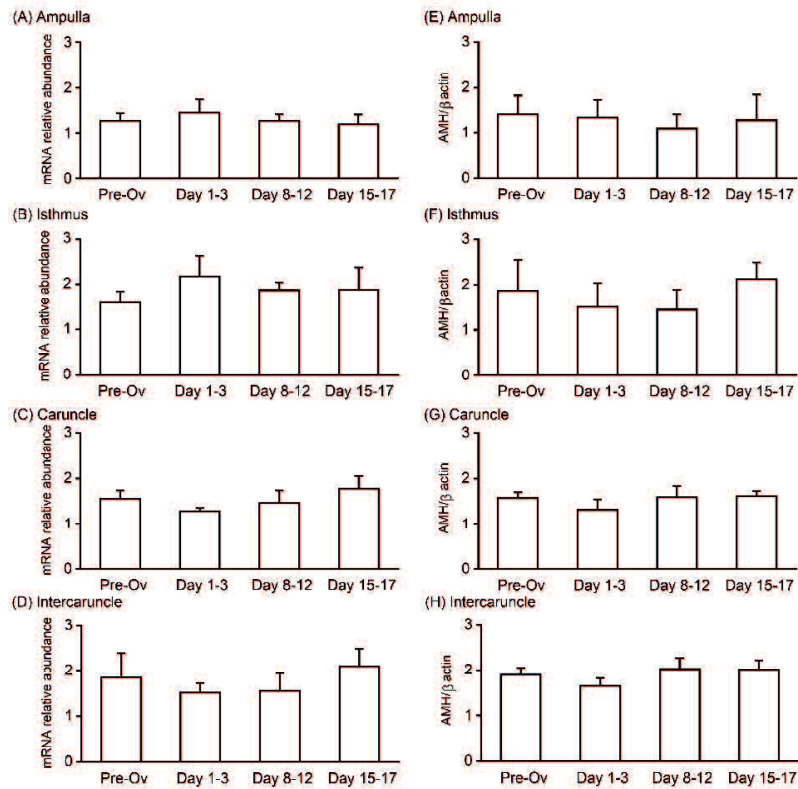


**Fig. 4.7.** No significant differences in the Changes in relative expression levels of AMH mRNA (determined by the RT-qPCR) or protein (determined by western blotting) (all data are shown as the mean  $\pm$  SEM) in the ampulla (A, E), isthmus (B, F), caruncle (C, G), or intercaruncle (D, H) samples of post-pubertal heifers during pre-ovulatory phase (Pre-Ov; day 19 to 21), day 1 to 3, day 8 to 12, or day 15 to 17. Relative *AMH* mRNA levels were determined by RT-qPCR and normalized to the geometric means of *C2orf29* and *SUZ12* levels. Relative AMH protein expression levels were determined by western blotting and normalized to those of  $\beta$ -actin. The same letters indicate no significant differences ( $P > 0.05$ ) across phases.

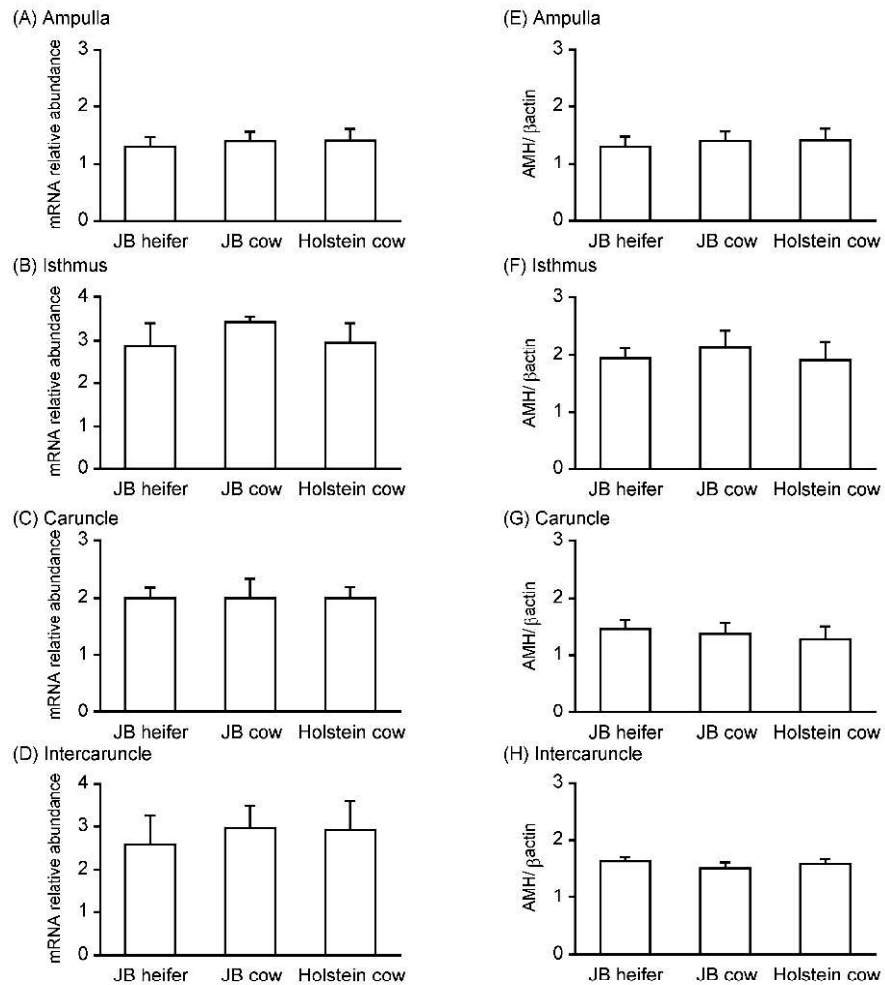


**Fig. 4.8.** No significant differences in the relative expression levels (shown as the mean  $\pm$  SEM) of *AMH* mRNA (determined by the RT-qPCR) or protein (determined by western blotting) in the ampulla (A, E), isthmus (B, F), caruncle (C, G), or intercaruncle (D, H) samples of young adult among post-pubertal JB heifers, JB cows, and Holsteins cows. The same letters indicate no significant differences ( $P > 0.05$ ) across phases.

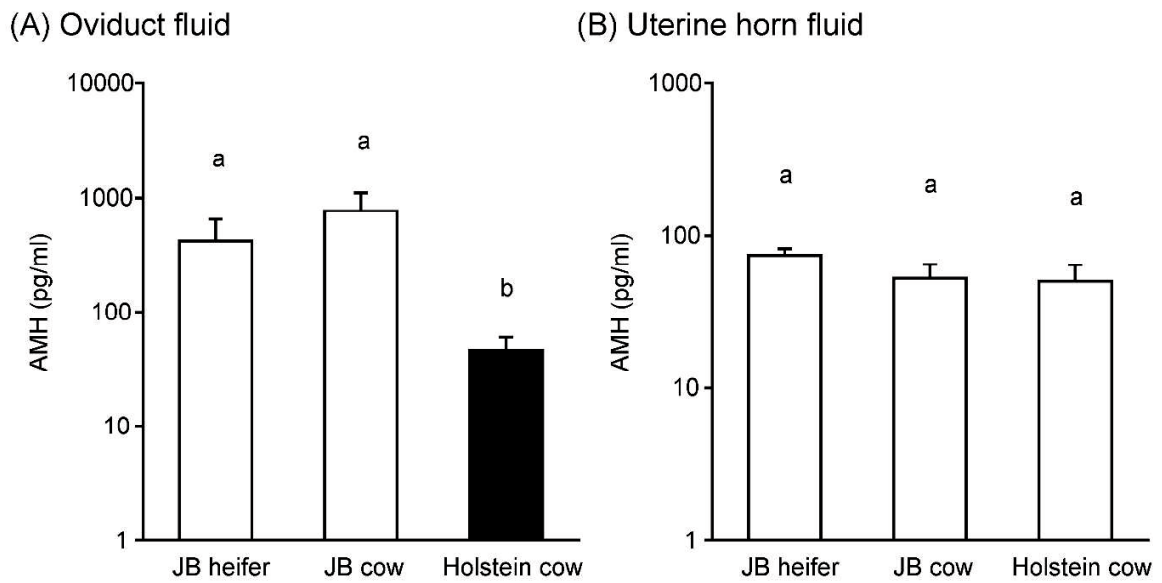


**Fig. 4.9.** AMH concentrations, as measured by enzyme immunoassays in the oviduct fluid on day 1 to 3 (A) or uterine fluid on day 8 to 14 (B), collected from post-pubertal JB heifers, JB cows, and Holsteins cows. Different letters indicate significant differences ( $P < 0.05$ ) among groups.

#### 4.4. Discussion

The results revealed robust high-intensity AMH signals in the tunica mucosa of the ampulla and isthmus, and in the glandular and luminal epithelium of endometria, where AMHR2 is constitutively expressed (Ferdousy *et al.* 2020). Little is known about AMH expression in the oviduct and endometrium in all species. However, a previous study utilizing immunohistochemistry detected AMH expression in the human endometrium (Wang *et al.* 2009) and human endometrial cancer tissue (Gowkielewicz *et al.* 2019). Recently, AMHR2 expression was discovered in healthy human endometrial tissues (Kim *et al.* 2019). We recently discovered that AMHR2 is expressed in the tunica mucosa of the ampulla and isthmus and the glandular and luminal epithelium of bovine endometria (Ferdousy *et al.* 2020), and this study validates previous findings. These data led to the speculation of potential roles of AMH and AMHR2 in these layers; however, little is known regarding AMH functions in the oviduct and endometrium. The roles of AMH in these layers might depend on the observed constitutive expression, the downstream cytoplasmic pathway of AMHR2, and other tissue-specific TGF- $\beta$  family members.

Of note, we need to have in mind that the contribution of extragonadal AMH secretion to the blood AMH concentration is unknown. However, no significant difference was observed in the AMH expression levels among the estrous phases in the ampulla, isthmus, caruncle, and intercaruncle tissues. Previous *in vivo* studies have not reported considerable changes in circulating AMH concentrations during the estrous cycle in ruminants (El-Sheikh *et al.* 2013; Pfeiffer *et al.* 2014; Koizumi & Kadokawa, 2017). Concurrent with the present findings, the 5'-flanking region upstream of the bovine AMH gene lacks the consensus response element sequences for estrogen and progesterone (Kereilwe *et al.* 2018). Therefore, AMH expression might not change during the estrous cycle in the tunica mucosa of the

ampulla and isthmus, and in the glandular and luminal endometrial epithelia. The constitutively expressed AMH in the layers of the oviduct and uterine horns might not play a temporal role, such as that during sperm capacitation and fertilization.

AMH shares an intracellular pathway with another TGF- $\beta$  family member, bone morphogenetic protein (BMP) (McLennan & Pankhurst 2015). Bovine oviduct epithelial cells express both BMP and BMP receptors, and BMPs might play autocrine roles at the epithelial lining of the oviduct (Valdecantos *et al.* 2017). Smads are the cytoplasmic pathway for BMP receptors in murine oviduct and uterus (Rodriguez *et al.* 2016). AMH induce Smad1/5/8 phosphorylation via AMHR2 in human granulosa cells (Merhi 2019). AMH signaling regulates expression of BMP receptor type 2, supports Smad signaling, and influences BMP-dependent signaling in non-small cell lung cancer (Beck *et al.* 2016). Furthermore, uteri from Smad1/5/4-AMHR2- conditional knockout females exhibit multiple defects in the stroma, epithelium, and smooth muscle layers, and fail to assemble a closed uterine lumen upon embryo implantation, with defective uterine decidualization that lead to pregnancy loss at early to mid-gestation (Rodriguez *et al.* 2016). Mossa & Ireland (2019) suggested that dairy cows with a low antral follicle count (follicles  $\geq 3$  mm in diameter) have lower blood concentrations of AMH and their endometrium is thinner than those with high antral follicle counts. Therefore, further studies must clarify whether AMH in bovine oviduct and uterus have important autocrine and/or paracrine roles in uterine function.

Our results on the effects of breed and age on such measurements should be interpreted with caution since we could not obtain specimens from young Holsteins heifers. However, despite no differences in the AMH expression levels were observed in the ampulla and isthmus among Holsteins cows and the JB heifers and cows, the AMH concentration in the oviduct fluids of old Holsteins cows was lower than that those in oviduct fluids from

JB heifers and cows. The comparable results between JB heifers and cows were unexpected since JB cows were reported to have higher blood AMH levels than post-pubertal heifers (Koizumi & Kadokawa, 2017). One possible explanation of our results relates to the relevant AMH source. While the AMH in the oviduct fluids may be a direct result of AMH secretion by the oviductal epithelial cells (and not from the blood circulating levels), the blood AMH concentration is not greatly affected by AMH secreted by the oviductal epithelia. However, Japanese Black cattle were fed for meat production, and old Holstein cows were infertile. Therefore, since these animals were raised under varied conditions not only different breed and age, it is difficult to interpret the results. Hence, further studies are needed to clarify age- or breed-related differences in the AMH concentration in fluid samples.

Western blotting showed differences in band strength or size between the oviducts and ovaries. The oviduct samples exhibited weaker bands for the mature C-terminal form of AMH than those of the ovary samples, suggesting that the oviducts store less mature C-terminal protein than the ovaries. The oviduct samples also exhibited weaker bands for the AMH precursor than those of the ovary samples. One possible reason for this difference is that the oviducts express lower levels of AMH precursor compared to the ovaries. Another possible explanation is that the oviducts secrete the C-terminal form soon after maturation without storing it subcellularly.

Western blotting showed differences in the number of full-length AMH bands among the ovary, ampulla, isthmus, caruncle, and intercaruncle. Since, different organs show different patterns of AMH O-glycosylation (Meczekalski *et al.* 2016; Skaar *et al.* 2011), therefore, differential glycosylation may explain the differences observed in the full-length form in our study. Collectively, these results show that bovine oviducts and endometria express AMH and likely secrete AMH into the oviduct and uterine fluids. AMH expression

might be useful to assess fertility status in bovines. Further studies must examine the roles of AMH in oviducts and the uterus.

In conclusion, these results show that bovine oviducts and endometria express AMH and likely secrete AMH into the oviduct and uterine fluids.

## **CHAPTER V**

**(Study III)**

**Specific locations and amounts of denatured collagen and  
collagen-specific chaperone, HSP47,  
in the oviducts and uteri of old cows as compared with those of heifers**

## Abstract

Collagen, the most abundant extra-cellular matrix in oviducts and uteri, performs critical roles in pregnancies. I hypothesised that the locations and amounts of both denatured collagen and the collagen-specific molecular chaperone, 47-kDa heat shock protein (HSP47), in the oviducts and uteri of old cows are different compared to those of young heifers because of repeated pregnancies. Since detecting damaged collagen in tissues is challenging, in the first part of this Chapter, we developed a new method that uses a denatured collagen detection reagent. Then, I compared damaged collagen in the oviducts and uteri between post-pubertal growing nulliparous heifers ( $22.1 \pm 1.0$  months old) and old multiparous cows ( $143.1 \pm 15.6$  months old). Further, I evaluated the relationship between denatured collagen and HSP47 by combining this method with fluorescence immunohistochemistry. Picro-sirius red staining showed collagen in almost all parts of the oviducts and uteri. Expectedly, damaged collagen was increased in the oviducts and uteri of old cows. However, damaged collagen and HSP47 were not located in the same area in old cows. The number of fibroblasts increased, suggesting the presence of fibrosis in the oviducts and uteri of old cows. These organs of old cows showed higher HSP47 protein amounts than those of heifers. However, the uteri, but not oviducts, of old cows showed lower *HSP47* mRNA amounts than those of heifers. These findings revealed the specific location and amounts of denatured collagen and HSP47 in the oviducts and uteri of old cows compared to those of heifers.

## 5.1. Introduction

Infertility increases after aging in various animals, including cows (Osoro and Wright 1992). However, little is known about the exact pathophysiological mechanisms in oviducts and uteri. Collagen, one of the most abundant ECM proteins, exerts a critical role in successful pregnancies, and abnormal collagen expression is associated with recurring miscarriages in women (Li *et al.* 2019, Shi *et al.* 2020). The bovine endometrium, similar to that of other mammals, changes morphologically throughout the oestrous cycle (Arai *et al.* 2013). Furthermore, dysregulation of ECM remodelling in bovine endometrium may impair fertility (Scolari *et al.* 2016).

Denaturation of collagen is increased due to various diseases, including cancer, osteoporosis, and arthritis (Fields 2013, Ito and Nagata 2019). Denatured collagen was studied by electron microscopy for corneal immune injury (Mohos and Wagner 1969). It was technically challenging to detect damaged collagen in tissues until the recent development of a collagen hybridising peptide (Zitnay *et al.* 2017) and a denatured collagen detection reagent (Takita *et al.* 2019). The latter is a biotin-labelled collagen-mimetic peptide that hybridises with the denatured portion of collagen. It enables the detection of denatured collagen via western blotting as well as through visualisation of heat damaged collagen fibrils in mouse fibroblasts (Takita *et al.* 2019).

Forty-seven kilodalton heat shock protein, HSP47, encoded by *SERPINH1*, is a sole procollagen-specific molecular chaperone that is essential for correct folding of the unique, triple-helical structure of collagen (Ito and Nagata 2019). HSP47 also plays important roles in the synthesis of collagen as well as in the prevention of procollagen aggregation (Duarte and Bonatto 2018). Therefore, HSP47 is central in detecting the location of active collagen synthesis in the oviducts and uteri.

In this study, we hypothesised that the locations and amounts of both denatured collagen and HSP47 in the oviducts and uteri of old cows are different compared to those of young heifers. In the first part of this study, we developed a new method using the denatured collagen detection reagent to compare young and old oviducts and uteri. Then, we evaluated the relationship between denatured collagen and HSP47 in heifers and old cows utilising this method followed by fluorescence immunohistochemistry. Further, we compared the amounts of the mRNA and protein of HSP47 in oviducts and uteri between the old cows and heifers.

## 5.2. Materials and Methods

### 5.2.1. Sample collection

All experiments were performed according to the Guiding Principles for the Care and Use of Experimental Animals in the Field of Physiological Sciences (Physiological Society of Japan) and approved by the Committee on Animal Experiments of Yamaguchi University.

We used a previously reported method (Ferdousy *et al.* 2020) to obtain the ampulla, isthmus, CAR, and ICAR areas as well as the uterine myometrium from healthy post pubertal, growing, young nulliparous JB heifers ( $22.1 \pm 1.0$  months old; Young group), and old multiparous JB beef cows ( $143.1 \pm 15.6$  months old;  $9 \pm 1$  parities; sacrificed at least 3 months after the last parturition; Old group) at a local abattoir. The heifers and cows were at days 2 to 3, 8 to 12, 15 to 17, or 19 to 21 of the oestrous cycle (day 0 = day of oestrus), as determined via macroscopic examination of the ovaries and uterus (Miyamoto *et al.* 2000). The samples collected were from the side ipsilateral to ovulation from days 2 to 3, 8 to 12, or 15 to 17 but were from the side ipsilateral to the dominant follicle from days 19 to 21. We collected at least five samples per group per day. Half of the samples (whole tissue fragment; about 1 cm length of ampulla and isthmus; about 5 mm in width, 5 mm in length, and 2 mm in thickness of CAR, ICAR, and myometrium) were frozen in liquid nitrogen and preserved at  $-80^{\circ}\text{C}$  until RNA or protein extraction was performed. The remaining half was embedded in a cryo-mould containing an optimum cutting temperature compound (Sakura Fintech Co. Ltd.), and then the cryo-mould was wrapped with an aluminium foil. The cryo-moulds were then frozen in liquid nitrogen and preserved at  $-80^{\circ}\text{C}$  until *in situ* detection of denatured collagen and immunohistochemistry studies were conducted.

Additionally, we measured the total collagen in tissue using picro-sirius red staining.

For this purpose, we obtained the ampulla, isthmus, CAR, and ICAR from four different young nulliparous heifers ( $21.5 \pm 0.6$  months old), and four old multiparous JB beef cows ( $148.8 \pm 12.0$  months old;  $9 \pm 1$  parities; sacrificed at least 3 months after the last parturition) at the local abattoir. The samples were stored in 4% PFA at 4°C for 16 h.

### **5.2.2. Development of the method for *in situ* detection of denatured collagen**

We developed a new method for *in situ* detection of denatured collagen. As described below, this method can be combined with fluorescent immunohistochemistry.

Unfixed tissue blocks were sectioned into 15- $\mu$ m-thick sections using a cryostat (CM1950, Leica Microsystems) and mounted on slides (MAS coat Super frost, Matsunami-Glass). Next, the tissue was fixed with 4% PFA in PBS for 15 min. Some sample sections from the young group were placed on slides treated with 100 °C PBS for 2 min (pre-heated slides) or with 25 °C accutase cell detachment solution (Nacalai Tesque) for 30 min (digested slides) to denature collagen, whereas others were treated with ice-cold PBS (non-treated slides). We used accutase because it is a proteolytic and collagenolytic enzyme, and it is not inhibited by the possible presence of calcium and magnesium in the tissues. We tried to use also collagenase, but the structures of the tissues were broken after staining, while accutase did not significantly damage the structure. Blocking was performed by incubating the tissue sections in PBS (0.5 mL) containing 10% normal goat serum (Wako Pure Chemicals) for 1 h at room temperature. Tissues were then treated with an avidin/biotin blocking kit (Vector Laboratories) following the manufacturer's protocol. After washing twice with PBS, the slide was loaded with 5  $\mu$ g/mL of denatured collagen detection reagent (Funakoshi) and incubated for 60 min at room temperature in a humid box. After washing twice with PBS, the tissues were incubated with streptavidin, Alexa Fluor 546 conjugate (diluted to 1  $\mu$ g/mL in PBS,

Thermo Fisher Scientific) and DAPI; (Wako Pure Chemicals) for 60 min at room temperature. After washing thrice, cover glasses were mounted using Vectashield HardSet Mounting Medium (Vector Laboratories).

Sections were observed with a confocal microscope (LSM710; Carl Zeiss) equipped with a 405 nm diode laser, 488 nm argon laser, 533 nm HeNe laser, and 633 nm HeNe laser. Images obtained by fluorescence microscopy were scanned with a 20× or 40× oil-immersion objective and recorded with a CCD camera system controlled by ZEN2012 black edition software (Carl Zeiss). The exact same microscope settings were used throughout immunofluorescence imaging of the ampulla, isthmus, CAR, ICAR, or myometrium to compare between young and old cows. We distinguished between the layers or parts of oviducts and uteri according to Banu *et al.* (2005), Hayashi *et al.* (2017), and Godoy-Guzman *et al.* (2018).

### **5.2.3. Picro-sirius red staining for total collagen**

The fixed tissues were dehydrated and embedded in paraffin using the Handed autokinette (model 1400P, Shiraimatsu Corp. Ltd.). Thin sections (10 µm thick) were cut with a sliding microtome (Yamato Kohki) attached onto a slide glass. The paraffin-embedded sections were de-parafinised thrice in xylene, for 5 min each, followed by de-alcohol in 100%, 100%, 90%, and 70% ethanol and ultrapure water for 5 min each. The slides were then covered in picro-sirius red staining solution (Picro-Sirius Red Stain Kit, ScyTek laboratories Inc.) for 1 h. Following staining, the slides were washed twice with 0.5% acetic acid solution. The sections were dehydrated through three changes of 100% ethanol and cleared in three changes of xylene. After attaching the cover slip with Entellan new mounting medium (Sigma-Aldrich), the stained sections were observed under a light microscope fitted

with a digital camera (Eclipse Ci, Nikon). The staining and light microscopy results showed collagen in red, muscle fibres and cytoplasm in yellow, and complex in orange.

#### **5.2.4. RT-PCR, sequencing of amplified products, and homology search in gene databases**

Total RNA (at least four per tissue) was extracted using the RNAzol RT isolation reagent (Molecular Research Centre Inc.) and treated with deoxyribonuclease. The concentration and purity of each RNA sample were evaluated by spectrophotometry (acceptable 260/280 nm ratio of absorbance, 1.8–2.1) and electrophoresis (28S:18S ratios were 2:1). Complementary DNA was synthesised using the Verso cDNA Synthesis Kit (Thermo Fisher Scientific). NRCs were prepared for RT-PCR; they were generated by treating the extracted RNA with the same deoxyribonuclease but not with cDNA synthetase.

To determine the amount of *HSP47* mRNA, a primer pair was designed by Primer Express v3.0 (Thermo Fisher Scientific) based on the reference sequence of bovine *HSP47* [ NCBI reference sequence of bovine *HSP47* is NM\_001046063]. Table 5.1 details the primers. PCR was performed using 20 ng of cDNA, 20 ng RNA as the NRC or water as the NTC, and polymerase (Tks Gflex DNA Polymerase, Takara Bio Inc.) under the following thermocycle conditions: 94 °C for 1 min for pre-denaturation followed by 35 cycles of 98°C for 10 s, 60°C for 15 s, and 68°C for 30 s. PCR products were separated on 1.5% agarose gel by electrophoresis with a molecular marker (Nippon Gene), stained with Gelstar (Lonza, Allendale), and observed using a CCD imaging system (GelDoc; Bio-Rad). The PCR products were purified with the NucleoSpin Extract II kit (Takara Bio Inc.) and then sequenced using one of the PCR primers and the Dye Terminator v3.1 Cycle Sequencing Kit (Thermo Fisher Scientific). The sequences obtained were used as query terms with which to

search the homology sequence using the BLAST (available on the NCBI website).

Table 5.1. Details of the primers for RT-PCR for *HSP47*

Gene	Primer	Sequence 5'-3'	Position		Size (bp)
			Nucleotide	Exon	
<i>HSP47</i>	Forward	GACAACCGAGGCTTCATGGT	770	4	470
	Reverse	AGCTCCTCACGCCCGTAGAT	1239	6	

### 5.2.5. Western blotting for HSP47 detection

Five samples per day in each tissue of each group (total of 20 samples in each tissue of each group); were assessed and analysed statistically. After electrophoresis and transfer to PVDF membrane, we used a Can Get Signal Immunoreaction Enhancer kit (Toyobo Co. Ltd) for membrane blocking (1 h at 25 °C), primary antibody reaction (1 h at 25 °C) with an anti-HSP47 rabbit polyclonal antibody (1:400,000 dilution with immunoreaction enhancer solution; AP7366B; Abcepta Inc.), and secondary antibody reaction (1 h at 25 °C) with goat anti-rabbit IgG horseradish peroxidase-conjugated antibody (Bethyl Laboratories Inc.; 1:400,000 dilution with immunoreaction enhancer solution). The anti-human HSP47 rabbit antibody recognizes the mature C-terminal form of human HSP47 (corresponding to amino acids 390 to 418; FLVRDTQSGSLLFIGRLVLRPKGDKMRDEL). This sequence had 100% homology to amino acids 390 to 418 of the mature C-terminal form of bovine HSP47 but no homology to other bovine proteins, as determined using protein BLAST (NCBI reference sequences of human and bovine HSP47 are NP\_001193943.1 and NP\_001039528.1, respectively).

The protein bands were visualised using an ECL-Prime chemiluminescence kit (GE Healthcare) and a CCD imaging system (LAS-3000 Mini; Fujifilm). The images were exported using the Multigauge (version 3.0; Fujifilm) software. To verify the specificity of the signals, we included several negative controls in which the primary antibodies had been omitted or normal rabbit IgG (Wako Pure Chemicals) antibodies were used instead of the primary antibodies. Signal specificity was also confirmed using negative controls in which the primary antibodies were pre-absorbed with 5 nM antigen peptide (Scrum Inc.).

The antibodies were removed from the PVDF membrane with a stripping solution (Nacalai Tesque) prior to the blocking and subsequent immunoblotting with an anti- $\beta$ -actin

mouse monoclonal antibody (1:400,000 dilution; Sigma-Aldrich).

All relevant bands were cropped from the exported file using Adobe Photoshop element ver. 2020 (Adobe, San Jose) and pasted onto a graph created using Delta Graph ver. 7.5.2J (Red rock software). Image Quant TL (version 8.2; Cytiva) software was used to measure the band sizes and volumes (calculated using rolling ball background subtraction). The protein amount of HSP47 was normalised against  $\beta$ -actin.

#### **5.2.6. RT-qPCR analysis of *HSP47***

After preparation of high-quality total RNA and cDNA synthesis using the previously described protocol, *HSP47* mRNA amount was compared among the young and old groups via the relative standard curve method of RT-qPCR and data analyses, as described previously (Nahar and Kadokawa 2017, Ferdousy *et al.* 2020). G\*Power 3 for windows (Faul *et al.* 2007) was used to estimate the required number of samples with an alpha-error probability of 0.05 and a statistical power of 0.95. Five cDNA samples per day in each tissue of each group (total of 20 cDNA samples in each tissue of each group), were assessed and analysed statistically.

To prepare external standards for amplified fragments of cDNA products containing target sequences for RT-qPCR of *HSP47*(800 bp) and two housekeeping genes, *C2orf29* (562 bp) and *SUZ12* (1169 bp), PCRs were conducted as described previously (Nahar and Kadokawa 2017). The primers were designed by Primer Express Software v3.0 (Table 5.2). The PCR-amplified products were purified to prepare the standards, as well as to verify the DNA sequence. Then, we prepared a 6-point relative standard by 10-fold diluting the PCR products for the relative standard method. *HSP47* mRNA levels were normalised to the geometric mean of the levels of the two house-keeping genes, *C2orf29* and *SUZ12*.

The mRNA level was measured in duplicate by RT-qPCR analyses with 20 ng cDNA, using CFX96 Real Time PCR System (Bio-Rad) and Power SYBR Green PCR Master Mix (Thermo Fisher Scientific), together with the 6-point relative standards, NTC, and NRC to generate the standard curve by plotting the log of the starting quantity of the dilution factor against the  $C_q$  value using appropriate software (CFXmanagerV3.1, Bio-Rad). Temperature conditions for all genes were as follows: 95°C for 10 min for pre-denaturation; five cycles each of 95°C for 15s and 66°C for 30s; and 40 cycles each of 95°C for 15s and 60°C for 60 s. Melting curve analyses were performed at 95°C for each amplicon and each annealing temperature to ensure the absence of smaller non-specific products, such as dimers. All the  $C_q$  values of the unknown samples ( $22.85 \pm 0.15$ ) were between the highest (8.00) and lowest (30.33) standards for *HSP47* in RT-qPCR. Further, all the  $C_q$  values of the unknown samples were between the highest and lowest standards for *C2orf29* or *SUZ12* in RT-qPCR. Reactions with a coefficient of determination ( $R^2$ ) > 0.98 and efficiency between 95 and 105% were considered optimised. The coefficients of variation of RT-qPCRs were less than 6%. The concentration of PCR products was calculated by comparing  $C_q$  values of unknown samples with the standard curve using CFXmanagerV3.1. Then, the *HSP47* amount was divided by the geometric mean of *C2orf29* and *SUZ12* in each sample.

Table 5.2. Details of the primers for RT-qPCRs for *HSP47*

Gene	Primer	Sequence 5'-3'	Position		Size (bp)
			Nucleotide	Exon	
<i>C2orf29</i>	Forward	AAGTTTTTTCTTTCCCAGCTCATG	666–688	2	562
	Reverse	CAGGAAGTTTGGCTGGAGTGA	1207– 1227	5	
<i>SUZ12</i>	Forward	GGAAGAGACTGCCTCCATTTGA	1019– 1040	10	1169
	Reverse	CCCTGAGACACCATCTGTTTCC	2166– 2187	16	
<i>HSP47</i>	Forward	TGTCGGGCAAGAAGGACCTA	1131	5	800
	Reverse	AAAATGGGGAGGAAAGTGGG	1930	6	
<i>HSP47</i>	Forward	ACAAGATGCGAGACGAGTTGT	1347	5	93
	Reverse	CCCTGTTTTCCCACCCATGT	1439	5&6	
	Reverse	TTGGCCTGCACACAAGAATG	1581– 1600	14	

### **5.2.7. Immunofluorescence staining and confocal microscopy**

For immunofluorescence staining, we randomly selected at least five tissue samples per day in each tissue of each group. To evaluate the association between HSP47-rich areas and denatured collagen-rich areas, the tissues on slides were washed once after incubation with streptavidin, Alexa Fluor 546 conjugate, and DAPI. Then, the sections were treated with 0.3% Triton X-100 for 15 min, blocked with 10% normal goat serum in PBS for 1 h at room temperature, and subjected to a primary antibody reaction with the anti-HSP47 antibody (1:1,000 dilution for overnight at 4°C). Subsequently, the samples were subjected to a secondary antibody reaction with Alexa Fluor 647 goat anti-rabbit IgG (diluted to 1 µg/mL, Thermo Fisher Scientific) and 1 µg/mL DAPI for 2 h at room temperature. After washing the sections four times, the slides were mounted in preparation for confocal microscopy. To verify the specificity of signals, we included several negative controls in which the primary antiserum had been omitted or pre-absorbed with 5 nM antigen peptide, or in which normal rabbit IgG was used instead of the primary antibody. We also included negative controls in which the secondary antibodies had been omitted or normal goat IgG (Wako Pure Chemicals) antibodies were used instead of the secondary antibodies. Signal specificity was also confirmed using negative controls in which the secondary antibodies were pre-absorbed with 5 nM normal rabbit IgG.

Additionally, we performed immunohistochemistry to identify whether cytokeratin-rich areas or vimentin-rich areas express HSP47. For this purpose, we included anti-bovine pan cytokeratin mouse monoclonal antibody or anti-bovine vimentin mouse monoclonal antibody (both from Sigma-Aldrich, and diluted as 1:1,000) in the primary antibody reaction, and Alexa Fluor 488 goat anti-mouse IgG (diluted to 1 µg/mL, Thermo Fisher Scientific) in the secondary antibody reaction.

### 5.2.8. Analysis of the 5'-flanking region of *SERPINH1*

The 5000-nucleotide sequence of the 5'-flanking region of the *SERPINH1* gene (chromosome 15: 54,737,997-54,748,417) was obtained using the online Ensembl Search Genome program (<http://www.ensembl.org>) against the bovine genome database (April, 2018, ARS\_UCD\_1.2/bosTau9). The sequence was analysed using Genetyx software v.13 (Genetyx) for the presence of consensus response element (RE) sequences for oestrogen—i.e., ERE (5'-GGTCANNNTGACC-3'), ERE-like sequence (5'-TGACCCCTGGGTCA-3') (Gruber et al., 2004), and half ERE (GGTCA, TGACC, or TGACT) (Liu et al., 1995), as well as for progesterone—i.e., PRE (5'-G/A G G/T AC A/GTGGTGTCT-3') (Geserick *et al.* 2005) and half PRE (5'-TGTTCT-3') (Tsai *et al.* 1988).

### 5.2.9. Statistical analysis

The statistical analyses were performed using Stat View version 5.0 for Windows (SAS Institute, Inc.). Grubb's test verified the absence of outliers. The Shapiro-Wilk's test and Kolmogorov-Smirnov Lilliefors test verified the normality of distribution of each variable. Two-factor ANOVA was used to evaluate the effect of age (young or old), stage (days 2 to 3, 8 to 12, 15 to 17, or 19 to 21), and interaction followed by post-hoc comparisons using Fisher's PLSD test for the data of RT-qPCR or western blotting for HSP47. The statistical significance of differences among stages was assessed by one-factor ANOVA followed by post-hoc comparisons using Fisher's PLSD test using a model consisting of variance from the effect of stage and the residual. The level of significance was set at  $P < 0.05$ . Data are expressed as means  $\pm$  SEM.

### 5.3. Results

Picro-sirius red staining showed red or orange colour in almost all parts of the ampullae, isthmuses, CAR, ICAR, and myometria (**Fig. 5.1**).

We successfully developed a new *in situ* assay for the detection of denatured collagen (**Fig. 5.2**). The non-treated young tissues showed a very subtle signal indicating the presence of denatured collagen (red). By contrast, the old samples, similar to the heated and enzyme-treated young tissues, showed a strong signal indicating the presence of denatured collagen in the lamina propria and muscular layer of the ampullae and isthmuses. In addition, the heated young uteri showed strong signals in the luminal epithelia and uterine stroma of CAR as well as in the glandular epithelia and uterine stroma of ICAR, and various cells in the uterine myometria.

PCR products of a size corresponding to that of *HSP47* (470 bp) were obtained from the ampullae, isthmuses, CAR, ICAR, and myometria, as revealed by agarose gel electrophoresis (**Fig. 5.3**). Neither the NTC nor any of the NRCs yielded any PCR-amplified products. A homology search against gene databases for the sequenced amplified products revealed bovine *HSP47* (NM\_001046063) as the best match, with a query coverage of 100%, an e-value of 0.0, and a maximum alignment identity of 99%. No other bovine genes displayed homology with the PCR product, indicating that the amplified product was indeed *HSP47*.

We combined the *in situ* detection method for denatured collagen with immunofluorescence staining of HSP47 in the ampulla (**Fig. 5.4A**), isthmus (**Fig. 5.4B**), CAR (**Fig. 5.5A**), ICAR (**Fig. 5.5B**), and myometrium (**Fig. 5.5C**). Robust, high-intensity fluorescence signals of denatured collagen were localised again in the above-mentioned areas of old samples but not in those of young samples. In addition, HSP47 signals were

localised in the epithelial layer and superficial stroma very near to the epithelial layer of oviducts of old individuals but only weakly in those of young individuals (**Fig.5.6**). HSP47 signals were localised in the epithelia and stroma of the CAR and ICAR of old and young individuals. HSP47 signals were localised in the myometrium of old individuals but not in those of young individuals. More importantly, HSP47 rich-areas (green) and denatured collagen-rich area (red) were different because there was little colocalisation (yellow) in the merged panels. There was no signal indicating that HSP47 had colocalised with denatured collagen in the lamina propria and muscular layers of ampullae and isthmuses. Therefore, HSP47-rich and denatured collagen-rich areas were different.

**Fig. 5.7** shows the results of western blot and outcomes of two-factor ANOVA. The western blot revealed HSP47 protein in all five specimens obtained from old cows, but only weak expression in those from young heifers (**Fig. 5.7**). Unexpectedly, an extra band at 25 kDa appeared only in old samples. The ANOVA revealed that the age effect was significant for the 47 kDa or 25 kDa bands in the ampulla, isthmus, CAR, ICAR, and myometrium, and old samples contained a higher amount of HSP47 than the young samples. The effect of stage was significant in almost all samples, except for the 47 kDa band in ampulla and isthmus, and 25 kDa band in the myometrium. The interaction between the effects of age and stage was significant only for 47 kDa and 25 kDa bands in the CAR.

**Fig. 5.8** shows the results of RT-qPCR, and outcomes of two-factor ANOVA. The age effect was significant in the CAR, ICAR, and myometrium, but not in the ampulla and isthmus. The effect of stage was significant in the ampulla, isthmus, and ICAR, but not in CAR and myometrium. The interaction between the effects of age and stage was significant only in the isthmus.

The 5'-flanking region of the bovine *SERPINH1* gene was analysed for EREs, PREs,

and similar sequences. Although there were no ERE, ERE-like, or PRE-sequences, 19 halves ERE (7 GGTCA, 7 TGACC, and 5 TGACT) and 3 halves PRE-sequences were identified.

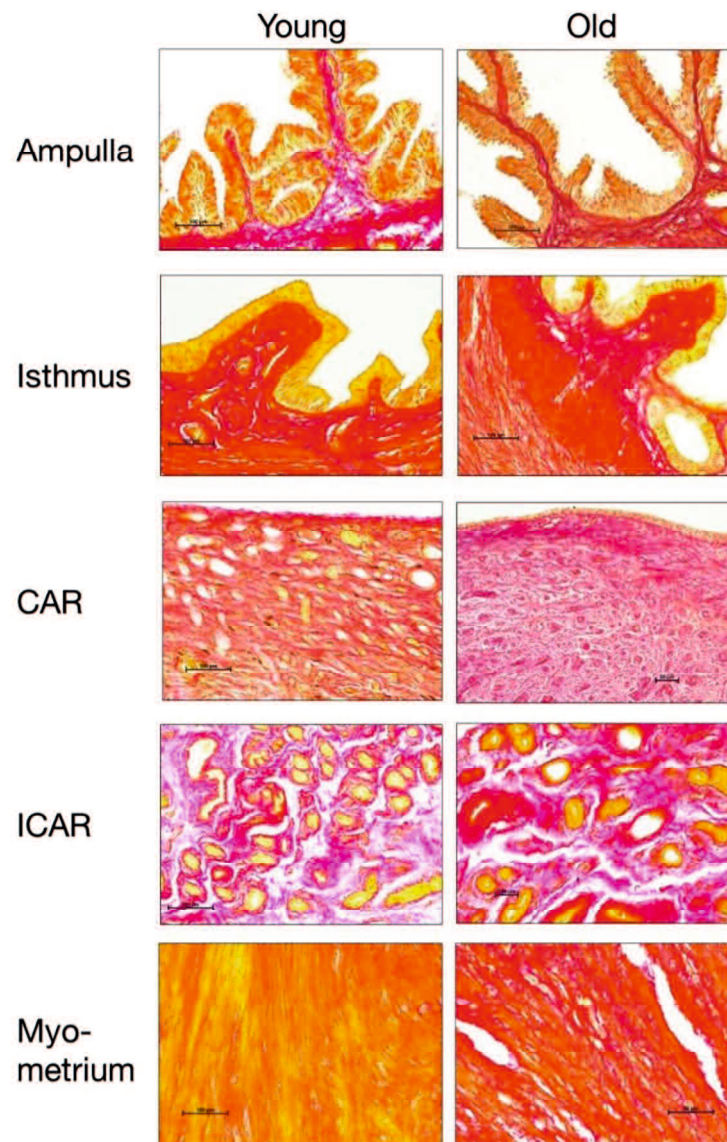


**Fig. 5.1.** Picro-sirius red staining for total collagen in ampulla, isthmus, and CAR and ICAR areas of the endometrium and myometrium in healthy post pubertal, growing and young nulliparous heifers (Young), and old multiparous JB beef cows (Old). The Picro-sirius red staining shows collagen in red, muscle fibres and cytoplasm in yellow, and complex in orange.

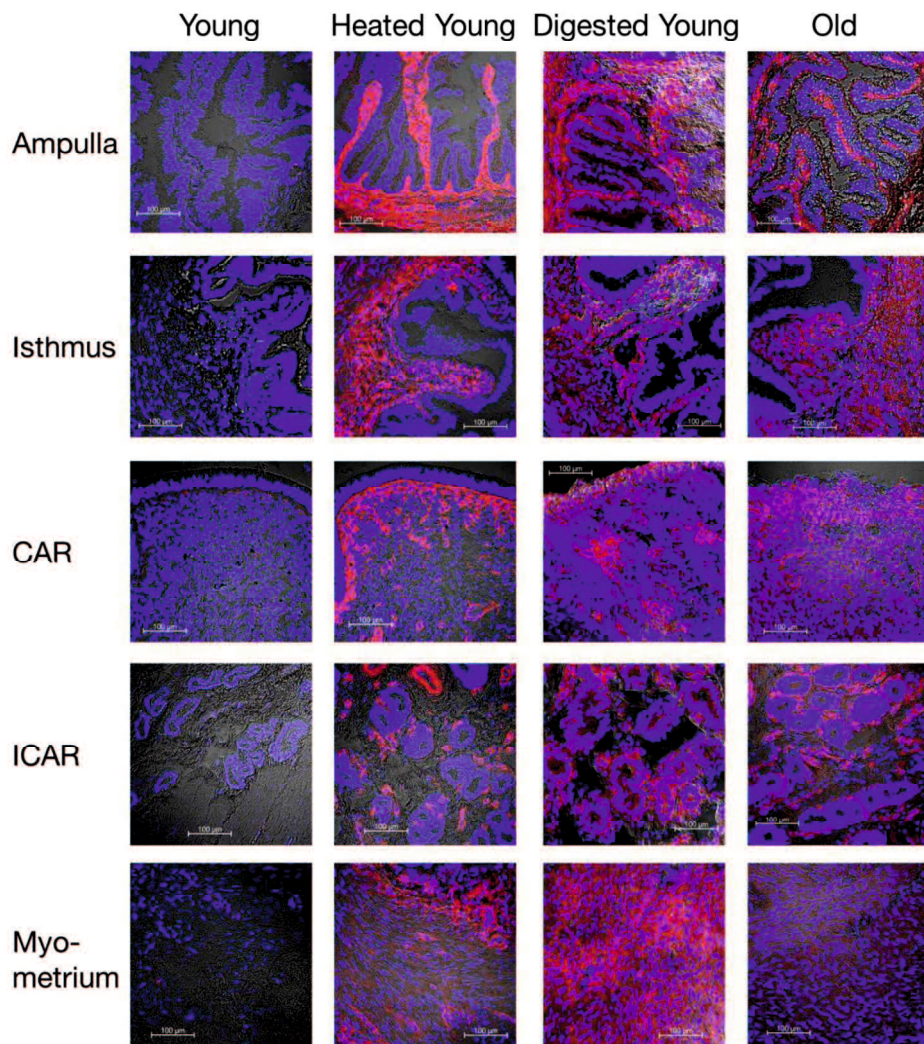


**Fig. 5.2.** *In situ* detection of denatured collagen. The no-heated, non-digested young tissues show very subtle signals of denatured collagen (red). In contrast, the old samples, in a manner similar to the heated or enzyme-digested young tissues, show strong signals corresponding to denatured collagen in the lamina propria and muscular layers of ampullae and isthuses; the stroma of CAR and ICAR; the glandular epithelium of ICAR; and various myometrial cells.

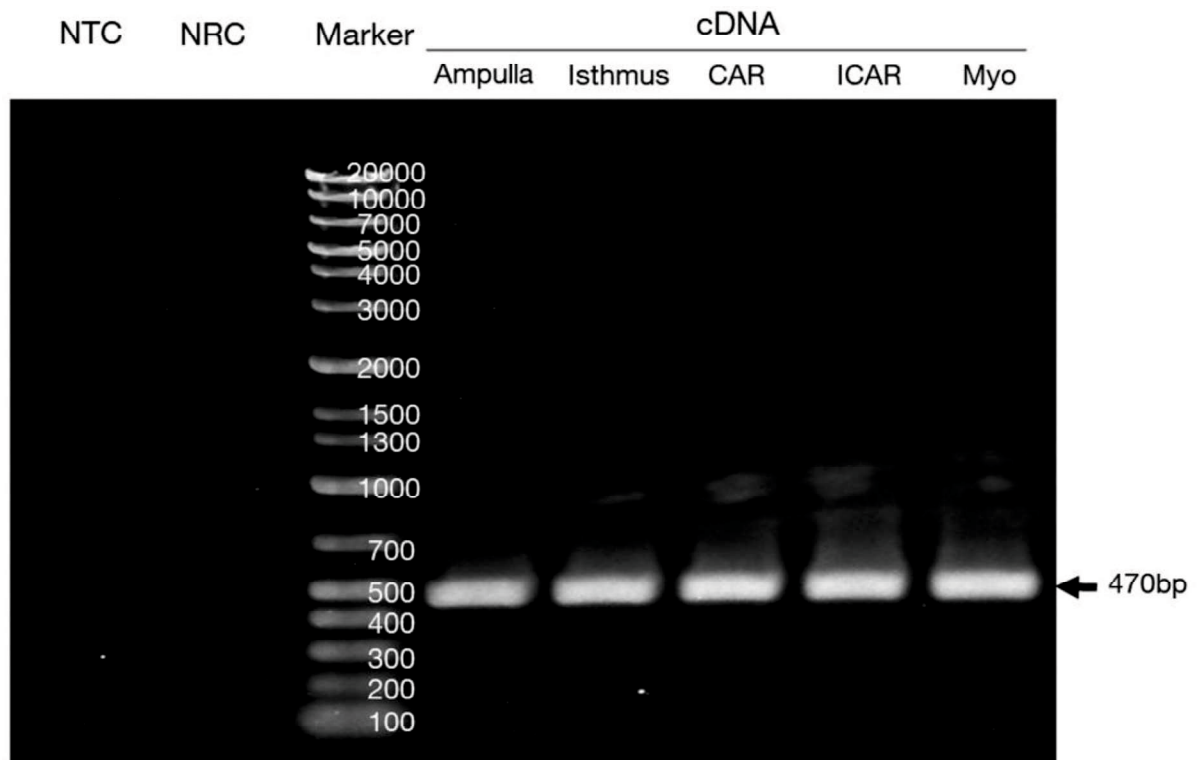


**Fig. 5.3.** Expression of *HSP47* detected via RT-PCR analysis. The electropherogram shows the size (470 bp) expected from PCR products of bovine *HSP47*-in the ampulla, isthmus, CAR, ICAR, and myometrium (Myo) in old cows. Bands were not present in the NTC and NRCs lanes.

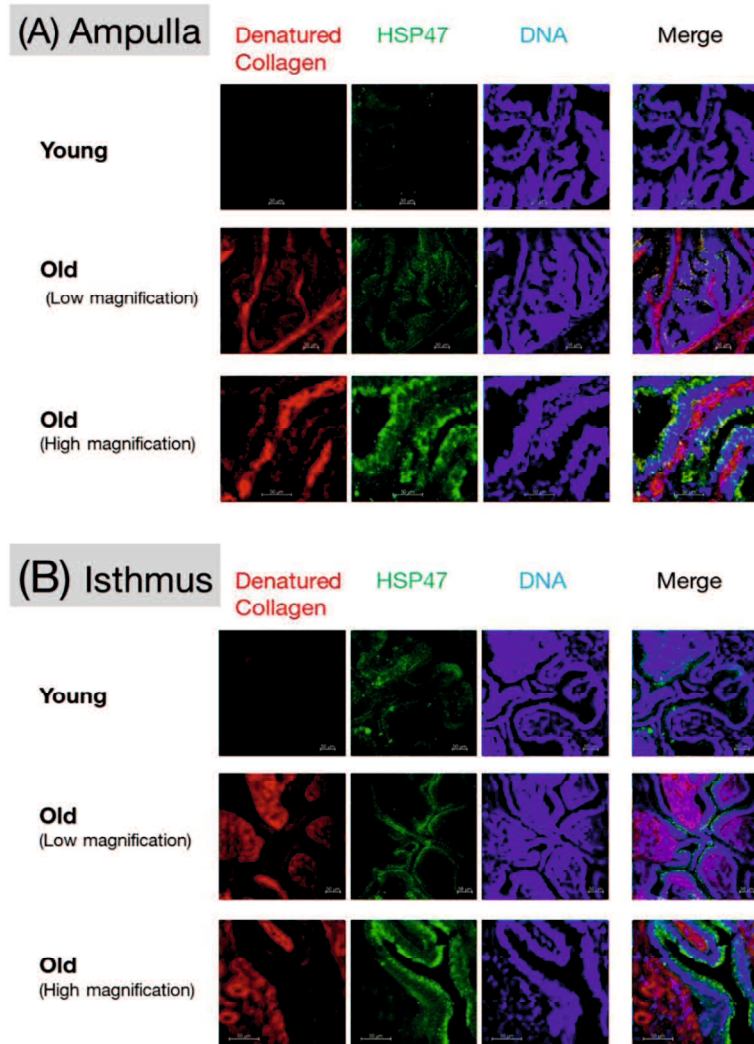


**Fig. 5.4.** Comparison of denatured collagen-rich areas (red) and HSP47-rich areas (green) in the ampullae or isthmuses (collected on day 3 of the oestrous cycle) of Young and Old groups. Nuclei are counterstained with DAPI (dark blue). Unlike the Young, the Old specimens showed strong signal corresponding to denatured collagen in the lamina propria and muscular layers. The Old specimens showed strong signal corresponding to HSP47 in the epithelia of tunica mucosa and superficial stroma. Not many signals corresponding to colocalisation (yellow) were present in the Merge panels; scale bars are 50  $\mu$ m.

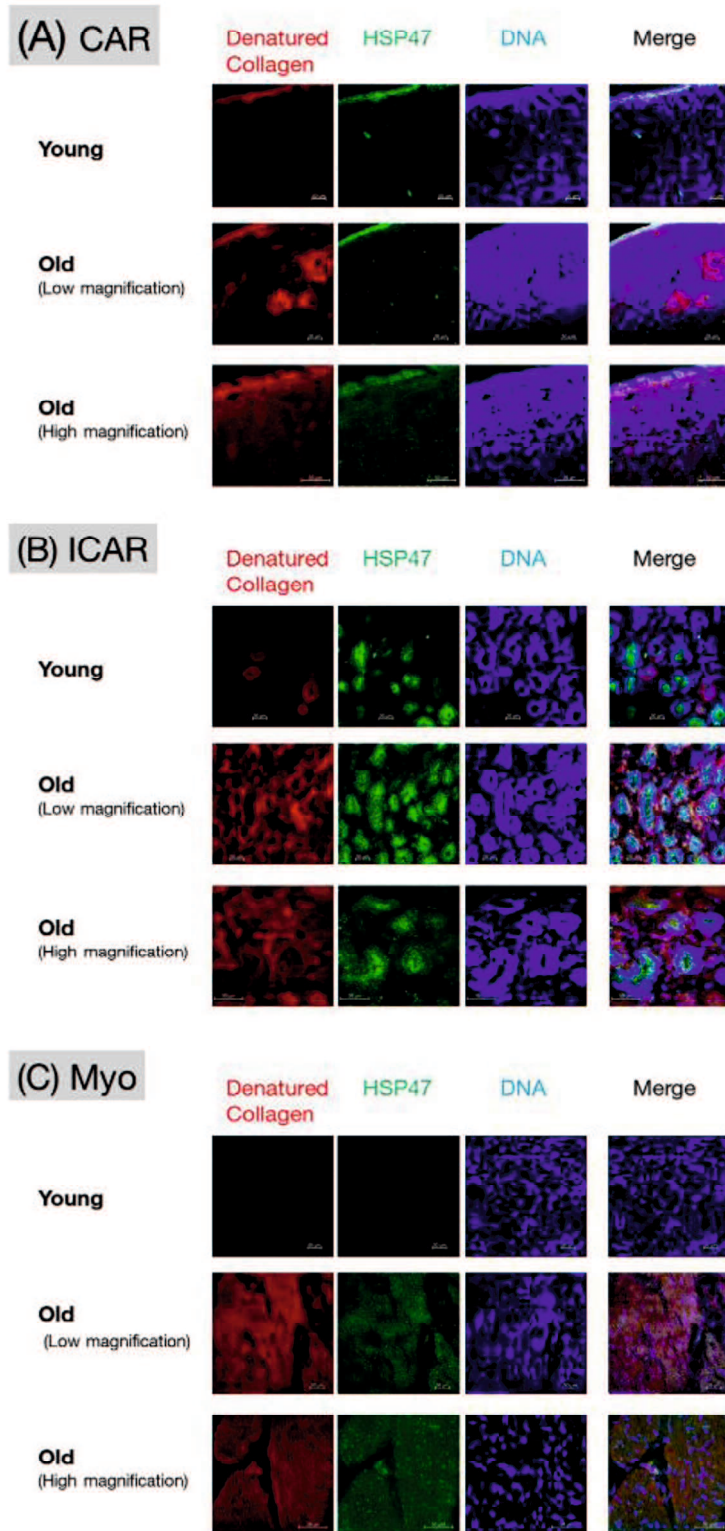


**Fig. 5.5.** Comparison of denatured collagen-rich areas (red) and HSP47-rich areas (green) in the CAR, ICAR, or Myo (collected on day 13 of the oestrous cycle) of Young and Old groups.

Nuclei are counterstained with DAPI (dark blue). Both the Young and Old specimens showed signals corresponding to both denatured collagen and HSP47 in luminal epithelia, glandular epithelia, and stroma. Unlike the Young, the Old specimens also showed strong signals corresponding to both denatured collagen and HSP47 in the stroma and myometria. Particularly, the number of fibroblasts (green dots) increased. However, not many signals corresponding to colocalisation (yellow) were present in the Merge panels; scale bars are 50  $\mu\text{m}$ . The dark patches in old myometria are broken parts.

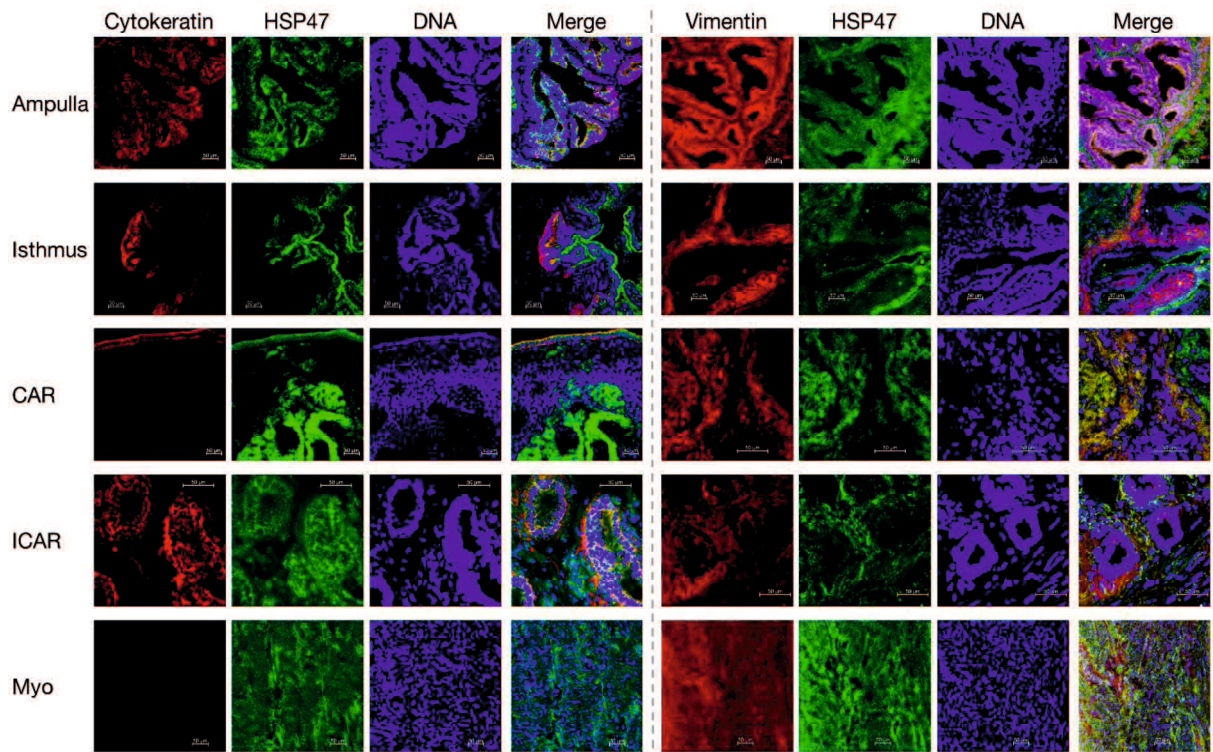


**Fig. 5.6.** Comparison of HSP47-rich areas (green) and cytokeratin- or vimentin-rich areas (red) in the ampullae or isthmuses (collected on day 3 of the oestrous cycle), or the CAR, ICAR, or Myo (collected on day 13 of the oestrous cycle) of Old groups. Nuclei are counterstained with DAPI (dark blue); scale bars are 50 μm.

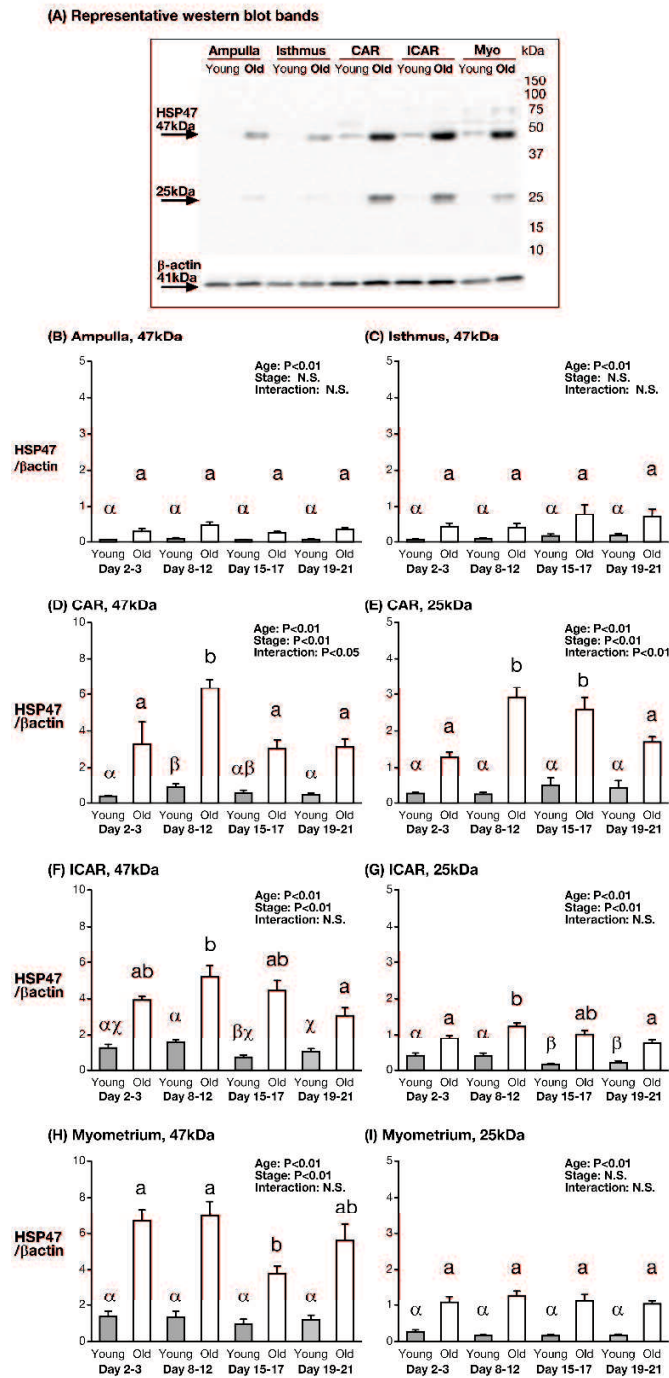


**Fig. 5.7.** Representative photos of western blotting analysis for HSP47 or anti- $\beta$ -actin mouse antibodies in extracts from ampulla, isthmus, CAR, ICAR, and myometrium (Myo) in the Young and Old groups (A). Relative HSP47 protein levels normalised to those of  $\beta$ -actin in the ampulla (B), isthmus (C), CAR (D), ICAR (E), or myometrium (F) in the Young and Old

groups. The header in the upper corner of each graph represents the results of two-factor ANOVA followed by Fisher's PLSD test, including the effect of age (Young or Old) and effect of stage and interaction. Greek letters ( $\alpha$ ,  $\beta$ , or  $\chi$ ) above the grey left-side bars indicate significant between-stage differences in expression in Young samples; letters (a, b, or c) above the white right-side bars indicate significant between-stage differences in expression in Old samples (one-factor ANOVA followed by Fisher's PLSD test). N.S., non-significant.

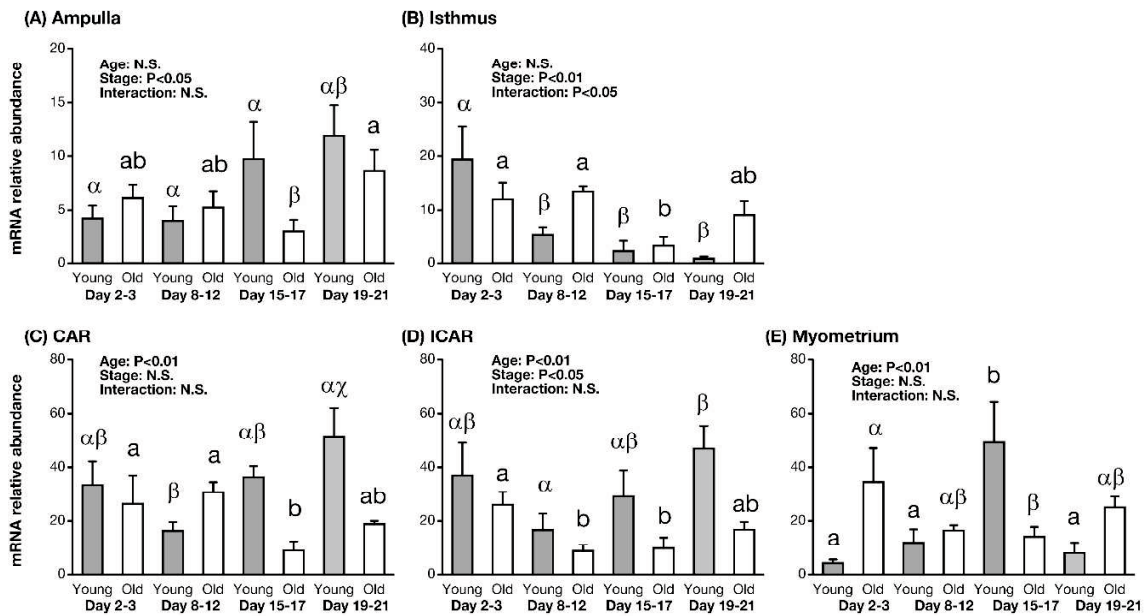


**Fig. 5.8.** Relative *HSP47* mRNA levels (mean  $\pm$  SEM) in the ampulla (A), isthmus (B), CAR (C), ICAR (D), or Myo (E) in healthy, post-pubertal growing nulliparous heifers (Young group) and old multiparous cows (Old group), as determined via RT-qPCR. Data were normalised to the geometric means of *C2orf29* and *SUZ12* levels. The header in the upper corner of each graph represents the results of two-factor ANOVA followed by Fisher's PLSD test, including the effect of age (Young or Old) and effect of stage and interaction. Greek letters ( $\alpha$ ,  $\beta$ , or  $\chi$ ) above the grey left-side bars indicate significant between-stage differences in expression in Young samples; letters (a, b or c) above the white right-side bars indicate significant between-stage differences in expression in Old samples (one-factor ANOVA followed by Fisher's PLSD test).

N.S. is abbreviation of non-significant.

#### 5.4. Discussion

We developed a new method that uses a denatured collagen detection reagent to identify denatured collagen-rich areas. The picro-sirius red stain showed red or orange colour in almost all parts of oviduct and uterus, including the epithelium. Boos (2000) reported the presence of collagen types I, III, IV, and VI in various parts of the uterus and the presence of collagen types IV and VI in the epithelium. We did not identify the collagen type in this study, but collagen was present in almost all parts of the oviduct and uteri. The results indicated that the levels of denatured collagen in old oviducts and uteri were higher than those in the oviducts and uteri of young ones. Thus, it is possible that repeated pregnancy and parturition increase the denatured collagen. Another possible reason for such an increase in the levels of denatured collagen may be infection and inflammation because lipopolysaccharides decrease collagen synthesis in myometrial explants from women (Wendremaire *et al.* 2013).

The tunica mucosa of oviducts and epithelia of the endometrium are located adjacent to the lumen, and thus, the structure of these layers may be susceptible to damage or frequent changes. Ovarian steroid hormones drive ECM remodelling in the bovine oviduct (Gonella-Diaza *et al.* 2018). Therefore, even young heifers may require collagen biosynthesis because these layers provide growth factors and nutrients for embryogenesis (Hugentobler *et al.* 2010; Besenfelder *et al.* 2012).

Little is known regarding HSP47 expression in the oviducts and uteri of all species. Therefore, we were unable to compare the data obtained by the current study with those of previous studies. The high HSP47 protein amounts observed in old oviducts and uteri compared with those in the young oviducts and uteri was somewhat unexpected because body weights of heifers were still in the phase of increasing (Inoue *et al.* 2020), and thus, we

speculated that increased size of the uteri and oviducts may also play a role in HSP47 expression. Little is known regarding postnatal changes associated with the sizes of bovine oviducts and uteri, as growth continues at least until 15 months of age in beef heifers (Honaramooz *et al.* 2004). However, the minimum age at first calving among about 2600 Japanese Black heifers was 21.4 months old (Inoue *et al.* 2020). Therefore, it was possible that the growth of oviducts and uteri of the young group was completed before sampling in this study.

We must be careful in interpreting the data obtained using the anti-HSP47 antibody for two reasons. First, the antibody is not recommended for immunohistochemistry in frozen sections by the supplier. However, we observed increased denatured collagen in the paraffin section in our preliminary trial using the denatured collagen detection reagent because the steps of paraffin embedding and deparaffinisation increased the denatured collagen. Second, we observed an extra 25 kDa band in the western blot. We could not find any paper reporting another size of HSP47. Therefore, we must be careful as the HSP47 signal in the immunohistochemistry results may have been caused by another protein. However, we performed western blotting using another anti-HSP47 mouse monoclonal antibody, clone M16.10A1 (Enzo Life Sciences, Inc.) and we observed both the 25 kDa and 47 kDa bands (Supplementary Figure 5.9). We tried to search similar proteins using the amino acid sequence of bovine HSP47 using protein BLAST. However, we could not find any protein with high homology. Therefore, further studies are required to identify the protein that the 25 kDa band corresponds to.

Importantly, HSP47 protein amount was increased in areas other than the denatured collagen-rich areas in old cows. These results suggested a possibility that collagen synthesis may not occur in denatured collagen-rich areas, indicating that a damaged structure may

remain uncured. This may explain the increased infertility observed in older beef cows (Osoro and Wright 1992).

However, this brings into question the physiological significance of increased HSP47 protein amount observed in other areas with less denatured collagen. Notably, an abnormal increase in collagen synthesis by fibroblasts induced by transforming growth factor (TGF)- $\beta$ 1 and its isoforms may lead to adenomyosis and ectopic endometria in women (Cheong *et al.* 2019). TGF- $\beta$ 1 may also exert important pathological effects on fibroblasts during equine endometriosis (Szostek-Mioduchowska *et al.* 2019). Although HSP47 is a key regulator of cell homeostasis, it also plays a role in fibrogenesis and fibrotic disorders in the liver, kidneys, and lungs. Excess HSP47 expression is an important step in collagen-related diseases, including keloids and fibrosis (Ito and Nagata, 2019). In addition, this study showed an increase in the number of fibroblasts in various parts of the oviducts and uteri, thereby suggesting fibrosis. Therefore, any increase in HSP47 protein amount may play an important role in inducing infertility in old cows.

The bovine endometrium is thicker on days 19–21 or days 2–3 than on other days (Sugiura *et al.* 2018). The highest amount of *HSP47* mRNA was observed in the ampulla, isthmus, CAR, and ICAR on either days 19–21 or days 2–3 in this study. Young oviducts and uteri showed a higher amount of *HSP47* mRNA than did old ones, whereas young oviducts and uteri showed a lower amount of HSP47 protein than did old ones. Based on these results, high levels of HSP47 protein may be required only temporarily in oviducts and uteri to avoid excess collagen synthesis, a possible cause for inflexibility. The HSP47 protein is bound to a ubiquitin-like protein, UBIN (Matsuda *et al.* 2001) and is degraded via the ubiquitin-proteasome system (Ito and Nagata 2016). Therefore, further studies are required to clarify the possibility that HSP47 protein is degraded via the ubiquitin-proteasome system

shortly after translation in young organs but is not degraded smoothly in old organs, resulting in abnormal collagen synthesis.

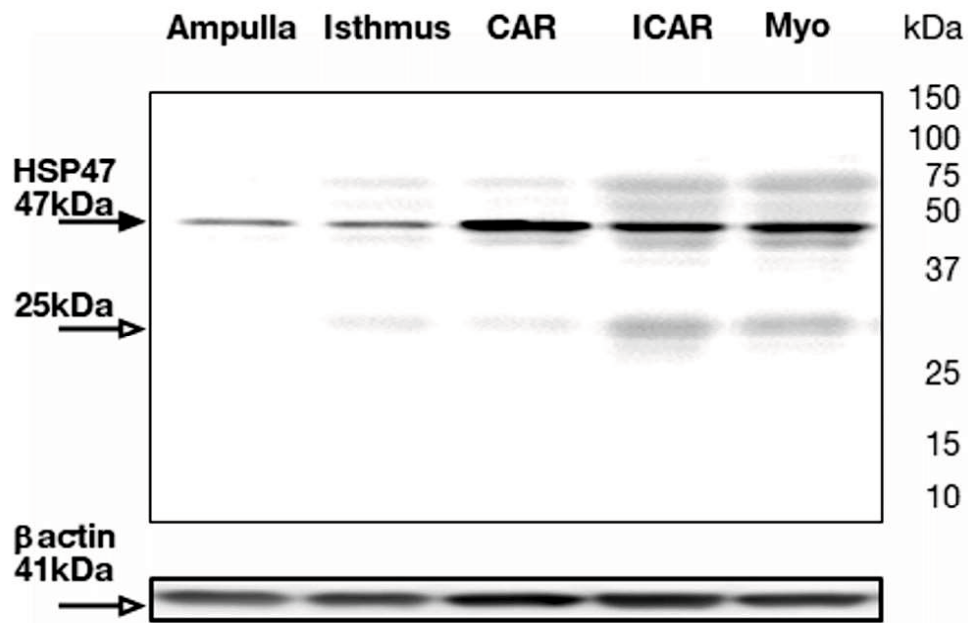
HSP47 is induced by cellular stresses, but it is also constitutively expressed, and its expression is always up- or down-regulated concomitantly with changes in the expression of various types of collagens, as reviewed by Ito and Nagata (2017). Therefore, a possible reason for the lower amount of *HSP47* mRNA observed in old organs is the increased collagen. We found 19 halves ERE and 3 half PRE-sequences in the 5'-flanking region of the bovine *SERPINH1* gene. A caveat here is that half ERE and PRE-like sequences are only five or six nucleotides long; such short sequence can appear at random at every 1024 ( $= 4^5$ ) or 2048 ( $= 4^6$ ) nucleotides. Thus, some of the identified sequences may not be involved in the control of gene expression. Detailed studies are required to clarify the mechanisms regulating HSP47 expression and the roles of oestradiol and progesterone.

HSP47 signals were observed in the epithelial layer and superficial stroma very near to the epithelial layer of oviducts and endometria of old individuals. HSP47 is expressed also in the surface epithelial cells of pneumonia (Kakugawa *et al.* 2005) and desmin-positive glomerular epithelium cells of the kidney (Razzaque and Taguchi 1999). Moreover, HSP47 expression in human nasal mucosa and lacrimal sac (obtained surgically) is associated with surgical outcome (Park *et al.* 2018). HSP47 induces mesenchymal phenotypes in mammary epithelial cells for cancer metastasis, and HSP47 is a hub of the ECM transcription network (Xiong *et al.* 2020). Therefore, further studies are required to clarify the relationship between HSP47 expression in the layers and fertility in cows.

Takita *et al.* (2019) produced a standard curve based on an EIA utilising the denatured collagen detection reagent and heated pure collagen (grade for culture dish coating). However, our attempts of immunoassays (HRP-conjugated streptavidin for EIA,

fluorochrome-conjugated streptavidin for fluorescent immunoassay, lanthanide-conjugated streptavidin for dissociation-enhanced lanthanide fluorescence immunoassay) failed to obtain a good parallel between the standard curve and serially diluted bovine oviduct or uterine extracts that were extracted using various methods. This was due to the samples showing strong matrix effects unlike pure collagen. Therefore, our comparison could be performed only on photographic images.

In conclusion, these findings revealed the specific location and amounts of damaged collagen and HSP47 in the oviducts and uteri of old cows compared to those in heifers.



**Supplementary Fig. 5.9.** Representative photos of western blotting using another anti-HSP47 mouse monoclonal antibody, clone M16.10A1 (Enzo Life Sciences, Inc.) or anti- $\beta$ -actin mouse antibodies in extracts from ampulla, isthmus, CAR, ICAR, and myometrium (Myo) in the Young and Old groups.

## **CHAPTER VI**

**(Study IV)**

**AMH stimulates HSP47 expression  
in bovine uterine epithelial cells but not myofibroblasts**

## **Abstract**

Uterine collagen is the most abundant extracellular matrix component of uterine ECM and plays a critical role in pregnancy. The HSP47 is the sole collagen-specific molecular chaperone. To investigate the mechanisms controlling HSP47 expression in uteri, I assessed the effect of AMH stimulation on HSP47 expression in cultured bovine uterine epithelial cells and myofibroblasts. Fluorescent immunohistochemistry confirmed the expression of AMHR2, AMH, and HSP47 in the epithelial, stromal, and myometrial layers of the uteri of JB cows. Fluorescent immunocytochemistry confirmed oxytocin receptor, AMHR2, AMH, HSP47, and collagen type-IV expression in cultured epithelial cells and myofibroblasts. Treatment of uterine epithelial cells and myofibroblasts with AMH at 10 or 100 ng/mL promoted ( $p < 0.05$ ) HSP47 expression in epithelial cells but not in myofibroblasts. The effect of AMH on HSP47 expression was suppressed by pre-treatment with the MEK/ERK inhibitor U0126 in epithelial cells, suggesting that AMH-induced HSP47 expression is mediated through the ERK pathway. In conclusion, these data showed that AMH stimulated HSP47 protein expression in bovine uterine epithelial cells, but not in myofibroblasts.

## 6.1. Introduction

Collagen, one of the most abundant constituents of the ECM, plays a critical role in a successful pregnancy, and abnormal collagen expression is associated with recurring miscarriages in women (Li *et al.* 2019a, Shi *et al.* 2020). The dysregulation of ECM remodeling in bovine endometrium may impair fertility (Scolari *et al.* 2016).

Collagen denaturation is increased in various diseases, including cancer, osteoporosis, and arthritis (Fields 2013, Ito and Nagata 2019). We recently showed that levels of denatured collagen are increased in the uteri of old cows due to repeated pregnancies using a new denatured collagen visualization method (Ferdousy and Kadokawa 2022). Subsequently, we discovered increased levels of the 47 kDa heat shock protein (HSP47), the sole procollagen-specific molecular chaperone, in the uteri of old cows as compared to young ones (Ferdousy and Kadokawa 2022). HSP47, the sole molecular chaperone encoded by *SERPINH1*, is essential for the correct folding of the unique triple-helical structure of collagen (Ito and Nagata 2019). HSP47 also plays an important role in the synthesis of collagen, as well as in the prevention of procollagen aggregation (Duarte and Bonatto 2018). However, the mechanisms regulating HSP47 in the uterus have not been investigated before.

AMH, a member of the TGF- $\beta$  family of proteins, is primarily secreted by the preantral and small antral follicles in female animals (Bhide and Homburg 2016). AMH expression is well-characterized in ovaries and plays an important role in regulating follicular development (Hernandez-Medrano *et al.* 2012) and inhibiting follicular atresia (Sefrioui *et al.* 2019). Concentrations of circulating AMH can help predict the number of high-quality embryos produced by various mammals, including cows and humans (Arouche *et al.* 2015; Sefrioui *et al.* 2019). Further, plasma AMH concentrations are positively correlated with pregnancy rates in various animals, including humans and cows (Ribeiro *et al.* 2014; Josso

2019). Because high-quality embryos and conception result from synchronous regulation by the sperm, ovum, and uteri, AMH may play an important role in maintaining appropriate condition of uterine for fertility. Recent studies have revealed the extragonadal roles of AMH mediated by the activation of its primary receptor, namely, AMHR2, in the anterior pituitary glands of rats and bovines (Garrel *et al.* 2016; Kereilwe *et al.* 2018). Importantly, women with low blood AMH concentrations have been shown to have a higher risk of miscarriage (Tarasconi *et al.* 2017; Lyttle *et al.* 2018). Furthermore, both bovine endometria and myofibroblasts express AMHR2 (Ferdousy *et al.* 2020a) and AMH (Ferdousy *et al.* 2020b). Endometria likely secrete AMH into the uterine fluids at least femtomolar level (Ferdousy *et al.* 2020b). These data suggest the role of AMH and AMHR2 in HSP47-rich areas of the uterus. However, the association between AMH and HSP47 expression has not been investigated before. Therefore, in this study, we assessed the role of AMH in regulating HSP47 expression in uterine epithelial cells and myofibroblasts.

## **6.2. Materials and Methods**

### **6.2.1. Sample collection**

All experiments were performed according to the Guiding Principles for the Care and Use of Experimental Animals in the Field of Physiological Sciences (Physiological Society of Japan) and approved by the Committee on Animal Experiments of Yamaguchi University.

We followed a previously reported method (Ferdousy *et al.* 2020a 2020b) to obtain the CAR and ICAR endometrium, and uterine myometrium from healthy postpubertal, growing, young nulliparous heifers ( $22.1 \pm 1.0$  months old) and old multiparous JB beef cows ( $N=5$ ,  $130.1 \pm 15.6$  months old;  $9 \pm 1$  parities; sacrificed at least 3 months after the last parturition) at a local abattoir. The heifers were at days 8 to 15 of the estrous cycle (day 0 = day of estrous), as determined via macroscopic examination of the ovaries and uterus (Miyamoto *et al.* 2000). The samples collected were from the side ipsilateral to the corpus luteum. We collected at least five samples per group per day. The middle area of the uterine horn was opened longitudinally using scissors, and CAR was carefully dissected so as not to include ICAR; subsequently, similarly ICAR endometrium areas, followed by myometrium areas were obtained. The collected samples were stored in 4% PFA at 4 °C for 16 h for immunohistochemistry.

### **6.2.2. Antibodies and blocking peptides for immunohistochemistry and immunocytochemistry**

For immunohistochemistry and immunocytochemistry, we used the anti-HSP47 rabbit polyclonal antibody (AP7366B; Abcepta Inc.) that we have previously used in bovine CAR, ICAR, and myometria (Ferdousy and Kadokawa 2022). The anti-human HSP47 rabbit antibody recognizes the mature C-terminal of human HSP47 (corresponding to amino acids 390-418; FLVRDTQSGSLLFIGRLVLRPKGDKMRDEL). This sequence has 100%

homology to amino acids 390-418 of the mature C-terminal of bovine HSP47 but no homology to other bovine proteins, as determined using protein BLAST (NCBI reference sequence: NP\_001193943.1 (human HSP47) and NP\_001039528.1 (bovine HSP47)). We also used blocking peptides for this antibody (P50454, Abcepta).

We also used the original anti-AMHR2 chicken antibody (Kereilwe *et al.* 2018) and anti-human AMH mouse monoclonal antibody (MCA2246T; Bio-Rad, Hercules, CA, US) to determine the expression of AMHR2 and AMH, respectively. We have previously used these antibodies to verify the expression of AMHR2 and AMH in bovine ovaries (Kereilwe *et al.* 2018; Kereilwe and Kadokawa 2019), as well as bovine CAR and ICAR (Ferdousy *et al.* 2020a, 2020b). We used the antigen peptide synthesized by Scrum Inc. as a blocking peptide for each of these antibodies.

Anti-bovine collagen IV rabbit polyclonal antibody (GTX44066, Genetex Inc.) was used for immunocytochemistry because both bovine uterine epithelial cells and myofibroblasts express collagen IV (Boos 2000). We used purified bovine collagen IV (Nitta Gelatin Inc.) as a blocking peptide for the antibody.

Both bovine uterine epithelial cells and myometrium express oxytocin receptor (Fuches *et al.* 1990). Therefore, we used anti-oxytocin receptor rabbit polyclonal antibody (BS-1314R, Bioss antibodies Inc.) for immunocytochemical oxytocin receptor detection. The antibody recognizes the C-terminal of mouse oxytocin receptor (corresponding to amino acids 325-388;

WIYMLFTGHLFHELVQRFLCCSARYLKGSRPGETSISKKSNSSTFVLSRRSSSQRSC

SQPSSA). This sequence has 90% homology to amino acids 329-391 of the C-terminal of

bovine oxytocin receptor

(WIYMLFTGHLFQELVQRFLCCSFRRLLKGSRPGETSVSKKSNSSTFVLSQYSSSQRR

CSQPSTL) but no homology to other bovine proteins, as determined using protein BLAST (NCBI reference sequence: NP\_001074616.1 (mouse) and NP\_776559.1 (bovine). We used the antigen peptide synthesized by Scrum Inc. as a blocking peptide for this antibody.

Epithelial cells are cytokeratin-positive and vimentin-negative, while fibroblasts are vimentin-positive and cytokeratin-negative (Yamamoto *et al.* 2014). Therefore, we performed immunocytochemistry to confirm the purity of cultured cells, using anti-bovine pancytokeratin mouse monoclonal antibody and anti-bovine vimentin mouse monoclonal antibody (C2931 and V2258, both from Sigma-Aldrich and diluted as 1:1,000) as primary antibodies and Alexa Fluor 488 goat anti-mouse IgG (1 µg/mL, Thermo Fisher Scientific) as secondary antibody. These antibodies have been used for immunocytochemistry in cultured bovine oviduct epithelial cells (García *et al.* 2017), as well as bovine CAR, ICAR, and myometria (Ferdousy *et al.* 2022).

### **6.2.3. Immunofluorescence staining and confocal microscopy**

After storage in 4% PFA in PBS at 4°C for 16 h, tissue blocks were placed in 30% sucrose-PBS until the blocks were infiltrated with sucrose. We used immunohistochemistry to detect ovarian and uterine AMH and AMHR2 as previously described (Kereilwe *et al.* 2018; Kereilwe and Kadokawa 2019; Ferdousy *et al.* 2020a, 2020b). Briefly, the fixed tissue blocks were placed in 30% sucrose PBS until the blocks were infiltrated with sucrose. The blocks were then frozen in an embedding medium (Tissue-Tek OCT compound; Sakura Finetechnical Co. Ltd) and maintained at -80°C. Next, the blocks were sectioned into 15-µm-thick cross-sections using a cryostat (Leica Microsystems Pty Ltd.) and mounted on microscope slides (MAS coat Superfrost; Matsunami-Glass). The sections were treated with 0.3 % triton X-100-PBS for 15 min and blocked by incubating them with 0.5 mL of PBS

containing 10% normal goat serum (Wako Pure Chemicals) for 1 hr at 25°C. The slides were incubated with a cocktail of primary antibodies containing the anti-AMH, anti-AMHR2, and anti-HSP47 antibodies (all diluted as 1:1,000) for 12 hr at 4 °C. After the primary antibody incubation, the sections were washed twice with PBS and then incubated with a cocktail of fluorochrome-conjugated secondary antibodies (Alexa Fluor 488 goat anti-chicken IgG, Alexa Fluor 546 goat anti-mouse IgG, and Alexa Fluor 647 goat anti-rabbit IgG [all diluted to 1 µg/mL, and all from Thermo Fisher Scientific]) and 1 µg/mL of 4', 6'-diamino-2-phenylindole (DAPI; Wako Pure Chemicals) for 4 hr at 25°C.

The stained sections on slides were observed by confocal microscopy (LSM710; Carl Zeiss) equipped with a diode laser 405 nm, argon laser 488 nm, and HeNe laser 533 nm. Images obtained by fluorescence microscopy were scanned with a 20×, 40×, 63× or 100× objective and recorded with a CCD camera system controlled by ZEN2012 black edition software (Carl Zeiss). The DAPI is shown in blue, and AMH is shown in green in the confocal images. To verify the specificity of the signals, we included several negative controls in which the primary antiserum had been omitted or pre-absorbed with 5 nM of the respective blocking peptide or in which normal rabbit IgG, normal mouse IgG, and normal chicken IgG (all from Wako Pure Chemicals) were used instead of the primary antibody. We also included negative controls in which the secondary antibodies had been omitted or normal goat IgG (Wako Pure Chemicals) were used instead of the secondary antibodies. Signal specificity was also confirmed using negative controls in which the secondary antibodies were pre-absorbed with 5 nM normal animal IgGs (all from Wako Pure Chemicals).

#### **6.2.4. Culture of bovine epithelial cells and treatment with AMH**

Uteri from adult (n = 6, 22 months old) non-pregnant healthy JB heifers were collected from a local slaughterhouse within 10-20 min after exsanguination. Experiments were repeated six times using each of the six different samples. The heifers were at days 8 to 15 of the oestrous cycle (day 0 = day of estrous), as determined via macroscopic examination of the ovaries and uterus (Miyamoto *et al.* 2000). According to the regulations of our university, we were disallowed from using the uterine cells of old cows for cell culture to avoid contamination by introducing mycoplasma in the culture room. Also, the thickness and condition of endometrium and myometrium were inappropriate for culture.

The uteri were transported in an icebox from the local slaughterhouse to the laboratory within 2 h of collection. Isolation and culture of bovine epithelial cells were carried out using previously described methods (Takahashi *et al.* 2001). Briefly, each uterine horn was filled with approximately 20-50 ml of Dulbecco's PBS containing 0.76% EDTA and pre-incubated for 1 h at 37 °C. Next, the uterine horns were cut vertically to expose the uterine lumen. Then uterine epithelium was scraped off by a surgical blade and incubated for 5 min at 37 °C in Dulbecco's Modified Eagle's Medium and Ham's F-12, 1:1 (DMEM/Ham's F-12; 08460-95, Nacalai Tesque) supplemented with 0.1% (W/V) collagenase (032-22364, Wako Pure Chemicals). The epithelial cells were then filtered (70 µm; PluriStrainer, PluriSelect Life Science), centrifuged (10 min at 100 × g), and then the suspended cells were centrifuged (10 min at 100 × g) in gradients of percoll (50, 25 and 12.5% v/v; Sigma Aldrich). The final pellets of epithelial cells were re-suspended in approximately 10 mL of DMEM/Ham's F-12 with 10% (v/v) fetal bovine serum (FBS; Thermo Fisher Scientific), 1× MEM nonessential amino acids (Thermo Fisher Scientific), 100 IU/mL penicillin (Nacalai Tesque), 100 µg/mL streptomycin (Nacalai Tesque), and 2 µg/mL amphotericin B (Sigma Aldrich). The cells

were counted using a cell counter (Model TC20, Bio-Rad). Trypan blue (0.5%) dye exclusion test revealed cell viability was > 95%. Then, 3 mL of cell suspension per well (at a density of  $0.33 \times 10^5$  cells/mL) were seeded in 6-well plates (Thermo Fisher Scientific) coated with gelatin (GLS250, Porcine skin, Nitta Gelatin Inc.) and cultured at 38.5 °C in a humidified atmosphere of 5% CO<sub>2</sub> and 95% air. Gelatin, instead of collagen, was used for coating as it is the molecular derivative of collagen obtained through the irreversible denaturation of collagen proteins. The molecular structure and function of gelatin and collagen are similar (Bello *et al.* 2020). The structure of collagen may vary with sources and seasons, which may affect results, unlike that by gelatin (Liu *et al.* 2015). Moreover, gelatin shows lower immunogenicity, lower potential for the formation of aromatic radicals, and is less expensive (Rose *et al.* 2014). The medium was changed every two days until the cells reached 70-80% confluence. The cells were then passaged using accutase (Nacalai Tesque). The cells so obtained were re-suspended in 10 mL DMEM/F12 containing 10% FBS, 1 × MEM nonessential amino acids, 100 IU/mL penicillin, and 100 µg/mL streptomycin. Then, 1 ml of cell suspension (at a density of  $1.0 \times 10^6$  cells/ml) was seeded in 12-well plates for the AMH test. The remaining cells were cultured in a microscopy chamber (µ-Slide 8 well high, ib80806, Ibidi) for three days for immunocytochemistry.

After epithelial cells reached 70-80% confluence, the medium was replaced with 720 µl DMEM/F12 containing 0.1% BSA (IgG-free Protease-free culture grade, 032-22364, Wako Pure Chemicals), 1% FBS, 1 × MEM nonessential amino acids, 100 IU/mL penicillin, and 100 µg/mL streptomycin and incubated at 38.5 °C for 2 h. Then 80 µl of medium containing increasing doses of bioactive human recombinant AMH (final concentrations of 0, 1, 10, 100 ng/mL; 100 ng/mL is 0.85 pM; R&D Systems] was added to the culture media and incubated for 8 h. The bioactive region in the carboxyl-terminal region of mature AMH

(Belville *et al.* 2004) of bovines (NP\_776315.1) and goats (XP\_017906255.1) has 96% homology with that of human AMH (NP\_000470.2), and the same recombinant human AMH product has effects on goat follicles (Rocha *et al.* 2016), bovine anterior pituitary cells (Kereilwe *et al.* 2018), and cultured pig granulosa and theca cells (Li *et al.* 2019b). A low FBS concentration medium has also been used in a previous study to evaluate the effects of 10 ng/mL of recombinant AMH on the expression of various genes in cultured pig granulosa and theca cells (Li *et al.* 2019b). For comparison, TGF wells were cultured without AMH and with bioactive human recombinant TGF- $\beta$ 1 (final concentration, 0.85 pM; Peptide Institute Inc., 100% homology with bovine sequence (NCBI reference sequence: NP\_000651.3 (human) and AAA30778.1 (bovine))).

After 8 h of culture the culture medium was removed, the cells were treated with 300  $\mu$ L of tissue protein extraction reagent (T-PER; Thermo Fisher Scientific) containing protease inhibitors (Halt protease inhibitor cocktail, Thermo Fisher Scientific), and the samples were stored at -80°C until western blotting.

#### **6.2.5. Culture of bovine uterine fibroblasts and treatment with AMH**

Uteri from adult (n=6, 22 months old; at days 8 to 15 of the oestrous cycle) non-pregnant healthy JB heifers were collected at a local slaughterhouse within 10–20 min after exsanguination. The experiment was repeated six times with each of the six different samples. Isolation and culture of bovine uterine myofibroblasts were carried out using a previously described method (Vangipuram *et al.* 2013). Briefly, small pieces of uterine horn tissue (about as cube 2 cm on a side) were transported in ice-cold HEPES buffer (NaCl, 137 mmol/L; KCl, 3 mmol/L; Na<sub>2</sub>HPO<sub>4</sub>, 0.7 mmol/L; n-2-hydroxyethyl piperazine ethanesulfonic acid (HEPES), 25 mmol/L; glucose, 10 mmol/L; CaCl<sub>2</sub>, 360  $\mu$ mol/L; pH 7.2)

from the local slaughterhouse to the laboratory within 2 h. The tissue was incubated in 70% alcohol for 1 min in order to kill epithelial cells. The tissue was washed twice in HEPES buffer. Then, the myometrium layer was separated from the other layers using a surgical scissor, and the myometrium was placed in HEPES buffer in a small dish and cut into small cubes (approximately as cube 2 mm on a side) using a surgical blade. The tissue pieces were washed three times in HEPES buffer and three pieces per well were placed into 6-well plates coated with gelatin and incubated at 38.5 °C in 5% CO<sub>2</sub> and 95% air in DMEM/F-12 supplemented with 10% FBS, 1 × MEM nonessential amino acids, 100 IU/mL penicillin, 100 µg/mL streptomycin, and 2 µg/mL amphotericin B until the cells reached 70-80% confluence. Then, the cells were passaged using accutase. Next, the cells were re-suspended in 10 mL DMEM/F-12 containing 10% FBS, 1 × MEM nonessential amino acids, 100 IU/mL penicillin, and 100 µg/mL streptomycin. Then, 1 ml of cell suspension (at a density of 1.0×10<sup>6</sup> cells/ml) was seeded in 12-well plates for the AMH test. The remaining cells were cultured in the microscopy chamber for three days for immunocytochemistry.

After myofibroblasts reached 70-80% confluence, the medium was replaced with 720 µl DMEM/F-12 containing 0.1% BSA, 1% FBS, 1 × MEM nonessential amino acids, 100 IU/mL penicillin, and 100 µg/mL streptomycin and incubated at 38.5°C for 2 h. Then 80 µl of the medium containing either recombinant AMH (final concentrations of 0, 1, 10, 100 ng/mL) or recombinant TGF (final concentration, 0.85 pM) was added to the culture media and incubated for 8 h. Then, the proteins were extracted using 300 µL of T-PER containing protease inhibitors and stored at -80°C until western blotting.

### **6.2.6. Fluorescent immunocytochemistry**

Cells attached to the microscopy chamber were treated with 4% PFA in PBS for 3 min. After washing with PBS, the cells were treated with 0.1% Triton X-100 in PBS for 3 min and blocked by 10% normal goat serum for 30 min at 25°C. Then a cocktail of primary antibodies containing the anti-AMHR2 antibody with either anti-HSP47, anti-cytokeratin, anti-vimentin, anti-oxytocin receptor, or anti-collagen antibodies (all diluted as 1:1,000) was added to each chamber and incubated for 2 h at 25°C. After incubation with primary antibodies, the cells were washed twice with PBS, and then a cocktail of fluorochrome-conjugated secondary antibodies (Alexa Fluor 488 goat anti-chicken IgG, Alexa Fluor 546 goat anti-mouse IgG, and Alexa Fluor 647 goat anti-rabbit IgG (all 1 µg/mL) and 1 µg/mL of DAPI was added to the microscopy chambers and incubated for 2 h at 25°C. Finally, the cells were washed with PBS, the stained cells were observed by confocal microscopy, and fluorescence microscopic images were obtained along a single plane. To verify the specificity of the signals, several negative controls were included in which the primary antiserum had been omitted or pre-absorbed with 5 nM antigen peptide or in which the normal mouse IgG had been used instead of the primary antibody. Signal specificity was also confirmed using negative controls in which the secondary antibodies were pre-absorbed with 5 nM normal IgGs.

### **6.2.7. Effect of inhibition of the ERK pathway on AMH-induced HSP47 expression**

We assessed the effect of ERK pathway inhibition on AMH-induced HSP47 expression in epithelial cells. Epithelial cells obtained from a different set of post-pubertal JB heifers (n = 6, 22 months old; at days 8 to 15 of the estrous cycle) were cultured using the aforementioned methods. The experiment was repeated six times using each of the six

different samples. After the cells reached 70-80% confluence, the old medium was replaced with 640 µl of the low FBS medium and incubated at 38.5°C for 2 h. Then, 80 µl of U0126 (ERK inhibitor; final concentration, 1 µM; Enzo Biochem, Inc.) were added to the culture and incubated for 30 min for pre-treatment. Gonadotropin secretion in cultured bovine anterior pituitary cells has been investigated before using the same dose of U0126 and pre-treatment time (Kereilwe *et al.* 2018). After the pre-treatment, 80 µl of the same diluted recombinant AMH (final concentration, 100 ng/mL) were added to culture media and further cultured for 8 h. The cell proteins were extracted using the 300 µL of T-PER containing protease inhibitors, and the sample was then stored at -80°C until western blotting.

#### **6.2.8. Western Blotting for HSP47 detection**

The total protein content of each sample was measured using a bicinchoninic acid kit (Thermo Fisher Scientific). The extracted protein sample was boiled with Sample Buffer Solution with Reducing Reagent (6x) for SDS-PAGE (09499-14; Nacalai Tesque) for 3 min at 100 °C. The protein samples (400 ng of total protein) were loaded onto a polyacrylamide gel (Any KD Criterion TGX gel, Bio-Rad) along with a molecular weight marker (Precision Plus Protein All Blue Standards; Bio-Rad). Then, the proteins were resolved using sodium dodecyl sulphate–polyacrylamide gel electrophoresis at 100 V for 90 min. The proteins were transferred on to PVDF membranes (Trans-blot turbo PVDF, Bio-Rad) with electroblotting at 2.5 A, 25 V, for 7 min using a Trans-blot Turbo system (Bio-Rad).

We used a Can Get Signal Immunoreaction Enhancer kit (Toyobo Co. Ltd) for blocking membrane (1 hour at 25 °C), primary antibody reaction (1 hour at 25 °C) with the anti-HSP47 rabbit polyclonal antibody (1:400,000 dilution with immunoreaction enhancer solution), and secondary antibody reaction (1 hour at 25 °C) with goat anti-rabbit IgG

horseradish peroxidase-conjugated antibody (Bethyl Laboratories Inc.; 1:400,000 dilution with immunoreaction enhancer solution).

The protein bands were visualised using an ECL-Prime chemiluminescence kit (GE Healthcare, Amersham, UK) and a CCD imaging system (LAS-3000 Mini; Fujifilm). The images were exported using the Multigauge (version 3.0; Fujifilm) software. To verify the specificity of the signals, we included several negative controls in which the primary antibodies had been omitted or normal rabbit IgG (Wako Pure Chemicals) antibodies were used instead of the primary antibodies. Signal specificity was also confirmed using negative controls in which the primary antibodies were pre-absorbed with 5 nM of antigen peptide.

The antibodies were removed from the PVDF membrane with a stripping solution (Nacalai Tesque) prior to the blocking and subsequent immunoblotting with an anti- $\beta$ -actin mouse monoclonal antibody (1:400,000 dilution; Sigma-Aldrich).

All relevant bands were cropped from the exported file using Adobe Photoshop element ver. 2020 (Adobe, San Jose), and pasted onto a graph created using DeltaGraph ver. 7.5.2J (Red rock software). ImageQuant TL (version 8.2; Cytiva, Marlborough) software was used to measure the band sizes and volumes (calculated using rolling ball background subtraction). The protein amount of HSP47 was normalised against  $\beta$ -actin.

### **6.2.9. Statistical analysis**

The statistical analyses were performed using StatView version 5.0 for Windows (SAS Institute, Inc.). Grubb's test verified the absence of outliers. The Shapiro-Wilk's test and Kolmogorov-Smirnov Lilliefors test verified the normality of distribution of each variable. One-factor analysis of variance was used to evaluate the effect of AMH treatments on epithelial cells and myoblasts, and post-hoc comparisons with Fisher's protected least

significant difference test were used to analyze western blotting data for HSP47. The level of significance was set at  $P < 0.05$ . Data are expressed as mean  $\pm$  standard errors of the mean (SEM).

### 6.3. Results

Immunohistochemistry confirmed the colocalization of AMHR2 and HSP47 in the luminal and glandular epithelium of CAR (**Fig. 6.1A, 6.1B**) and ICAR (**Fig. 6.1C, 6.1D**) of endometria. The stroma layer of CAR and myometria (**Fig. 6.1E, 6.1F**) showed AMHR2-negative, AMHR2-negative, and HSP47-positive epithelial cells, as well as AMHR2-positive, AMH-positive, and HSP47-positive myofibroblasts.

We observed more than  $10^3$  cells for each uterine epithelium by immunocytochemistry and confirmed that the 100% purity of the epithelial cells by confirming cytokeratin-positivity (**Fig. 6.2A**) and vimentin-negativity (**Fig. 6.2B**). Furthermore, all the cultured epithelial cells were AMHR2-positive (**Fig. 6.2A, 6.2B, and 6.2C**) and showed colocalization of the oxytocin receptor with AMHR2 (**Fig. 6.2A**). All the cultured epithelial cells were collagen type IV-positive (**Fig. 6.2C**). Both oxytocin receptors and AMHR2 were aggregated at the periphery (probably surface) of each cell or the cytokeratin-positive (**Fig. 6.2A**), HSP47-positive (**Fig. 6.2B**), or collagen IV-positive (**Fig. 6.2C**) areas (probably cytoplasm) of each cell.

We observed more than  $10^3$  cells for each uterine epithelium by immunocytochemistry and confirmed that the 100% purity of the myofibroblasts by confirming vimentin-positivity (**Fig. 6.3A**) and cytokeratin-negativity (**Fig. 6.3B**). Myofibroblasts were thinner and wider than the epithelial cells. All the cultured myofibroblasts were AMHR2-positive (**Fig. 6.3A, 6.3B, and 6.3C**) and showed co-localization of the oxytocin receptor with AMHR2 (**Fig. 6.3A**). All the cultured myofibroblasts were collagen type IV-positive (**Fig. 6.3C**). Both oxytocin receptors and AMHR2 were aggregated at the periphery (probably surface) of each cell. However, stronger AMHR2 signals were observed at the cytokeratin-positive (**Fig. 6.3A**), HSP47-positive (**Fig. 6.3B**), or collagen IV-positive (**Fig. 6.3C**) area of each cell.

**Fig 6.4** shows representative photos of western blotting for HSP47 in extracts from cultured uterine epithelial cells treated with increasing concentrations of AMH. A main 47 kDa band corresponding to HSP47 and a weak 75 kDa band were observed for the control and all treatments. Treatment with 10 and 100 ng/ml AMH increased HSP47 expression corresponding to the 47 kDa band, while treatment with 100 ng/ml AMH only increased the expression of the protein corresponding to the 75 kDa band. In contrast, treatment with the same molar concentration (0.85 pM) of TGF- $\beta$ 1 did not affect the expression of either of the proteins.

**Fig 6.5** shows representative photos of western blotting for HSP47 in extracts of the myofibroblasts treated with increasing concentrations of AMH. All the tested concentrations of AMH and TGF- $\beta$ 1 did not increase the expression of HSP47 corresponding to the 47 kDa band and the protein corresponding to the 75 kDa band.

**Fig 6.6** shows representative photos of western blotting for HSP47 in extracts of the cultured epithelial cells treated with 100 ng/ml of AMH with or without pre-treatment with the MEK/ERK inhibitor U0126. U0126 treatment alone had no significant effect on HSP47 expression. However, U0126 pre-treatment inhibited the 100 ng/ml of AMH-mediated increase in HSP47 expression.

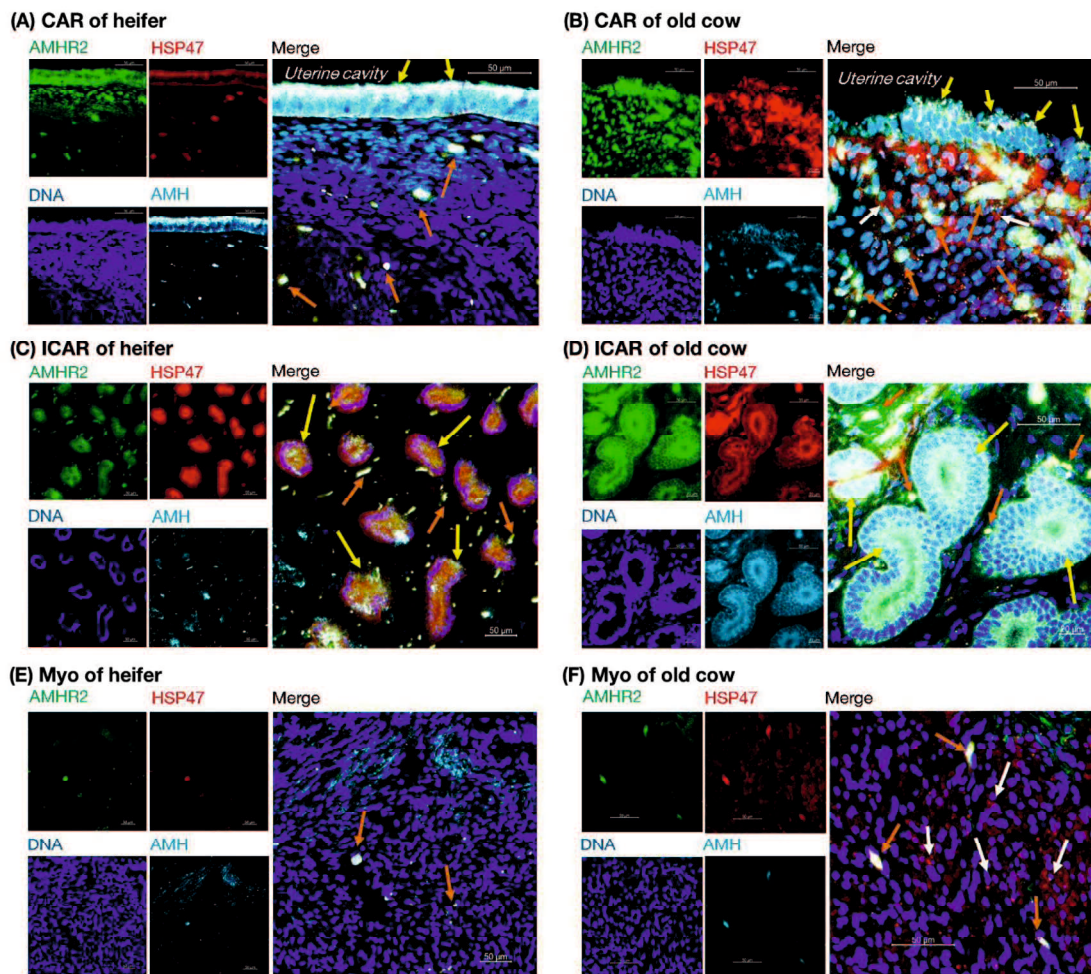


**Fig. 6.1.** Comparison of AMHR2-rich areas (green), AMH-rich areas (light blue), and HSP47-rich areas (red) in the CAR, ICAR, and uterine myometrium (Myo) (collected on day 3 of the oestrous cycle) of young heifer (22 months old) and old cows (130 months old, collected on day 13 of the estrous cycle). Nuclei are counterstained with DAPI (dark blue). The specimens showed signals corresponding to both AMHR2 and HSP47 in luminal epithelia, glandular epithelia, and stroma. The Merge panels show signals indicating the colocalization (yellow arrows) of AMHR2 and HSP47. AMHR2-negative, AMH-negative, and HSP47-positive epithelial cells are indicated by white arrows and appear abundantly in

the CAR (A) and Myo (C). AMHR2-positive, AMH-positive, and HSP47-positive myofibroblasts are indicated by brown arrows. The dark patches in old myometria are broken parts. Scale bars: 50  $\mu$ m.

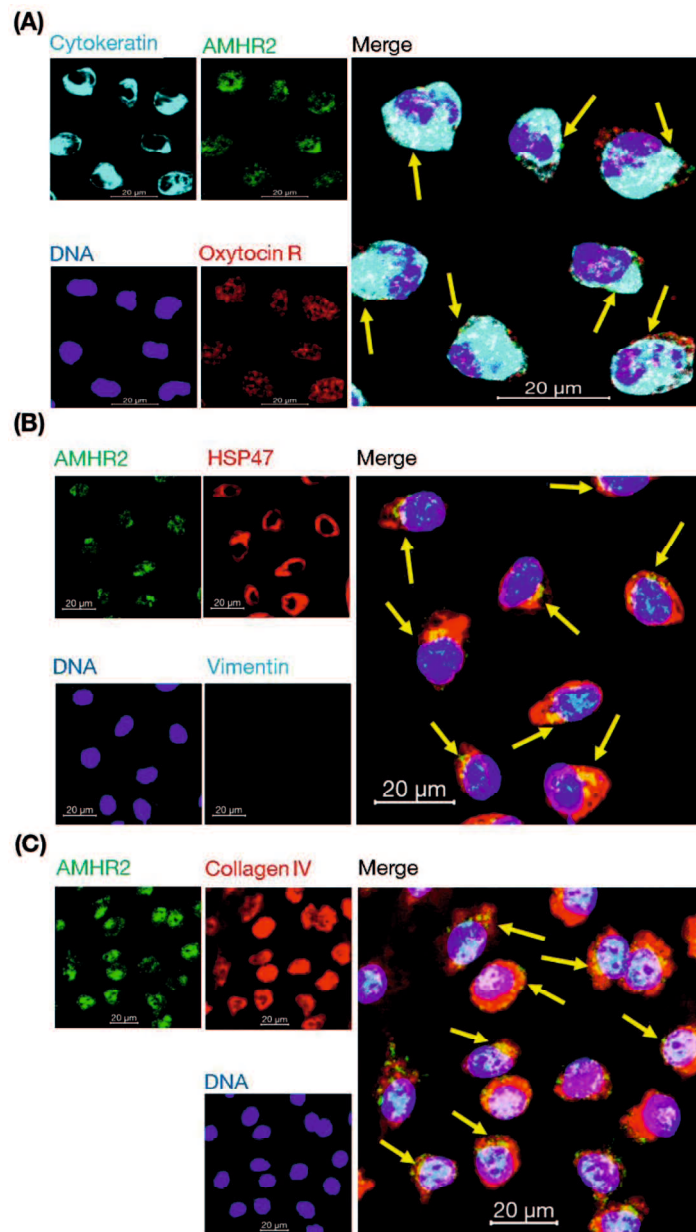


**Fig. 6.2.** Immunocytochemistry of cultured uterine epithelial cells for AMHR2 (green) with oxytocin receptor (A), HSP47 (B), or collagen type IV (C). Immunocytochemistry confirmed that all the cultured cells were cytokeratin-positive (A) and vimentin-negative (B), verifying pure epithelial cell culture. Scale bar: 20  $\mu\text{m}$ .

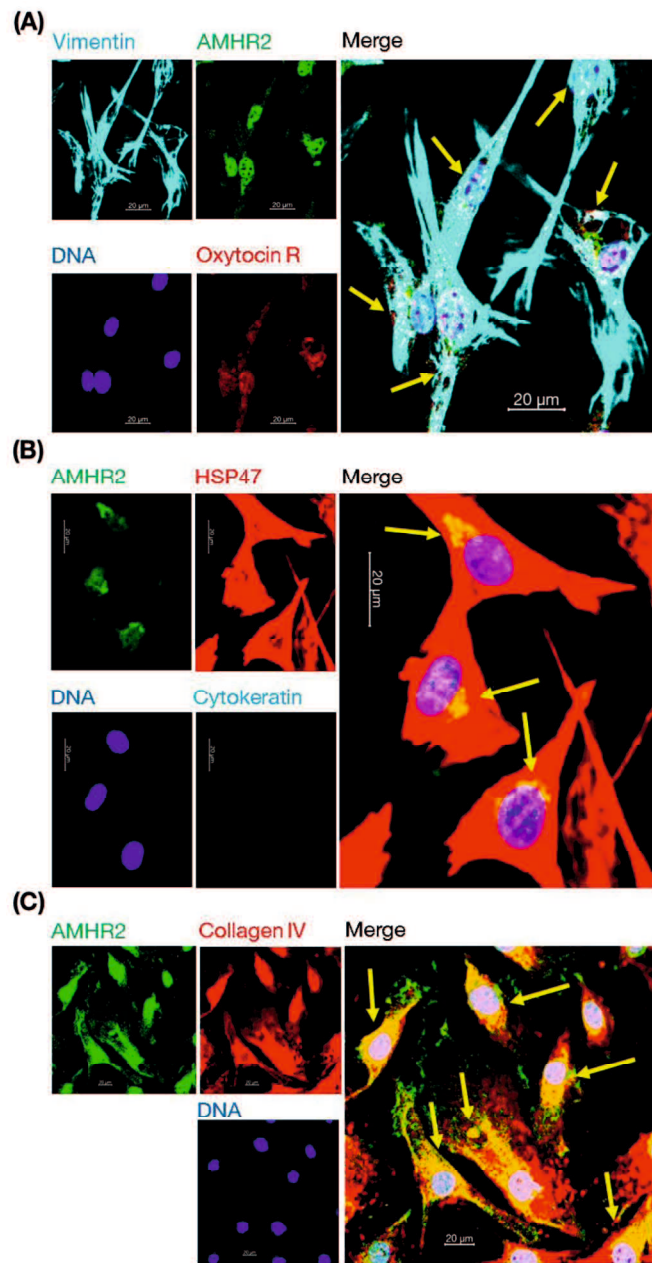


**Fig. 6.3.** Immunocytochemistry of cultured uterine myofibroblasts for AMHR2 (green) with oxytocin receptor (A), HSP47 (B), or collagen type IV (C). Immunocytochemistry confirmed that all the cultured cells were vimentin-positive (A) and cytokeratin-negative (B), verifying pure myofibroblast culture. Scale bar: 20 μm.

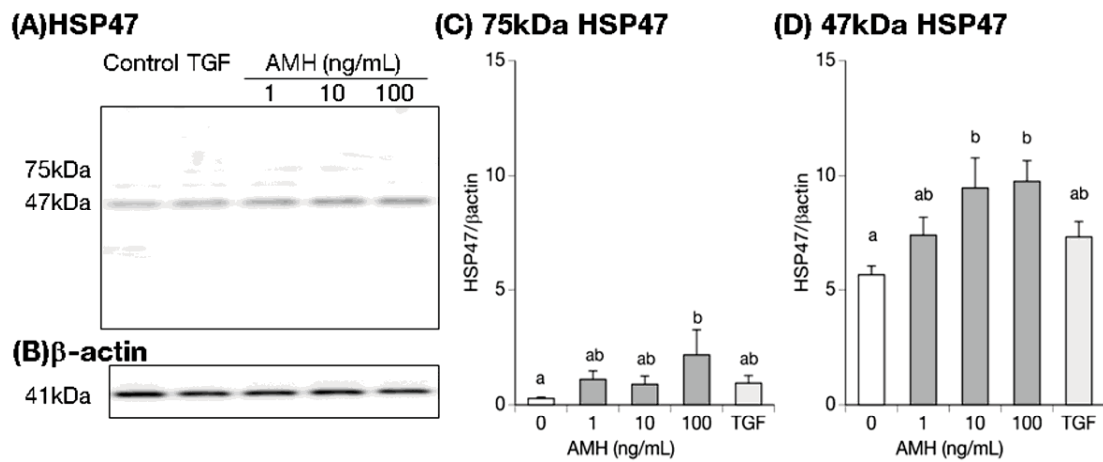


**Fig. 6.4.** Representative photos of western blotting for HSP47 (A) or  $\beta$ -actin (B) using extracts of cultured uterine epithelial cells treated with AMH [final concentrations, 0, 1, 10 ng/mL, or 100 ng/mL (0.85 pM)], or with TGF- $\beta$ 1 (final concentration, 0.85 pM). A dark 47 kDa band corresponding to HSP47 and a weak 75 kDa band were observed for control and all treatments. HSP47 levels were normalized to that of  $\beta$ -actin in both bands. The different letters (a or b) above the bars indicate significant difference in HSP47 expression due to different treatments (One-factor ANOVA followed by Fisher's PLSD test).

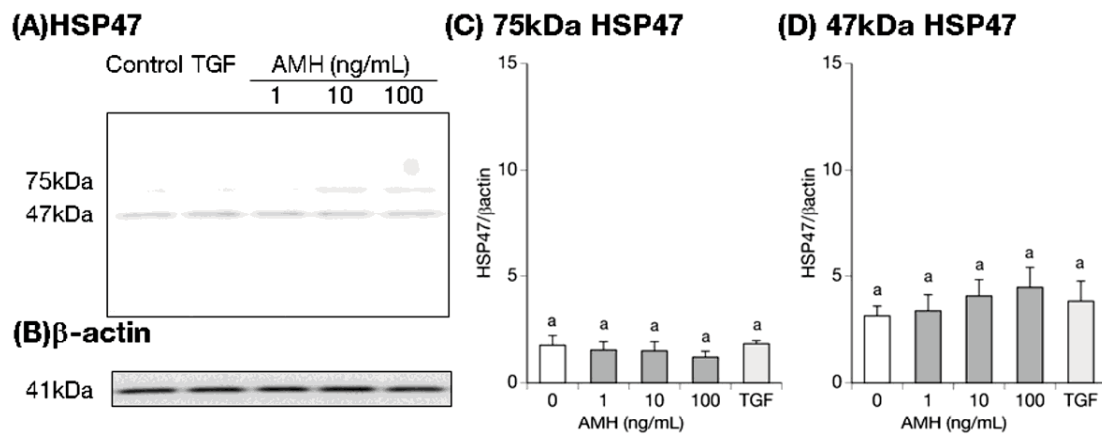
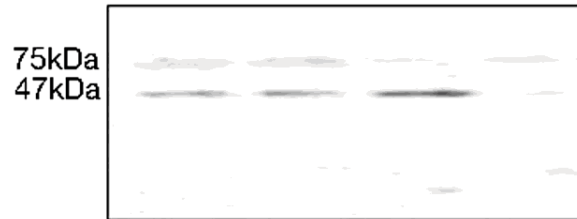


**Fig. 6.5.** Representative photos of western blotting for HSP47 (A) or  $\beta$ -actin (B) using extracts of cultured uterine myofibroblasts treated with AMH [final concentrations, 0, 1, 10 ng/mL, or 100 ng/mL (0.85 pM)], or TGF- $\beta$ 1 (final concentrations, 0.85 pM). A main 47 kDa band corresponding to HSP47 and a weak 75 kDa band were observed. HSP47 levels were normalized to that of  $\beta$ -actin in both bands. The same letters (a) above the bars indicate no significant differences in HSP47 expression due to different treatments (One-factor ANOVA followed by Fisher's PLSD test).

**(A) HSP47**

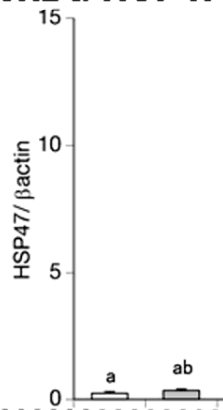
U0126 (mM)	0	1	0	1
AMH (ng/mL)	0	0	100	100



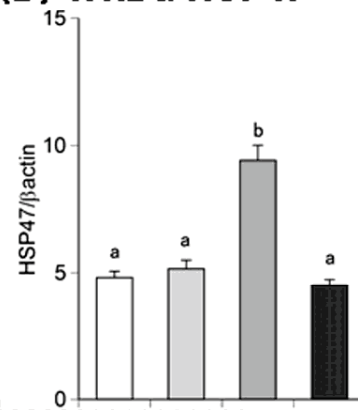
**(B)  $\beta$ -actin**



**(C) 75kDa HSP47**



**(D) 47kDa HSP47**



U0126 (mM)	0	1	0	1
AMH (ng/mL)	0	0	100	100

**Fig. 6.6.** Representative photos of western blotting for HSP47 (A) or  $\beta$ -actin (B) using extracts of cultured uterine epithelial cells treated with AMH (final concentrations, 100 ng/mL) with or without pre-treatment with U0126. The different letters (a or b) above the bars indicate significant difference in HSP47 expression due to different treatments (One-factor ANOVA followed by Fisher's PLSD test).

#### 6.4. Discussion

We previously found increased levels of the heat shock protein HSP47, the sole procollagen-specific molecular chaperone, in the uteri of old than young cows (Ferdousy and Kadokawa 2022). However, the mechanisms regulating HSP47 in the uterus remain elusive. We previously reported the expression of AMHR2 (Ferdousy *et al.* 2020a), AMH (Ferdousy *et al.* 2020b), and HSP47 (Ferdousy and Kadokawa 2022) in the endometrium and stroma layers of young and old bovine uteri. However, the association between AMH and HSP47 has not been investigated before. In this study, we found that AMH induces HSP47 expression in uterine epithelial cells. Immunohistochemistry showed the co-localization of AMHR2 and HSP47 in the epithelial layers, reinforcing our previous findings. Endometria likely secrete AMH into the uterine fluid (Ferdousy *et al.* 2020b). We previously reported the strong expression of HSP47 in the epithelial layer and superficial stroma near the epithelial layer of endometrium layers in the uteri of both young and old cows (Ferdousy and Kadokawa 2022). Therefore, AMH may be transported via blood or uterine fluids and may play autocrine and paracrine roles in epithelial layers to control collagen synthesis by controlling HSP47 expression. HSP47 is also expressed in the surface epithelial cells in pneumonia (Kakugawa *et al.* 2005) and in desmin-positive glomerular epithelial cells of the kidney (Razzaque and Taguchi 1999). HSP47 expression in the human nasal mucosa and the lacrimal sac is associated with surgical outcomes (Park *et al.* 2018). HSP47 induces mesenchymal phenotypes in mammary epithelial cells for cancer metastasis, and HSP47 is a hub of the ECM transcription network (Xiong *et al.* 2020). The epithelial layer of the endometrium is located adjacent to the lumen, and thus its structure may be susceptible to damage or change. Therefore, HSP47 expression may be increased here to support collagen biosynthesis because these layers provide growth factors and nutrients for embryogenesis

(Hugentobler *et al.* 2010).

The present data did not support the hypothesis that AMH induces HSP47 expression in myofibroblasts. Unlike the epithelium, the uterine myometrium is not located adjacent to the lumen, and its structure may not be susceptible to damage or change. However, this may also be due to the short life of HSP47 and subpopulations of myofibroblasts. The HSP47 protein is bound to a ubiquitin-like protein, UBIN (Matsuda *et al.* 2001), and is degraded via the ubiquitin-proteasome system (Ito and Nagata 2016). Therefore, the absence of the effect of AMH on HSP47 may be attributed to HSP47 degradation via the ubiquitin-proteasome system in the cultured myofibroblasts. The recent advances in single-cell biology have revealed that fibroblasts are a heterogeneous population with distinct phenotypes, which exert both beneficial and detrimental effects in human kidney diseases (Arai *et al.* 2021), fibrotic skin keloid (Deng *et al.* 2021), and pancreatic cancer (Ogawa *et al.* 2021). Also, uterine myofibroblasts are divided into several subpopulations, that is, highly myogenic and nonmyogenic types (Kobayashi *et al.* 2020), and Thy 1-positive and Thy 1-negative types of myofibroblasts (Koumas *et al.* 2001). Therefore, further studies are required to clarify uterine myofibroblasts and their role in age-related infertility.

AMH mediates its effects through the activation of AMHR2. Little is known about the cytoplasmic pathways downstream of AMHR2 activation. Recombinant human AMH activates the ERK pathway in Sertoli cells (Rehman *et al.* 2017). We demonstrated that U0126, a MEK/ERK inhibitor, inhibited AMH-mediated HSP47 expression in epithelial cells. Therefore, we postulate that AMH induces HSP47 expression via the ERK pathway.

This study has some limitations that we could not address. We observed a weak 75 kDa band in the western blot. We searched for proteins with a similar amino acid sequence to bovine HSP47 using protein BLAST; however, we did not identify a protein with high

homology to bovine HSP47. Therefore, further studies are required to identify the protein corresponding to the 75 kDa band. Furthermore, we could not quantify the effect of AMH on HSP47 expression because HSP47 mRNA levels were too low to measure by RT-qPCR. HSP47 expression is always upregulated or downregulated with changes in the expression of various types of collagens, as reviewed by Ito and Nagata (2017). Therefore, a possible reason for the low levels of HSP47 mRNA may be such systems.

In this study, 0.85 pM of AMH, but not TGF- $\beta$ 1, stimulated HSP47 in the bovine uterine epithelium. In order to increase HSP47 expression, minimum required concentration of TGF $\beta$ 1 is 4 uM (Kim et al. 2019) in nasal fibroblasts, and 40uM (Nakayama et al. 2008) in human lung fibroblasts. Therefore, TGF- $\beta$ 1 at the micromolar levels may stimulate HSP47. An abnormal increase in collagen synthesis by myofibroblasts induced by TGF- $\beta$ 1 and its isoforms may lead to adenomyosis and ectopic endometria in women (Cheong *et al.* 2019). TGF- $\beta$ 1 may also exert important pathological effects on myofibroblasts during equine endometriosis (Szostek-Mioduchowska *et al.* 2019). Therefore, we could not deny any pathological role of TGF- $\beta$ 1 in bovine uteri.

In conclusion, AMH stimulates HSP47 expression in bovine uterine epithelial cells but not myofibroblasts. Moreover, AMH-induced HSP47 expression is likely mediated by the ERK pathway.

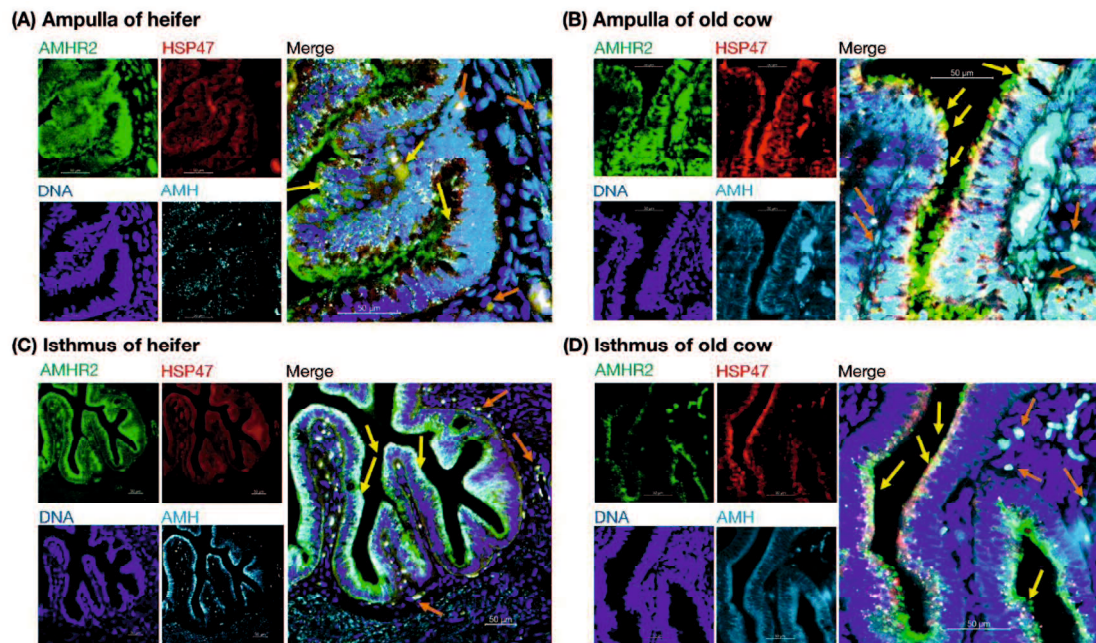


**Fig. 6.7. Supplementary Fig. 1.** Comparison of AMHR2-rich areas (green), AMH-rich areas (light blue), and HSP47-rich areas (red) in the ampullae or isthuses (collected on day 3 of the estrous cycle) of young heifer (22 months old) and old cow uteri (130 months old). Nuclei are counterstained with DAPI (dark blue). The old specimens showed strong signals corresponding to both AMHR2 and HSP47 in the epithelia of tunica mucosa and superficial stroma. The merge panels show signals corresponding to colocalization of AMHR2 with HSP47 (yellow arrows). AMHR2-positive, AMH-positive, and HSP47-positive myofibroblasts are indicated by brown arrows. Scale bars: 50  $\mu$ m.

## **CHAPTER VII**

### **General Discussion and Conclusion**

## 7.1. General discussion

I hypothesized that AMH secreted from preantral and small antral follicles etc. regulate the oviducts and endometria in the study I. Then, I discovered the mRNA and protein of AMHR2 in the oviducts and endometria of heifers and cows. Immunofluorescence analysis using anti-bovine AMHR2 antibody revealed robust high-intensity signals in the tunica mucosa of ampulla and isthmus, and in the glandular and luminal epithelium of endometria, leading to the speculation the potential AMHR2 roles in these layers. The preantral and small antral follicles are not silent majority in ovaries.

In addition to the AMH's endocrine roles, I investigated whether bovine oviducts and endometria produce AMH for paracrine and autocrine signaling. The study II discovered that bovine oviducts and endometria express AMH, and secrete AMH into the oviduct and uterine fluids. This data suggested that AMH has paracrine and autocrine roles, similar with other important hormones (e.g. GnRH, inhibin, and activin).

Cow fertility decreases with age, but the oviductal and endometrial pathomechanisms are not understood well. Blood AMH concentrations are influenced by age in cows (Koizumi and Kadokawa 2017); old JB cows have significantly higher blood AMH concentrations than young JB cows throughout the postpartum period (Koizumi and Kadokawa 2017). Therefore, the AMH and AMHR2 in oviducts and endometria may contribute to infertility cows after aging. I compared the AMH and AMHR2 expression between old Holsteins and young and old JB females in the study I and II. No significant difference was observed in AMH and AMHR2 expression in the oviducts and endometria among old Holsteins and young and old JB cows. However, the AMH concentration in the oviduct fluid, but not in the uterine horn fluid of Holsteins cows, was lower than that those in JB heifers and cows'

females. The results for the effects of breed and age on AMH expression should be interpreted with caution because we could not obtain oviducts and endometria from young Holsteins. However, the difference in AMH concentration may be explained by a difference among breeds or any factor related to breed.

In the study III, I observed the denatured collagen and HSP47 in oviducts and uteri. The damaged collagen was increased in not only uteri but also oviducts of old JB cows. The high HSP47 protein amounts observed in old oviducts and uteri compared with those in the young oviducts. However, HSP47 expression located apart from the damaged collagen in the uteri of old JB cows. Excess HSP47 expression is an important step in collagen-related diseases, including keloids and fibrosis (Ito and Nagata, 2019). Also this study showed an increased fibroblasts in various parts of the oviducts and uteri, thereby this study discovered also fibrosis in old JB cows. Therefore, damaged collagen and abnormal increase of HSP47 may be important caused for infertility in old JB cows.

In the study IV, AMH stimulates HSP47 expression in bovine uterine epithelial cells and fibroblasts. Therefore, the study supported the hypothesis that AMH increase HSP47 expression in both epithelial cells and fibroblasts. The AMH stimulation of HSP47 expression was suppressed by pre-treatment with the ERK inhibitor. The study IV suggested AMH may be an important part of the infertility in aged cows.

## **7.2. Conclusion**

In conclusion, this thesis discovered the AMH and AMHR2 in bovine oviducts and uteri, which have important roles for collagen synthesis via HSP47.

## References

- Abe, H., and Hoshi, H. (2008). Morphometric and ultrastructural changes in ciliated cells of the oviductal epithelium in prolific Chinese Meishan and Large White pigs during the oestrous cycle. *Reprod Dom Anim.* 43: 66–73.
- Akbarinejad, V., Gharagozlou, F., Vojgani, M., Shourabi, E., and Makiabadi, M. J. M. (2019). Inferior fertility and higher concentrations of anti-Mullerian hormone in dairy cows with longer anogenital distance. *Domest. Anim. Endocrinol.* 68, 47-53.
- Alward, K.J., and Bohlen, J.F. (2020). Overview of Anti-Müllerian hormone (AMH) and association with fertility in female cattle. *Reprod Domest Anim.* 55, 3-10.
- Arai, H., Sato, Y., and Yanagita, M. (2021). Fibroblast heterogeneity and tertiary lymphoid tissues in the kidney. *Immunol. Rev.* 302, 196-210.
- Arai, M., Yoshioka, S., Tasaki, Y., and Kiyoshi Okuda, K. (2013). Remodeling of bovine endometrium throughout the estrous cycle. *Anim. Reprod. Sci.* 142, 1-9.
- Arouche, N., Picard, J. Y., Monniaux, D., Jamin, S. P., Vigier, B., Josso, N., Cate, R. L., Clemente, N. d., and Taieb, J. (2015). The BOC ELISA, a ruminant-specific AMH immunoassay, improves the determination of plasma AMH concentration and its correlation with embryo production in cattle. *Theriogenology*, 84, 1397-1404.
- Banu, S.K., Arosh, J.A., Chapdelaine, P., and Fortier, M.A. (2005). Expression of prostaglandin transporter in the bovine uterus and fetal membranes during pregnancy. *Biol. Reprod.* 73, 230-6.
- Beck, T.N., Korobeynikov, V.A., Kudinov, A.E., Georgopoulos, R., Solanki, N.R., Andrews-Hoke, M., Kistner, T.M., Pépin, D., Donahoe, P.K., Nicolas, E., Einarson, M.B., Zhou, Y., Bumber, Y., Proia, D.A., Serebriiskii, I.G., and Golemis, E.A. (2016). Anti-Müllerian Hormone Signaling Regulates Epithelial Plasticity and Chemoresistance in Lung Cancer. *Cell Rep.* 16, 657-71.

- Bello, A.B., Kim, D., Kim, D., Park, H., and Lee, S.H. (2020). Engineering and functionalization of gelatin biomaterials: from cell culture to medical applications. *Tissue. Eng. Part. B. Rev.* 26, 164-180.
- Belville, C., Van, Vlijmen, H., Ehrenfels, C., Pepinsky, B., Rezaie, A. R., Picard, J. Y., Josso, N., di Clemente, N., and Cate, R.L. (2004). Mutations of the anti-mullerian hormone gene in patients with persistent mullerian duct syndrome: biosynthesis, secretion, and processing of the abnormal proteins and analysis using a three-dimensional model. *Mol. Endocrinol.* 18, 708-721.
- Besenfelder, U., Havlicek, V., and Brem, G. (2012). Role of the oviduct in early embryo development. *Reprod. Domest. Anim.* 47, 156–163.
- Bhide, P., and Homburg, R. (2016). Anti-Müllerian hormone and polycystic ovary syndrome. *Best Pract. Res. Clin. Obstet. Gynaecol.* 37, 38-45.
- Binelli, M., Gonella-Diaza, A.M., Mesquita, F.S., and Membrive, C.M.B. (2018). Sex Steroid-Mediated Control of Oviductal Function in Cattle. *Biology (Basel).* 7, E15.
- Boos, A. (2000). Immunohistochemical assessment of collagen types I, III, IV and VI in biopsy samples of the bovine uterine wall collected during the oestrous cycle. *Cells Tissues Organs* 167, 225-38.
- Campbell, B. K., Clinton, M., and Webb, R. (2012). The role of anti-Müllerian hormone (AMH) during follicle development in a monovulatory species (sheep). *Endocrinology*, 153, 4533-4543.
- Chaney, H.L., Grose, L.F., Charpigny, G., Behura, S.K., Sheldon, I.M., Cronin, J.G., Lonergan, P., Spencer, T.E., and Mathew, D.J. (2021). Conceptus-induced, interferon tau-dependent gene expression in bovine endometrial epithelial and stromal cells, *Biol. Reprod.* 104, 669–683.

- Chenoweth, P. J. (1994). Aspects of reproduction in female *Bos indicus* cattle: a review. *Aust. Vet. J.* 71, 422-426.
- Cheong, M.L., Lai, T.H., and Wu, W.B. (2019). Connective tissue growth factor mediates transforming growth factor  $\beta$ -induced collagen expression in human endometrial stromal cells. *PLoS One*, 14, e0210765.
- Cox, C.I., and Leese, H.J. (1997). Retention of functional characteristics by bovine oviduct and uterine epithelia *in vitro*. *Anim. Reprod. Sci.*; 46, 169–178.
- Croxatto, H. B. (2002). Physiology of gamete and embryo transport through the fallopian tube. *Reprod. Biomed. Online* 4, 160–169.
- Deng, C.C., Hu, Y.F., Zhu, D.H., Cheng, Q., Gu, J.J., Feng, Q.L., Zhang, L.X., Xu, Y.P., Wang, D., Rong, Z., and Yang, B. (2021). Single-cell RNA-seq reveals fibroblast heterogeneity and increased mesenchymal fibroblasts in human fibrotic skin diseases. *Nat. Commun.* 12, 3709.
- Dewailly, D., Andersen, C. Y., Balen, A., Broekmans, F., Dilaver, N., Fanchin, R., Griesinger, G., Kelsey, T. W., Marca A. L., Lambalk, C., Mason, H., Nelson, S. M, Visser, J.A., Wallace, W. H., and Anderson, R. A. (2014). The physiology and clinical utility of anti-Müllerian hormone in women. *Hum. Reprod. Update*, 20, 370–385.
- Duarte, B.D.P., and Bonatto, D. (2018). The heat shock protein 47 as a potential biomarker and a therapeutic agent in cancer research. *J. Cancer. Res. Clin. Oncol.* 144, 2319-28.
- El-Banna, A. A., and Hafez, E. S. (1970). Egg transport in beef cattle. *Sci. J. Anim. Sci.* 30, 430–432.
- El-Sheikh Ali, H., Kitahara, G., Nibe, K., Yamaguchi, R., Horii, Y., Zaabel, S., and Osawa,

- T. (2013). Plasma anti-Müllerian hormone as a biomarker for bovine granulosa-theca cell tumors: comparison with immunoreactive inhibin and ovarian steroid concentrations. *Theriogenology*, 80, 940-949.
- Erickson, B. H., Reynolds, R. A., and Murphree, R. L. (1976). Ovarian characteristics and reproductive performance of the aged cow. *Biol. Reprod.* 15, 555-560.
- Ernst, E., Oxvig, C., Kumar, A., Kalra, B., and Andersen, C. Y., (2015). Proteolytic processing of anti-Müllerian hormone differs between human fetal testes and adult ovaries. *Mol. Hum. Reprod.* 21, 571–582.
- Faul, F., Erdfelder, E., Lang, A.G., and Buchner, A. (2007). G\*Power 3: a flexible statistical power analysis program for the social, behavioral, and biomedical sciences. *Behav. Res. Methods* 39, 175-91.
- Faure, E., Gouédard, L., Imbeaud, S., Cate, R., Picard, J. Y., Josso, N., and di Clemente, N. (1996). Mutant isoforms of the anti-Müllerian hormone type II receptor are not expressed at the cell membrane. *J. Biol. Chem.* 271, 30571-30575.
- Ferdousy, R.N., and Kadokawa, H. (2022). Specific locations and amounts of denatured collagen and collagen-specific chaperone HSP47 in the oviducts and uteri of old cows as compared to those of heifers. *Reprod. Fertil. Dev.* 34, 619-632.
- Ferdousy, R.N., Kereilwe, O., and Kadokawa, H. (2020a). Anti-Müllerian hormone receptor type 2 (AMHR2) expression in bovine oviducts and endometria: comparison of AMHR2 mRNA and protein abundance between old Holstein and young and old Wagyu females. *Reprod. Fertil. Dev.* 32, 738-747.
- Ferdousy, R.N., Kereilwe, O., and Kadokawa, H. (2020b). Anti-Müllerian hormone is expressed and secreted by bovine oviductal and endometrial epithelial cells. *Anim. Sci. J.* 91, e13456.

- Fields, G.B. (2013). Interstitial collagen catabolism. *J. Biol. Chem.* 288, 8785-8793.
- Fuchs, A.R., Behrens, O., Helmer, H., Liu, C.H., Barros, C.M., and Fields, M.J. (1990). Oxytocin and vasopressin receptors in bovine endometrium and myometrium during the estrous cycle and early pregnancy. *Endocrinology*, 127, 629-36.
- García, E.V., Hamdi, M., Barrera, A.D., Sánchez-Calabuig, M.J., Gutiérrez-Adán, A., and Rizos, D. (2017). Bovine embryo-oviduct interaction in vitro reveals an early cross talk mediated by BMP signaling. *Reproduction*, 153, 631-643.
- Garrel, G., Racine, C., L'Hôte, D., Denoyelle, C., Guigon, C. J., di Clemente, N., and Cohen-Tannoudji, J. (2016). Anti-Müllerian hormone: a new actor of sexual dimorphism in pituitary gonadotrope activity before puberty. *Sci. Rep.* 6, 23790.
- Geserick, C., Meyer, H.A., and Haendler, B. (2005). The role of DNA response elements as allosteric modulators of steroid receptor function. *Mol. Cell. Endocrinol.* 236, 1-7.
- Gharagozlou, F., Akbarinejad, V., Youssefi, R., and Rezagholizadeh, A. (2013). Low concentration of anti-Müllerian hormone in mares with delayed uterine clearance. *J. Equine Vet. Sci.* 34, 575-577.
- Godoy-Guzmán, C., Nuñez, C., Orihuela, P., Campos, A., and Carriel, V. (2018). Distribution of extracellular matrix molecules in human uterine tubes during the menstrual cycle: a histological and immunohistochemical analysis. *J. Anat.* 233, 73-85.
- Gonella-Diaza, A. M., Mesquita, F. S., Lopes, E., Silva, K. R. d., Cogliati, B., Strefezzi R. D. F., and Binelli, M. (2018). Research Article Sex steroids drive the remodeling of oviductal extracellular matrix in cattle. *Biol. Reprod.* 99, 590–599.
- Gowkielewicz, M., Lipka, A., Piotrowska, A., Szadurska-Noga, M., Nowakowski, J. J., Dzięgiel, P. and Majewska, M. (2019). Anti-Müllerian hormone expression in

- endometrial cancer tissue. *Int. J. Mol. Sci.* 20, E1325.
- Gray, C.A., Bazer, F.W., and Spencer, T.E. (2001). Effects of neonatal progestin exposure on female reproductive tract structure and function in the adult ewe. *Biol. Reprod.* 64, 797–804.
- Gruber, C.J., Gruber, D.M., Gruber, I.M., Wieser, F., and Huber J.C. (2004). Anatomy of the estrogen response element. *Trends Endocrinol. Metab.* 15, 73-78.
- Hayashi, K.G., Hosoe, M., Kizaki, K., Fujii, S., Kanahara, H., Takahashi, T., and Sakumoto, R. (2017). Differential gene expression profiling of endometrium during the mid-luteal phase of the estrous cycle between a repeat breeder (RB) and non-RB cows. *Reprod. Biol. Endocrinol.* 15, 20.
- Herath, S., Williams, E. J., Lilly, S. T., Gilbert, R. O., Dobson, H., Bryant, C. E., and Sheldon, I. M. (2007). Ovarian follicular cells have innate immune capabilities that modulate their endocrine function. *Reproduction*, 134, 683–693.
- Hernandez-Medrano, J. H., Campbell, B. K., and Webb, R. (2012). Nutritional influences on folliculogenesis. *Reprod. Domest. Anim. Suppl.* 4, 274-282.
- Hillmer, M., Marth, C.D., Meyerholz, M.M., Klaus-Halla, D., Schoon, H.A., Weber, F., Schuberth, H.J., and Zerbe, H. (2020). Gene expression in bovine endometrial cells and blood-derived neutrophils stimulated by uterine secretions. *Theriogenology*, 157, 458-466.
- Hirayama, H., Naito, A., Fujii, T., Sugimoto, M., Takedomi, T., Moriyasu, S., Sakai, H., and Kageyama, S. (2019). Effects of genetic background on responses to superovulation in Japanese Black cattle. *J. Vet. Med. Sci.* 81, 373-378.
- Hirschhorn, T., di Clemente, N., Amsalem, A. R., Pepinsky, R. B., Picard, J. Y., Smorodinsky, N. I., Cate, R. L., and Ehrlich, M. (2015). Constitutive negative

- regulation in the processing of the anti-Müllerian hormone receptor II. *J. Cell Sci.* 128, 1352-1364.
- Holt, W.V., and Fazeli, A. (2010). The oviduct as a complex mediator of mammalian sperm function and selection. *Mol. Reprod. Dev.* 77: 934–943.
- Honaramooz, A., Aravindakshan, J., Chandolia, R.K., Beard, A.P., Bartlewski, P.M., Pierson, R.A., and Rawlings, N.C. (2004). Ultrasonographic evaluation of the pre-pubertal development of the reproductive tract in beef heifers. *Anim. Reprod. Sci.* 80, 15-29.
- Hugentobler, S. A., Sreenan, J. M., Humpherson, P. G., Leese, H. J., Diskin, M. G., and Morris, D. G. (2010). Effects of changes in the concentration of systemic progesterone on ions, amino acids and energy substrates in cattle oviduct and uterine fluid and blood. *Reprod. Fertil. Dev.* 22, 684–694.
- Hunter, R. H. (2005). The Fallopian tubes in domestic mammals: how vital is their physiological activity? *Reprod. Nutr. Dev.* 45, 281–290.
- Inoue, K., Hosono, M., Oyama, H., and Hirooka, H. (2020). Genetic associations between reproductive traits for first calving and growth curve characteristics of Japanese Black cattle. *Anim. Sci. J.* 91, e13467.
- Ito, S., and Nagata, K. (2016). Mutants of collagen-specific molecular chaperone Hsp47 causing osteogenesis imperfecta are structurally unstable with weak binding affinity to collagen. *Biochem. Biophys. Res. Commun.* 469, 437-42.
- Ito, S., and Nagata, K. (2017). Biology of Hsp47 (Serpin H1), a collagen-specific molecular chaperone. *Semin. Cell. Dev. Biol.* 62, 142-151.
- Ito, S., and Nagata, K. (2019). Roles of the endoplasmic reticulum-resident, collagen-specific molecular chaperone Hsp47 in vertebrate cells and human disease. *J. Biol.*

Chem. 294, 2133-2141.

Josso, N. (2019). Anti-Müllerian hormone: a look back and ahead. *Reproduction*, 158, F81-F89.

Kadokawa, H., and Martin, G. B. (2006). A new perspective on management of reproduction in dairy cows: the need for detailed metabolic information, an improved selection index and extended lactation. *J. Reprod. Dev.* 52, 161-168.

Kakugawa, T., Mukae, H., Hayashi, T., Ishii, H., Nakayama, S., Sakamoto, N., Yoshioka, S., Sugiyama, K., Mine, M., Mizuta, Y., and Kohno, S. (2005). Expression of HSP47 in usual interstitial pneumonia and nonspecific interstitial pneumonia. *Respir. Res.* 6, 57.

Kamomae, H. (2012). Reproductive disturbance. In ‘Veterinary Theriogenology’. (Eds T. Nakao, S. Tsumagari and S. Katagiri.) pp. 283-340. (Buneidou Press: Tokyo, Japan) [in Japanese]

Kelly, R. W., Carr, G. G., and Critchley, H. O. (1997). A cytokine switch induced by human seminal plasma: an immune modulation with implications for sexually transmitted disease. *Hum. Reprod.* 12, 677–681.

Kereilwe, O., and Kadokawa, H. (2019). Bovine gonadotrophs express anti-Müllerian hormone (AMH): Comparison of AMH mRNA and protein expression levels among old Holsteins and young and old Japanese black females. *Reprod. Fertil. Dev.* 31, 810-819.

Kereilwe, O., Pandey, K., Borromeo, V., and Kadokawa, H. (2018). Anti-Müllerian hormone receptor type 2 is expressed in gonadotrophs of postpubertal heifers to control gonadotrophin secretion. *Reprod. Fertil. Dev.* 30, 1192-1203.

Kim, J.H., MacLaughlin, D.T., and Donahoe, P.K. (2014). Müllerian inhibiting

- substance/anti-Müllerian hormone: A novel treatment for gynecologic tumors. *Obstet Gynecol Sci.* 57, 343-57.
- Kim, S.M., Kim, Y.O., Lee, M.K., Chung, Y.J., Jeung, I.C., Kim, M.R., and Kim, J.H. (2019). Müllerian inhibiting substance/anti-Müllerian hormone type II receptor protein and mRNA expression in the healthy and cancerous endometria. *Oncol. Lett.* 17, 532-538.
- Kim, S.Y., Moon, H.M., Lee, M.K., Chung, Y.J., Song, J.Y., Cho, H.H., Kim, M.R., and Kim, J.H. (2018). The expression of Müllerian inhibiting substance/anti-Müllerian hormone type II receptor in myoma and adenomyosis. *Obstet. Gynecol. Sci.* 61, 127-134.
- Kobayashi, H., Kishi, Y., and Matsubara, S. (2020). Mechanisms underlying adenomyosis-related fibrogenesis. *Gynecol. Obstet. Invest.* 85, 1-12.
- Koizumi, M., and Kadokawa, H. (2017). Positive correlations of age and parity with plasma anti-Müllerian hormone concentrations in Japanese Black cows. *J. Reprod. Dev.* 63, 205-209.
- Kolle S, Dubielzig S, Reese S, Wehrend A, König P, Kummer W. (2009). Ciliary transport, gamete interaction, and effects of the early embryo in the oviduct: ex vivo analyses using a new digital video microscopic system in the cow. *Biol Reprod.* 81, 267-274.
- Kolle, S., Reese, S., and Kummer, W. (2010). New aspects of gamete transport, fertilization, and embryonic development in the oviduct gained by means of live cell imaging. *Theriogenology*, 73, 786–795.
- Koumas, L., King, A.E., Critchley, H.O., Kelly, R.W., and Phipps, R.P. (2001). Fibroblast heterogeneity: existence of functionally distinct Thy 1(+) and Thy 1(-) human female reproductive tract fibroblasts. *Am. J. Pathol.* 159, 925-935.

- Kumar, A., Kalra, B., Patel, A., McDavid, L., and Roudebush, W. E. (2010). Development of a second-generation anti-Müllerian hormone (AMH) ELISA. *J. Immunol. Methods*, 362, 51–59.
- Li, Y., Gao, D., Xu, T., Adur, M.K., Zhang, L., Luo, L., Zhu, T., Tong, X., Zhang, D., Wang, Y., Ning, W., Qi, X., Cao, Z., and Zhang, Y. (2019b). Anti-Müllerian hormone inhibits luteinizing hormone-induced androstenedione synthesis in porcine theca cells. *Theriogenology*, 142, 421-432.
- Li, M., Yao, L., Xin M., and Gao, M. (2019a). Dysregulation of collagen expression in peri-implantation endometrium of women with high ovarian response, *J. Obstet. Gynaecol. Res.* 45, 1035-1044.
- Liu, D., Nikoo, M., Boran, G., Zhou, P., and Regenstein, J.M. (2015). Collagen and gelatin. *Annu. Rev. Food. Sci. Technol.* 6, 527-557.
- Liu, D., Xiong, F., and Hew, C.L. (1995). Functional analysis of estrogen-responsive elements in chinook salmon (*Oncorhynchus tshawytscha*) gonadotropin II beta subunit gene. *Endocrinology* 136, 3486-93.
- Lyttle, S. B. M., Jukic, A. M. Z., and Steiner, A. Z. (2018). Antimüllerian hormone as a risk factor for miscarriage in naturally conceived pregnancies. *Fertil. Steril.* 109, 1065-1071.
- Maciejewska-Jeske, M., and Lukaszuk, K. (2016). Fertility in women of late reproductive age: the role of serum anti-Müllerian hormone (AMH) levels in its assessment. *J. Endocrinol. Investing.* 39, 1259-1265.
- Mamsen, L. S., Petersen, T. S., Jeppesen, J. V., Møllgard, K., Grøndahl, M. L., Larsen, A., Matsuda, M., Koide, T., Yoriuzzi, T., Hosokawa, N., and Nagata K. (2001). Molecular cloning of a novel ubiquitin-like protein, UBIN, that binds to ER targeting signal

- sequence. *Biochem. Biophys. Res. Commun.* 280, 535-40.
- McLennan, I.S., and Pankhurst, M.W., (2015). Anti-müllerian hormone is a gonadal cytokine with two circulating forms and cryptic actions. *J. Endocrinol.* 226, R45-57.
- Meczekalski, B., Czyzyk, A., Kunicki, M., Podfigurna-Stopa, A., Plociennik, L., Jakiel, G., Merhi, Z. (2019). Vitamin D attenuates the effect of advanced glycation end products on anti-Mullerian hormone signaling. *Mol. Cell. Endocrinol.* 479, 87-92.
- Miyamoto, Y., Skarzynski, D. J., and Okuda, K. (2000). Is tumor necrosis factor alpha a trigger for the initiation of endometrial prostaglandin F(2alpha) release at luteolysis in cattle? *Biol. Reprod.* 62, 1109-1115.
- Mohos, S.C., and Wagner, B.M. (1969). Damage to collagen in corneal immune injury. Observation of connective tissue structure. *Arch. Pathol.* 88, 3-20.
- Mossa, F., Jimenez-Krassel, F., Scheetz, D., Weber-Nielsen, M., Evans, A.C.O., and Ireland, J.J. (2017). Anti-Müllerian Hormone (AMH) and fertility management in agricultural species. *Reproduction.* 154, R1-R11.
- Mossa, F., and Ireland, J, J. (2019). Physiology and endocrinology symposium: Anti-Mullerian hormone: a biomarker for the ovarian reserve, ovarian function, and fertility in dairy cows. *J Anim Sci*, 97, 1446-1455.
- Nahar, A., and Kadokawa, H. (2017). Expression of macrophage migration inhibitory factor (MIF) in bovine oviducts is higher in the postovulatory phase than during the oestrus and luteal phase. *Reprod. Fertil. Dev.* 29, 1521-1529.
- Nahar, A., Maki, S., and Kadokawa, H. (2013). Suppressed expression of granulocyte macrophage colony-stimulating factor in oviduct ampullae of obese cows. *Anim. Reprod. Sci.* 139, 1-8.
- Nakahari, T., Nishimura, A., Shimamoto, C., Sakai, A., Kuwabara, H., Nakano, T., Tanaka,

- S., Kohda, Y., Matsumura, H., and Mori, H. (2011). The regulation of ciliary beat frequency by ovarian steroids in the guinea pig Fallopian tube: interactions between oestradiol and progesterone. *Biomed Res.* 32, 321–328.
- Ogawa, Y., Masugi, Y., Abe, T., Yamazaki, K., Ueno, A., Fujii-Nishimura, Y., Hori, S., Yagi, H., Abe, Y., Kitago, M., and Sakamoto, M. (2021). Three distinct stroma types in human pancreatic cancer identified by image analysis of fibroblast subpopulations and collagen. *Clin. Cancer. Res.* 27, 107-119.
- Osoro, K., and Wright, I. A. (1992). The effect of body condition, live weight, breed, age, calf performance, and calving date on reproductive performance of spring-calving beef cows. *J. Anim. Sci.* 70, 1661-1666.
- Paradisi, R., Vicenti, R., Macciocca, M., Seracchioli, R., Rossi, S., and Fabbri, R. (2016). High cytokine expression and reduced ovarian reserve in patients with Hodgkin lymphoma or non-Hodgkin lymphoma. *Fertil. Steril.* 106, 1176-1182.
- Park, J., Lee, J., and Baek, S. (2018). Pathologic features and expression of heat shock protein 47 in the nasal mucosa and lacrimal sac: does it influence the surgical outcome of endoscopic endonasal dacryocystorhinostomy? *Eye (Lond).* 32, 1432-1439.
- Pfeiffer, K. E., Jury, L. J., and Larson, J. E. (2014). Determination of anti-Müllerian hormone at estrous during a synchronized and a natural bovine estrous cycle. *Domest. Anim. Endocrinol.* 46, 58-64.
- Pohler, K.G., Geary, T.W., Atkins, J.A., Perry, G.A., Jinks, E.M., and Smith, M.F. (2012). Follicular determinants of pregnancy establishment and maintenance. *Cell Tissue Res.* 349, 649-664.
- Poole, D. H., Ocón-Grove, O. M., and Johnson, A. L. (2016). Anti-Müllerian hormone

- (AMH) receptor type II expression and AMH activity in bovine granulosa cells. *Theriogenology* 86, 1353-1360.
- Quayle, A. J. (2002). The innate and early immune response to pathogen challenge in the female genital tract and the pivotal role of epithelial cells. *J. Reprod. Immunol.* 57, 61–79.
- Ray, I.L., Dumas, M., Sagot, P., and Bardou, M., (2013). Effects of leptin on lipopolysaccharide-induced remodeling in an in vitro model of human myometrial inflammation. *Biol. Reprod.* 88, 45.
- Razzaque, M.S., and Taguchi, T. (1999). Role of glomerular epithelial cell-derived heat shock protein 47 in experimental lipid nephropathy. *Kidney Int. Suppl.* 71, S256-9.
- Rehman, Z.U., Worku, T., Davis, J.S., Talpur, H.S., Bhattarai, D., Kadariya, I., Hua, G., Cao, J., Dad, R., Farmanullah, Hussain, T., and Yang, L. (2017). Role and mechanism of AMH in the regulation of Sertoli cells in mice. *J. Steroid Biochem. Mol. Biol.* 174, 133-140.
- Rekawiecki, R., Rutkowska, J., and Kotwica, J. (2012). Identification of optimal housekeeping genes for examination of gene expression in bovine corpus luteum. *Reprod. Biol.* 12, 362–367.
- Rey, R., Lukas-Croisier, C., Lasala, C. and Bedecarras, P. (2003). AMH/MIS: What we know already about the gene, the protein and its regulation. *Mol. Cell Endocrinol.* 211, 21–31.
- Ribeiro, E. S., Bisinotto, R. S., Lima, F. S., Greco, L. F., Morrison, A., Kumar, A., Thatcher, W. W., and Santos, J. E. (2014). Plasma anti-Müllerian hormone in adult dairy cows and associations with fertility. *J. Dairy Sci.* 97, 6888-6900.
- Rocha, R. M., Lima, L. F., Carvalho, A. A., Chaves R. N., Bernuci, M. P., Rosa-e-Silva, A.

- C., Rodrigues, A. P., Campello, C. C., and Figueiredo, J. R. (2016). Immunolocalization of the Anti-Müllerian Hormone (AMH) in Caprine Follicles and the Effects of AMH on In Vitro Culture of Caprine Pre-antral Follicles Enclosed in Ovarian Tissue. *Reprod. Domest. Anim.* 51, 212-219.
- Rodriguez, A., Tripurani, S.K., Burton, J.C., Clementi, C., Larina, I., and Pangas, S.A. (2016). SMAD signaling is required for structural integrity of the female reproductive tract and uterine function during early pregnancy in mice. *Biol. Reprod.* 95, 1-16.
- Rose, J.B., Pacelli, S., Haj, A.J.E., Dua, H.S., Hopkinson, A., White, L.J., and Rose, F.R.AJ. (2014). Gelatin-based materials in ocular tissue engineering. *Materials (Basel)*. 7, 3106-3135.
- Scheffer, J. A. B., Scheffer, B., Scheffer, R., Florencio, F., Grynberg, M., and Lozano, D. M. (2018). Are age and anti-Müllerian hormone good predictors of ovarian reserve and response in women undergoing IVF? *JBRA Assist Reprod.* 22, 215-220.
- Scolari, S.C., Pugliesi, G., Strefezzi, R.F., Andrade, S.C., Coutinho, L.L., and Binelli, M. (2016). Dynamic remodeling of endometrial extracellular matrix regulates embryo receptivity in cattle. *Reproduction*, 153, 49-61.
- Sefrioui, O., Madkour, A., Aboulmaouahib, S., Kaarouc, I., and Louanjli, N. (2019). Women with extreme low AMH values could have in vitro fertilization success. *Gynaecol. Endocrinol.* 35, 170-173.
- Seifer, D. B., and Merhi, Z. (2014). Is AMH a regulator of follicular atresia? *Assist. Reprod. Genet.* 31, 1403-1407.
- Shi, J.W., Lai Z.Z., Yang, H.L., Yang, S.L., Wang, C.J., Ao, D., Ruan, L.Y., Shen, H.H., Zhou, W.J., Mei, J., Fu, Q., and Li, and M.Q. (2020). Collagen at the maternal-fetal interface in human pregnancy. *Int. J. Bio.l Sci.* 16, 2220-2234.

- Signorile, P.G., Petraglia, F., and Baldi, A. (2014). Anti-mullerian hormone is expressed by endometriosis tissues and induces cell cycle arrest and apoptosis in endometriosis cells. *J. Exp. Clin. Cancer Res.* 33, 46.
- Skaar, K. S, Nobrega, R. H., Magaraki, A., Olsen, L. C., Schulz, R. W., and Male, R. (2011). Proteolytically activated, recombinant anti Mullerian hormone inhibits androgen secretion, proliferation, and differentiation of spermatogonia in adult zebrafish testis organ cultures. *Endocrinology*, 152, 3527-3540.
- Sugiura, T., Akiyoshi, S., Inoue, F., Yanagawa, Y., Moriyoshi, M., Tajima, M., and Katagiri S. (2018). Relationship between bovine endometrial thickness and plasma progesterone and estradiol concentrations in natural and induced estrous. *J. Reprod. Dev.* 64, 135-43.
- Szóstek-Mioduchowska, A., Słowińska, M., Pacewicz, J., Skarzynski., D.J., and Okuda, K. (2020). Matrix metalloproteinase expression and modulation by transforming growth factor- $\beta$ 1 in equine endometrosis. *Sci. Rep.* 10, 1119.
- Takahashi, H., Iga, K., Sato, T., Takahashi, M., and Okano, A. (2001). Isolation and culture of bovine endometrial epithelial cells in a serum-free culture system. *J. Reprod. Dev.* 47, 181-187.
- Takita, K.K., Fujii, K.K., Ishii, K., and Koide, T. (2019). Structural optimization of cyclic peptides that efficiently detect denatured collagen. *Org. Biomol. Chem.* 17, 7380-7.
- Tang, L., Zhang, H., Lei, L., Gong, S., Zhou, Z., Baseman, J., and Zhong, G. (2013). Oviduct infection and hydrosalpinx in dba1/j mice is induced by intracervical but not intravaginal inoculation with *Chlamydia muridarum*. *PLoS One* 8, e71649.
- Tarasconi, B., Tadros, T., Ayoubi, J. M., Belloc, S., de Ziegler, D., and Fanchin, R. (2017). Serum antimullerian hormone levels are independently related to miscarriage rates

- after in vitro fertilization-embryo transfer. *Fertil. Steril.* 108, 518-524.
- Taylor, H.S. (2018). Role of the uterus in fertility, pregnancy, and developmental programming. *Fertil and Steril*, 110, 849-850.
- Tsai, S.Y., Carlstedt-Duke, J., Weigel, N.L., Dahlman, K., Gustafsson, J.A., Tsai, M.J., and O'Malley, B.W. (1988). Molecular interactions of steroid hormone receptor with its enhancer element: evidence for receptor dimer formation. *Cell.* 55, 361-9.
- Valdecantos, P.A., Miana, R.D.C.B., García, E.V., García, D.C., Roldán-Olarte, M., and Miceli, D.C. (2017). Expression of bone morphogenetic protein receptors in bovine oviductal epithelial cells: evidence of autocrine BMP signaling. *Anim. Reprod. Sci.* 185, 89-96.
- Vandesompele, J., De Preter, K., Pattyn, F., Poppe, B., Van Roy, N., De Paepe, A., and Speleman, F. (2002). Accurate normalisation of real-time quantitative RT-PCR data by geometric averaging of multiple internal control genes. *Genome Biol.* 3, research0034.1–research0034.11.
- Vangipuram, M., Ting, D., Kim, S., Diaz, R., and Schüle, B. (2013). Skin punch biopsy explant culture for derivation of primary human fibroblasts. *J. Vis. Exp.* 77, e3779.
- Walker, C. G, Meier, S., Mitchell, M. D., Roche, J. R., and Littlejohn, M. (2009). Evaluation of real-time PCR endogenous control genes for analysis of gene expression in bovine endometrium. *BMC Mol. Biol.* 10, 100.
- Wang, J., Dicken, C., Lustbader, J.W., and Tortoriello, D.V. (2009). Evidence for a Mullerian-inhibiting substance autocrine/paracrine system in adult human endometrium. *Fertil. Steril.* 91, 1195-1203.
- Wathes, D. C. (2012). Mechanisms linking metabolic status and disease with reproductive outcome in the dairy cow. *Reprod. Domest. Anim.* 47, 304-312.

- Wendremaire, M., Mourtialon, P., Goirand, F., Lirussi, F., Barrichon, M., Hadi, T., Garrido, C., Ray, I.L., Dumas, M., Sagot, P., and Bardou, M. (2013). Effects of leptin on lipopolysaccharide-induced remodeling in an in vitro model of human myometrial inflammation. *Biol. Reprod.* 88, 45.
- Xiong, G., Chen, J., Zhang, G., Wang, S., Kawasaki, K., Zhu, J., Zhang, Y., Nagata, K., Li, Z., Zhou, B.P., and Xu, R. (2020). Hsp47 promotes cancer metastasis by enhancing collagen-dependent cancer cell-platelet interaction. *Proc. Natl. Acad. Sci. U. S.A.* 117, 3748-3758.
- Yamamoto, Y., Kobayashi, Y., and Okuda, K. (2014). Purified culture systems for bovine oviductal stromal cells. *J. Reprod. Dev.* 60, 73-77.
- Yániz, J.L., Santolaria, P., Rutllant, J., López-Béjar, M., and López-Gatius, F. (2000). A scanning electron microscopic study of the peritoneal mesothelium covering the genital tract and its ligaments in the cow. *Anat Histol Embryol.* 29, 149–155.
- Zhai, J., Vannuccini, S., Petraglia, F., and Giudice, L.C. (2020). Adenomyosis: Mechanisms and Pathogenesis. *Semin Reprod Med.* 38, 129-143.
- Zhang, Y., Wang, Q., Wang, H., and Duan, E. (2017). Uterine Fluid in Pregnancy: A Biological and Clinical Outlook. *Trends Mol Med.* 23, 604-614.
- Zitnay, J.L., Li, Y., Qin, Z., San, B.H., Depalle, B., Reese, S.P., Buehler, M.J., Yu, S.M., and Weiss, J.A. (2017). Molecular level detection and localization of mechanical damage in collagen enabled by collagen hybridizing peptides. *Nat. Commun.* 8, 14913.